INFRA-SLOW NEURAL OSCILLATIONS: A GATEWAY TO UNDERSTANDING COGNITION AND BRAIN AGING

YUJIA AO

Thesis submitted to the University of Ottawa
in partial Fulfillment of the requirements for the
Doctorate in Philosophy degree in Neuroscience

Department of Cellular and Molecular Medicine
Faculty of Medicine
University of Ottawa

TABLE OF CONTENTS

Acknowledgements

In *Time and Free Will*, Henri Bergson reminds us that inner life, in its successive and singular phases, cannot be fully captured by fixed terms of language. This difficulty is familiar even to native speakers, let alone an international student who entered the English-speaking world only four years ago. Therefore, I write these acknowledgements with a simple purpose: to express my gratitude as sincerely and honestly as I can.

I was born in Yingshan, a small town in southwest China. My parents and I began our life with very little, sharing a room of thirty square meters with my grandparents. Neither of my parents had the opportunity to attend university, but their work gradually improved our family life. We had our own home, enough food, and, very importantly for me, books. In my earliest memories, there was a large bookshelf in my room, and a world map attached on the wall beside my bed.

My parents would read Andersen's fairy tales to me before sleep, or point to countries and oceans and ask me to name them. For a long time, I confused Australia with Canada: both countries seemed vast, distant, and developed. Even their Chinese names shared one character. What I worked hard to distinguish was that Australia's capital was Canberra, not Sydney, and Canada's was Ottawa, not Toronto. I still remember that my mother once talked with great admiration about a documentary on Canadian agriculture that she had watched in high school. At that time, Canada seemed like a distant and unreachable place.

Twenty years later, I am writing these words in my office in the Royal Ottawa Hospital. In this sense, this thesis is not only an academic document, but also a small trace across time and space. To everyone who has helped me along the way, I would like to express my sincere thanks.

First, I would like to thank my thesis supervisor, Dr. Georg Northoff. He gave me the opportunity to do research in his lab and provided a space where I could develop my own ideas. I am grateful for his scientific imagination, his openness to new ideas, and the independence he allowed me during my PhD. This freedom was very important for my growth as a researcher,

and I learned from him that good research requires both imagination and rigor.

I would like to thank my thesis advisory committee members, Dr. Stuart Fogel, Dr. Natalia Jaworska, and Dr. Lauri Tuominen, for their guidance and suggestions throughout my doctoral studies. I also thank my thesis examination committee, Dr. Natalia Jaworska, Dr. Paul Albert, Dr. Andra Smith, and Dr. Xujun Duan, for their time, careful reading, and thoughtful evaluation of this thesis. I am also grateful for Dr. Albert's course, which was one of the most valuable learning experiences during my PhD.

My academic journey began before PhD. Dr. Yifeng Wang, my master's supervisor, offered me resources, funding, and guidance that continued well beyond my master's degree. Many of the basic things I know about doing research were first learned in his lab. He opens the door of the science world to me.

In Ottawa, I had the great fortune of knowing Ms. Valerie Knowles, a deeply knowledgeable author whose work focuses on Canadian history and immigration. She opened her home to me and helped make a foreign city feel more familiar. I will always remember the conversations I had with her, her husband David, her brother Colin, and her old friend Paula, and the good times I spent with her dogs Robbie and Lucy on Piccadilly Ave. This experience reminded me that life outside the lab is also worth paying attention to.

I would also like to thank my labmates: Yasir, Jingyu, I-Fei, Owen, Angelica, Bianca, Lorenzo, Andreas, and Josh. Thank you for your help, conversations, and company during these years. A PhD can sometimes be a lonely process, especially when facing uncertainty for a long time. Having people around made this journey easier. I also thank Qi Wu and Jintao Xing, my academic brothers, who are completing their doctoral studies at Sichuan Normal University and the University of Louvain. I look forward to the day when we can celebrate together.

To my old friends from high school: Chuke Meng, Minsong Yang, Ziqiang Jiang, Wenkai Feng, and Yiqian Wan. Although we no longer play Dota 2 as often as before, we have taken up a new game together: investing in stocks. It seems that the time-series analysis I use for neural signals does not work so well for market fluctuations, but this game has been good

fun, and has shown me something of the real world beyond academia. Your friendship has been part of my life for many years, and I value it very much.

Most of all, I want to thank my parents. You have always supported me, even when I am far away on the other side of the ocean. I still remember losing a bet to my father about how to calculate the area of a triangle. We also played many games of chess together. The outcomes were usually balanced, though I still suspect that some of my victories were allowed by him. My mother is one of the most capable and tough women I have ever known. Her support has been with me throughout my entire education.

I would also like to dedicate special thanks to my late grandparents. My grandfather was a gentle and wise man, who taught me how to remain calm in any circumstance. My grandmother was one of the warmest and most spirited people I have ever known; because of her, my childhood was a happy one. This thesis is dedicated to them.

As I come to the end of my PhD, this journey was imperfect, and so was I. But I made it through — independently, and with more toughness than I expected. If, in the years to come, I am fortunate enough to leave even a small trace in the development of science, I will regard it as a great honor. And it would also be a gentle answer to the boy from a small town, who once looked at the map beside his bed and wondered how far the world could be.

Abbreviation Table

Abbreviation	Full term
5-HT	5-Hydroxytryptamine (serotonin)
5-HT1A	5-Hydroxytryptamine 1A receptor
ACW	Autocorrelation Window
AD	Alzheimer's disease
ADHD	Attention-Deficit/Hyperactivity Disorder
ALFF	Amplitude of Low-Frequency Fluctuation
ANOVA	Analysis of Variance
ATP	adenosine triphosphate
BF	Basal Forebrain
BOLD	Blood-Oxygen-Level-Dependent
BSV	Brain Signal Variability
CIFTI	Connectivity Informatics Technology Initiative file format
CI	Confidence Interval
CompCor	Component-Based Noise Correction
DAN	Dorsal Attention Network
DLB	Dynamic Layer Model of the Brain
DMN	Default Mode Network
DPABI	Data Processing & Analysis for Brain Imaging
DPARSFA	Data Processing Assistant for Resting-State fMRI
EEG	Electroencephalography
EPI	Echo-Planar Imaging
FC	Functional Connectivity
FD	Framewise Displacement

Abbreviation	Full term
FDR	False Discovery Rate
FFT	Fast Fourier Transform
fMRI	Functional Magnetic Resonance Imaging
FPN	Frontoparietal Network
GABA	γ-aminobutyric acid
GradCPT	Gradual-Onset Continuous Performance Task
GS	Global Signal
GSCORR	Global Signal Correlation
GS-TV	Global Signal Topography Variability with Age
HCP	Human Connectome Project
HCP-MMP	Human Connectome Project Multimodal Parcellation
HRF	Hemodynamic Response Function
ICA	Independent Component Analysis
INT	Intrinsic Neural Timescales
ISO	Infra-Slow Oscillations
KL	Kullback–Leibler
LC	Locus Coeruleus
LC–NE	Locus Coeruleus–Norepinephrine
L-DOPA	Levodopa (L-3,4-dihydroxyphenylalanine)
LFP	Local Field Potential
lfSSBR	Low-Frequency Steady-State Brain Response
MEG	Magnetoencephalography
MRI	Magnetic Resonance Imaging
NFFT	Number of Fast Fourier Transform Points

Abbreviation	Full term
NIRS	Near-Infrared Spectroscopy
NMDA	N-Methyl-D-Aspartate
NREM	Non-Rapid Eye Movement
PF	Peak Frequency
PLE	Power-Law Exponent
PSD	Power Spectral Density
ROI	Region of Interest
rs-fMRI	Resting-State Functional Magnetic Resonance Imaging
RT	Reaction Time
SD	Standard Deviation
SE	Sample Entropy
SMN	Somatomotor Network
SSEP	Steady-State Evoked Potential
SWU	Southwest University
tDCS	Transcranial Direct Current Stimulation
TMS	Transcranial Magnetic Stimulation
TR	Repetition Time
TE	Echo Time
VAN	Ventral Attention Network
VIS	Visual Network

Abstract

Infra-slow oscillations (ISO) constitute a dominant component of spontaneous and task-related brain activity, yet their functional and organizational significance is still not fully understood. Traditionally, infra-slow blood-oxygen-level-dependent (BOLD) fluctuations have often been treated as nonspecific drift, physiological noise, or a background feature of resting-state activity. This thesis examines an alternative view: that ISO reflects the structured spatiotemporal brain dynamics, constrained by intrinsic temporal properties of the brain and relevant to cognition and aging.

Across three studies, this thesis investigates ISO from complementary perspectives. Study 1 examines the time-domain organization of ISO by testing whether infra-slow phase dynamics are constrained by intrinsic neural timescales (INT). Using resting-state and naturalistic movie-watching functional magnetic resonance imaging (fMRI) data, this study shows that infra-slow phase progression is not uniform across the oscillatory cycle. Instead, the BOLD instantaneous frequency varies systematically across phase components and is negatively related to regional INT, such that regions with longer timescales show slower phase progression. This relationship persists across rest and task states, suggesting that ISO dynamics are related to stable temporal properties of the brain.

Study 2 examines the frequency-domain organization of ISO by focusing on scale-free dynamics during sustained attention. It shows that the power-law exponent (PLE), indexing scale-free infra-slow organization, mediates the relationship between BOLD signal variability and behavioral variability. These findings suggest that infra-slow scale-free dynamics provide a background temporal feature through which neural variability becomes behaviorally relevant.

Study 3 extends this framework to brain aging by examining global infra-slow connectivity across the adult lifespan. The results demonstrate that global infra-slow functional connectivity becomes less differentiated/more homogenous with age across both spatial and frequency dimensions. Importantly, this spatiotemporal dedifferentiation remains evident after controlling for physiological and vascular confounds, supporting the interpretation that aging

reorganizes, rather than simply degrades, the ISO.

Together, these findings support the view that ISO is not only nuisance activity but a dynamical structure of the human brain. By linking infra-slow dynamics to intrinsic neural timescales, scale-free spectral organization, behavioral variability, and lifespan reorganization, this thesis provides a spatiotemporal framework for understanding how slow brain activity contributes to cognition and brain aging.

Keywords: infra-slow oscillations; intrinsic neural timescales; scale-free dynamics; BOLD variability; behavioral variability; brain aging; fMRI

PREFACE: ARTICLES INCLUDED IN THESIS, COPYRIGHTS, AUTHOR CONTRIBUTIONS, APPROVALS OBTAINED TO CONDUCT THE RESEARCH

Manuscript 1: Ao, Y., Catal, Y., Lechner, S., Hua, J., Northoff, G., 2024. Intrinsic neural timescales relate to the dynamics of infraslow neural waves. NeuroImage 285, 120482.

Author contributions: **Ao, Y.**: Conceptualization, Data curation, Formal analysis, Investigation, Methodology, Software, Validation, Visualization, Writing – original draft, Writing – review & editing. **Catal, Y.**: Software, Validation, Writing – review & editing. **Lechner, S.**: Software, Validation, Writing – review & editing. **Hua, J.**: Validation, Writing – review & editing. **Northoff, G.**: Conceptualization, Investigation, Methodology, Project administration, Resources, Supervision, Validation, Writing – review & editing.

Approvals: The MRI datasets used in this study are from the Human Connectome Project (https://db.humanconnectome.org). The HCP scanning protocol was approved by the local Institutional Review Board at Washington University in St. Louis.

Manuscript 2: Ao, Y., Klar, P., Catal, Y., Wang, Y., Northoff, G., 2025. Infra-slow scale-free dynamics modulate the connection of neural and behavioral variability during attention. Commun. Biol. 8, 1057.

Author contributions: **Ao, Y.**: Conceptualization, Data curation, Formal analysis, Investigation, Methodology, Software, Validation, Visualization, Writing – original draft, Writing – review & editing. **Klar, P.**: Methodology, Software, Writing – review & editing. **Catal, Y.**: Methodology, Software, Writing – review & editing. **Wang, Y.**: Methodology, Resources, Writing – review & editing. **Northoff, G.**: Conceptualization, Investigation,

Methodology, Project administration, Resources, Supervision, Validation, Writing – review & editing.

Approvals: The experimental and scanning procedures received approval from the Ethics Committee of the Institute of Brain and Psychological Sciences at Sichuan Normal University, following the Declaration of Helsinki.

Manuscript 3: Ao, Y., Yang, C., Drewes, J., Jiang, M., Huang, L., Jing, X., Northoff, G., Wang, Y., 2023. Spatiotemporal dedifferentiation of the global brain signal topography along the adult lifespan. Hum. Brain Mapp. 44, 5906–5918.

Author contributions: **Ao, Y.**: Conceptualization, Data curation, Formal analysis, Methodology, Software, Validation, Visualization, Writing – original draft, Writing – review & editing. **Yang, C.**: Data curation, Software, Validation, Writing – review & editing. **Drewes, J.**: Writing - review & editing. **Jiang, M.:** Writing - review & editing. **Huang, L.**: Writing - review & editing. **Jing, X.**: Writing – review & editing. **Northoff, G.:** Conceptualization, Supervision, Resources, Writing – review & editing. **Wang, Y.:** Conceptualization, Investigation, Methodology, Project administration, Resources, Supervision, Validation, Writing – review & editing.

Approvals: The project was approved by the Research Ethics Committee of the Brain Imaging Center of Southwest University, following the Declaration of Helsinki.

Statement on the use of AI tools: During the preparation of this thesis, the author used large language model (ChatGPT, Claude) for language editing (grammar, phrasing, and readability) of text written by the author. No AI tool was used for data analysis, interpretation of results, or the development of scientific arguments.

1 Introduction

1.1 Context: Infra-slow oscillations: a structured component of brain dynamics

Cognitive processes unfold across a hierarchy of temporal scales, and neural activity reflects this organization through rhythmic and oscillatory dynamics that structure information integration over time (Buzsáki, 2025; Buzsáki & Draguhn, 2004). Much of our understanding of the psychological functions of neural oscillations comes from faster frequency bands measured with electroencephalogram (EEG) and magnetoencephalography (MEG) (e.g., theta, alpha, beta, and gamma), where oscillatory activity has been linked to perception, attention, and memory (Herbst & Landau, 2016; Wilckens et al., 2018). At the opposite end, very slow biological rhythms such as circadian and circannual cycles are typically studied in relation to physiological regulation (like arousal) rather than moment-to-moment neural processing.

Between these two well-characterized domains lies infra-slow oscillatory activity (ISO, 0.01–0.5 Hz), a frequency range that is slow enough to support long-range temporal integration, yet fast enough to remain embedded within ongoing neural dynamics (see Figure 1). Despite being a dominant component of functional magnetic resonance imaging (fMRI) and electrophysiological signals, the functional and organizational significance of ISO remains poorly understood. This conceptual gap has attracted growing attention in recent years (Gutierrez-Barragan et al., 2022; Hiltunen et al., 2014; Mitra et al., 2018), raising a fundamental question: how infra-slow dynamics contribute to the temporal organization of brain activity across cognitive states and the human lifespan.

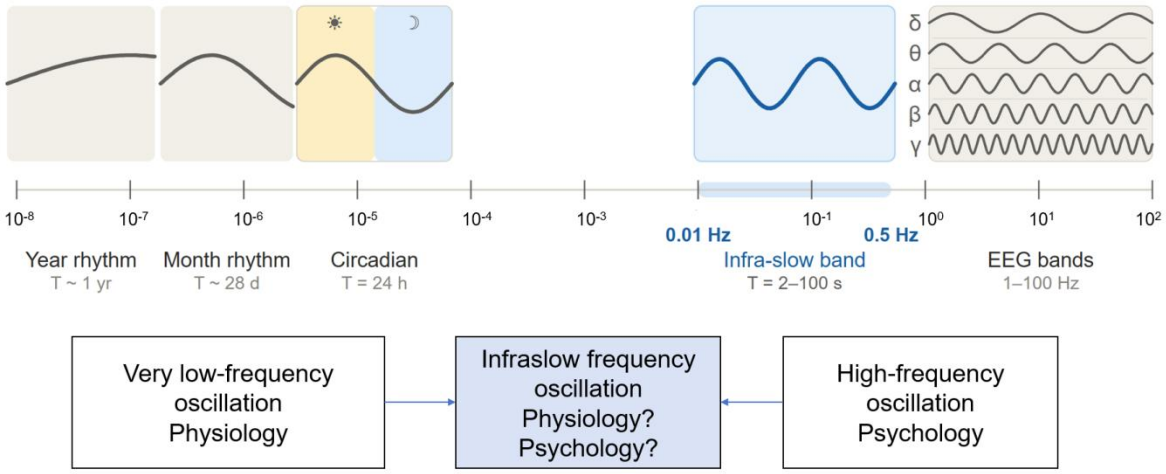

Figure 1. Infra-slow frequency oscillation within the hierarchy of biological and neural timescales.

Despite this growing interest, we still lack a unified framework that explains how infra-slow dynamics are organized, what constrains them, and why they matter for cognition and development (e.g. see Biswal and Uddin, 2025). Infra-slow dynamics were historically treated as nuisance fluctuations or physiological noise, yet accumulating evidence indicates that they may carry structured information about brain state, forming an underlying basis that has been metaphorically described as the brain's "dark energy" (Gong & Zuo, 2025; Raichle, 2006). The central challenge, therefore, is to move beyond revealing the presence of infra-slow fluctuations and to identify the organization principles that make them mechanistically interpretable and behaviorally relevant. Therefore, the goal of this thesis is to conceptualize ISO as structured spatiotemporal brain dynamics, which is constrained by intrinsic neural timescale (INT) and scale-free temporal organization, and to examine how ISO relates to cognitive variability during sustained attention as well as to systematic reorganization across the adult lifespan.

1.2 Literature review

1.2.1 The ubiquitous infra-slow oscillation

ISO generally refers to slow fluctuations in the 0.01–0.5 Hz range, with cycles lasting from a few seconds to several minutes. These fluctuations are not necessarily regular or sinusoidal. Their amplitude and cycle duration can vary over time, and the resulting dynamics are often better described as quasi-periodic. Thus, ISO does not require a perfectly repeating waveform. What matters here is that the signal retains an identifiable phase structure, allowing different points of the cycle, such as peaks, troughs, rising periods, and falling periods, to be distinguished. Treating ISO in this way also makes it possible to examine whether different phases of the slow fluctuation are associated with different neural states (Maris et al., 2016; Walters et al., 2007).

A notable feature of ISO is their broad generality across conditions and modalities. Aladjalova was among the first to record infra-slow oscillations from spontaneous cortical potentials in rabbits (Aladjalova, 1957). Subsequently, infra-slow oscillations have been observed in cortical electrical activity across multiple species, including cats (Norton & Jewett, 1965), rats (Penttonen et al., 1999), monkeys (Leopold et al., 2003), and human (Ko et al., 2011). Single-electrode recording studies further showed that neuronal firing in the thalamus of monkeys and rats, as well as in the basal ganglia of rats, contains prominent infra-slow oscillatory components (Albrecht & Gabriel, 1994; Ruskin et al., 1999; Werner & Mountcastle, 1963). ISO dynamics have been reported across diverse physiological and psychological states, including rest, task engagement, sleep, and mental disorders, and across multiple brain systems (e.g., cortex, thalamus, hippocampus, and midbrain) (Cooper et al., 2025; Dong et al., 2013; Kjaerby et al., 2025; C. Yang et al., 2023). Importantly, ISO is not confined to electrophysiology: converging evidence suggests that infra-slow dynamics are expressed in fMRI BOLD activity (usually 0.01-0.1 Hz) and are mirrored by slow behavioral fluctuations during sustained performance and cognitive aging, such as reaction-time variability and detection stability (Grady & Garrett, 2018; Y. Wang et al., 2018; H. Zhang et al., 2015). Taken together, these cross-modal observations support the view that ISO may index slowly evolving internal states, for instance, changes in arousal or vigilance that simultaneously shape large-

scale neural activity and moment-to-moment behavior (Liu & Falahpour, 2020; Wong et al., 2013).

Beyond their ubiquity, ISO exhibits systematic spatiotemporal organization. Spatially, infra-slow dynamics are not uniform across the cortex: both local activity and inter-regional interactions show region- and network-specific patterns in infra-slow power, phase relationships, and travelling waves (Bolt et al., 2022; Raut et al., 2021). Temporally, ISO dynamics can also be frequency-structured within the infra-slow range, suggesting that different infra-slow components may reflect partially distinct modes of large-scale coordination rather than a single undifferentiated fluctuation (Gong & Zuo, 2025; Yu et al., 2025). However, the relative contributions of such frequency sources and how they interact to produce coherent macro-scale infra-slow organization remain actively debated. This motivates a central question that guides the present thesis: the key issue is not whether ISO exists, but what organizational principles constrain their dynamics and make them functionally meaningful.

1.2.2 The neural substrate of ISO

1.2.2.1 Subcortical hubs supporting infra-slow dynamics

A growing body of work suggests that infra-slow oscillations are supported by subcortical hub systems that interact with cortical dynamics through widespread broadcast pathways. A useful distinction is between structures that can sustain infra-slow rhythmicity locally and systems that modulate its large-scale expression (e.g., amplitude, coherence, and phase coordination). Within this framework, the thalamus and basal forebrain (BF) have emerged as prominent candidates because they combine intrinsic slow processes with anatomically diffuse projections capable of shaping cortex-wide brain states (Hughes et al., 2011; Kropotov, 2022; Xie et al., 2025).

In the thalamus, relay nuclei can exhibit infra-slow rhythmicity even in isolated preparations, indicating that these dynamics can arise from local cellular and circuit mechanisms and do not strictly depend on intact corticothalamic loops (Lőrincz et al., 2009). Moreover, thalamic infra-slow activity can persist when fast ionotropic glutamatergic transmission is blocked, suggesting that ISO does not depend exclusively on fast excitatory

synaptic transmission and may instead involve slower cellular, synaptic, and extrasynaptic mechanisms, including metabotropic signaling and volume transmission (S. W. Hughes et al., 2011). Proposed mechanisms include gradual ionic concentration shifts and slow neuron–glia signaling. In particular, infra-slow glial Ca^{2+} events may promote ATP release, which is subsequently converted to adenosine. Activation of adenosine A1 receptors on thalamocortical neurons opens inwardly rectifying K^{+} channels and produces prolonged hyperpolarization, providing a potential mechanism through which glial metabolic and purinergic signaling can modulate neuronal excitability over tens of seconds to minutes (Lőrincz et al., 2009; Watson, 2018). Consistent with this view, astrocytes show spontaneous Ca^{2+} oscillations and propagating Ca^{2+} waves at infra-slow timescales, which may modulate neuronal excitability through gliotransmission (Kuga et al., 2011; Kuroda et al., 2023), and relates to BOLD activity (Schwalm et al., 2017). Given the thalamus' central position in thalamocortical coordination, these properties provide a plausible route by which infra-slow phase structure could be broadcast and stabilized across large-scale cortical networks (Neske, 2016).

Complementing thalamic contributions, the BF may shape infra-slow dynamics through its widespread cholinergic and modulatory projections (Kropotov, 2022). In non-human primates, Turchi et al. (2018) reversibly inactivated subregions of the nucleus basalis of Meynert (NBM) by local microinfusion of the GABA receptor agonist muscimol. This manipulation produced a pronounced reduction in spontaneous cortical fMRI fluctuations, particularly at frequencies below 0.05 Hz, with the strongest effects in cortical regions receiving direct projections from the inactivated NBM subregion. These findings provide causal evidence that basal-forebrain input contributes to the expression of large-scale infra-slow fluctuations (Turchi et al., 2018). Clinically, this perspective aligns with observations that disorders involving BF degeneration are often accompanied by disrupted slow network dynamics and impaired vigilance regulation (Teipel et al., 2005). More recently, resting-state fMRI in individuals across the Alzheimer's disease (AD) pathological spectrum showed that fractional amplitude of low-frequency fluctuations (fALFF) within the NBM decreased with increasing AD-related pathology, and baseline NBM activity predicted subsequent functional degeneration of the entorhinal cortex (Mieling et al., 2023). These human findings suggest that

compromise of the basal forebrain cholinergic system is accompanied by altered low-frequency spontaneous activity, although they do not yet establish that cortical ISO alterations in AD are caused specifically by NBM degeneration.

Together, the thalamus and BF provide a plausible anatomical and mechanistic substrate for ISO generation and propagation, in which slow glial, metabolic, and neuromodulatory processes impose long intrinsic timescales on neuronal excitability and, through broad projection systems, coordinate large-scale brain states relevant to arousal and attention (Raut et al., 2021).

1.2.2.2 Neurotransmitter modulation of ISO

ISO is shaped not only by local cellular substrates but also by brain-wide neuromodulatory systems that gate the emergence of infra-slow dynamics. At the circuit level, recurrent glutamatergic networks interacting with astrocytes provide a structural and dynamical basis for ISO generation by introducing long effective time constants through slow synaptic and cellular mechanisms. For example, glutamatergic granule cells in the dentate gyrus express a population ISO (~0.01–0.03 Hz) during cyclic non-rapid eye movement (NREM) sleep, supported by N-methyl-D-aspartate (NMDA) and metabotropic glutamate receptors, together with slow after-hyperpolarizing currents that enable sustained depolarizations and gradual state transitions (Neske, 2016; Pirttimaki et al., 2017; Turi et al., 2025).

Beyond these local mechanisms, monoaminergic systems appear to gate ISO-linked substates by biasing processing modes and regulating vigilance. During phases of decreasing serotonin levels, hippocampal sharp-wave ripples and other memory-related events occur more frequently. In contrast, increasing serotonin levels are associated with elevated arousal, including reduced EEG coherence and increased motor activity (Cooper et al., 2025). In addition, disruption of serotonergic signaling or selective blockade of 5-hydroxytryptamine 1A (5-HT1A) receptors abolishes dentate gyrus ISO and impairs memory consolidation (Turi et al., 2025). These findings suggest that serotonin functions as a slow neuromodulatory signal that biases the brain toward internal processing or toward responsiveness to the external environment. In parallel, the locus coeruleus–norepinephrine (LC–NE) system provides a

prominent brain-wide infra-slow modulation of excitability, synchrony, and vigilance (C. Tong et al., 2025). LC firing exhibits robust ISO (~0.02 Hz) that organize NREM substates (e.g., sensory insulation versus arousal), and related infra-slow fluctuations extend into wakefulness, tracking pupil-linked attentional dynamics and large-scale network reconfiguration (Kjaerby et al., 2025). Collective evidence further indicates phase coupling between LC activity and cortical ISO during goal-directed behavior (Xiang et al., 2023; Yellin et al., 2015)

In contrast, dopamine is less likely to function as an ISO pacemaker. Instead, dopaminergic signaling may regulate the stability, gain, and plasticity of slow network dynamics. Computational work implicates D1-dependent plasticity in minute-scale fluctuations, and empirical studies suggest that dopamine depletion can promote exaggerated low-frequency oscillations, whereas increasing dopaminergic tone (e.g., levodopa (L-DOPA)) tends to normalize infra-slow activity and reduce pathological hypersynchrony (Kobayashi et al., 2017; Walters et al., 2007). Clinical evidence supports this regulatory role: patients with Parkinson's disease, a condition characterized by dopamine deficiency, exhibit abnormally high-amplitude low-frequency (<0.1 Hz) oscillations in EEG and fMRI when off medication, and L-DOPA administration reduces and normalizes these ISOs (Kwak et al., 2012). Relatedly, dopamine-deficient states are associated with excessive slow-wave synchronization and altered resting-state connectivity across cortical networks (Spoa et al., 2025). Together, these findings suggest that dopamine stabilizes slow network dynamics, limiting pathological over-synchronization while supporting flexible and adaptive network states.

Direct causal evidence for a subcortical origin of ISO in humans remains limited, because selective perturbation of deep neuromodulatory nuclei is generally not feasible in human studies. Nevertheless, pharmacological neuroimaging provides indirect support for the involvement of these systems in shaping infra-slow BOLD dynamics. For example, serotonergic manipulation with the selective serotonin reuptake inhibitor citalopram alters resting-state functional connectivity in healthy individuals, including reduced amygdala–prefrontal connectivity and dose-dependent changes in default-mode network connectivity as a function of serotonin-transporter occupancy (McCabe & Mishor, 2011; Schrantee et al., 2018). Cholinergic modulation also affects low-frequency BOLD activity: in patients with

Alzheimer's disease, treatment with the acetylcholinesterase inhibitor donepezil produces regional changes in the amplitude of low-frequency fluctuation (ALFF), some of which are associated with cognitive improvement (H. Yang et al., 2021). These human pharmacological findings therefore support a modulatory role of serotonergic and cholinergic systems in low-frequency brain dynamics, although they do not demonstrate that any single subcortical structure acts as a unique generator of human ISO.

In summary, ISO reflects a multilevel organizing principle emerging from interactions between intrinsic circuit mechanisms and global neuromodulatory control. Despite substantial progress in identifying cellular, glial, and neuromodulatory mechanisms capable of generating and shaping infra-slow dynamics, much of the evidence derives from animal models or invasive preparations. In humans, where direct access to these mechanisms is limited, the central challenge is therefore not to establish the existence of infra-slow activity, but to develop clear methods that link it to cognition and behavior at the macroscale. At the same time, this sensitivity has placed infra-slow BOLD dynamics at the center of longstanding debates about physiological noise versus neural relevance, motivating explicit tests of their behavioral significance.

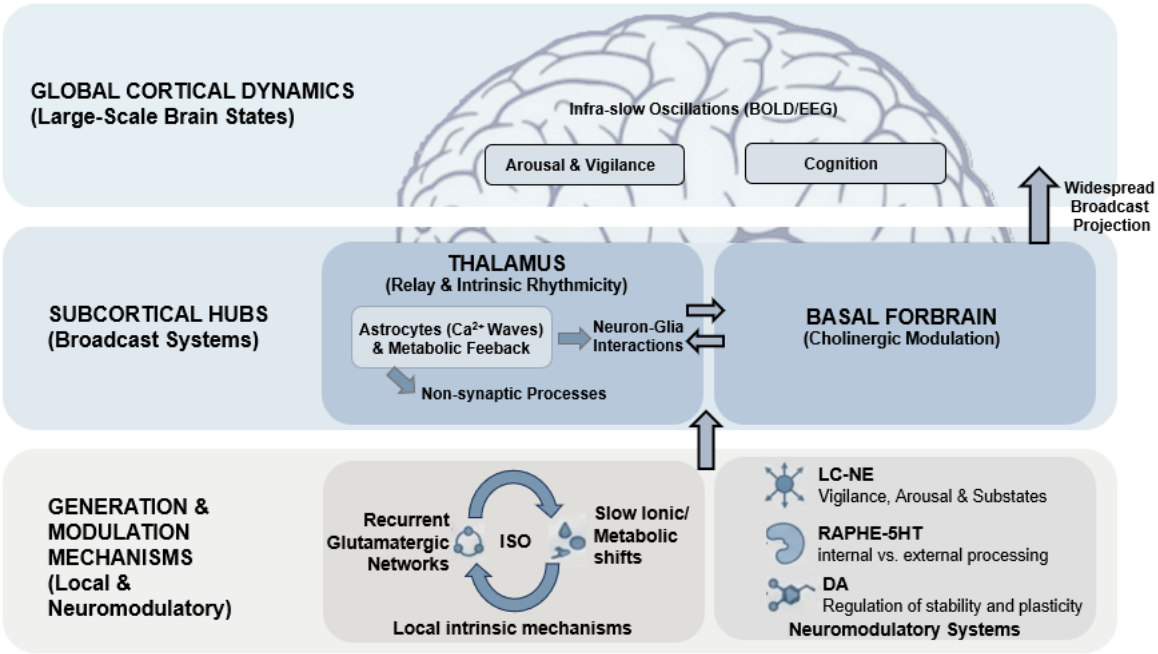

Figure 2. Multilevel mechanisms underlying Infra-slow neural oscillation (ISO): ISO arises from

interactions across hierarchical levels. Local cellular processes (e.g., glutamatergic circuits, neuron–glia interactions, and slow ionic/metabolic dynamics) support their generation, while subcortical hubs such as the thalamus and basal forebrain integrate and broadcast these signals. Neuromodulatory systems (locus coeruleus-norepinephrine, raphe–5HT, dopamine) further regulate their expression, enabling ISO to shape large-scale cortical dynamics related to arousal, vigilance, and cognition.

1.2.3 Behavioral relevance of ISO

Accumulating evidence suggests that ISO is behaviorally relevant, yet their functional contribution differs from that of classical fast rhythms. Because ISO unfolds over seconds to minutes, they are unlikely to index moment-to-moment cognitive operations directly; instead, they appear to modulate the global efficiency and stability of cognition by shaping cortical excitability, neurovascular responsiveness, and large-scale communication routes over extended timescales (Buzsáki, 2006; Wolff et al., 2022). Electrophysiological studies have proposed that slower oscillations preferentially support coordination across distributed regions, whereas faster oscillations are more strongly associated with local processing (Von Stein & Sarnthein, 2000). However, this relationship is not absolute, as high-frequency activity can also synchronize across widely separated cortical sites (Dickey et al., 2022). This hypothesis can be directly tested by examining whether frequency-resolved functional coupling decays with anatomical distance at different rates, with a steeper distance-dependent decay at higher frequencies providing support for the proposed frequency–distance relationship. In fMRI, multiple BOLD-derived metrics, including functional connectivity (FC), regional homogeneity, and low-frequency amplitude measures, show band-limited characteristics, and several studies report frequency-specific associations with network topology, clinical alterations, and behavioral performance, implying that distinct infra-slow ranges may support different functions rather than reflecting undifferentiated “noise” (Grady & Garrett, 2018; Luo et al., 2015; Y. Wang, Zou, et al., 2020; X.-N. Zuo et al., 2010). For example, Achard et al. (2006) showed that resting-state functional networks exhibit a small-world topology, characterized by high local clustering together with short average path lengths, thereby supporting both local segregation and efficient global integration—most prominently within the 0.03–0.06 Hz range (Achard et al., 2006). Likewise, pre-stimulus infra-slow BOLD fluctuations have been reported to predict near-threshold perception, consistent with a gating role of ongoing ISO dynamics on

conscious access and performance variability (Northoff, 2017).

Beyond frequency, ISO amplitude (ALFF) and brain signal variability (BSV) have been associated with cognitive performance across several domains. For example, BOLD variability has been related to accuracy and reaction time during perceptual processing, accuracy and reaction time during spatial working memory, and mean and trial-to-trial variability of reaction time during face recognition (Gao et al., 2018; Guitart-Masip et al., 2016; Y. Wang et al., 2018). These findings complement conventional activation-centric approaches, which primarily characterize cognition in terms of condition-averaged changes in mean BOLD amplitude, by showing that moment-to-moment signal variability can provide additional and partly independent information about cognitive performance (Lewis et al., 2016). Under frequency-tagging paradigms, periodically presented stimuli (e.g., 0.1 Hz) can induce a steady-state brain response at the tagged frequency while redistributing infra-slow power, typically suppressing power below the task frequency and enhancing power at the task frequency (Y. Wang et al., 2018; Y.-F. Wang et al., 2014, 2016). Together, these results indicate that ISO signatures reflect an interaction between intrinsic activity, neurovascular dynamics, externally imposed temporal structure, and reorganization in different states like aging.

However, much of this existing literature operationalizes ISO using static or single-aspect features (fixed band-pass filtering, time-averaged amplitude summaries, or phase examined in isolation) which may be insufficient to capture a defining property of ISO: slow, structured, and state-dependent dynamics. Time-resolved analyses of ISO phase synchronization and dynamic phase-locking reveal that large-scale coupling strength fluctuates rhythmically at very low frequencies, consistent with ongoing formation and dissolution of functional modules and shifting brain states (Gutierrez-Barragan et al., 2022; Maris et al., 2016; Omidvarnia et al., 2016). Moreover, the behavioral impact of stimulation or task onset can depend on the instantaneous ISO phase, and ISO-related coupling changes are often expressed along rising/falling segments rather than simply at peaks/troughs, suggesting a regulatory mechanism distinct from high-frequency oscillations (Huang et al., 2017; Monto et al., 2008). These observations motivate moving beyond static ISO descriptors toward integrative, time-resolved frameworks that jointly model frequency content, variability, and phase dynamics

within a unified spatiotemporal account, thereby better characterizing how ISO shapes behavioral variability and cognitive efficiency over extended timescales (Northoff, 2024).

1.2.4 Measurement of ISO in fMRI: from static to dynamic

While neurovascular contributions to the dynamics of BOLD signal cannot be excluded, the key methodological tension is not whether infra-slow BOLD oscillations contain physiological and vascular components but whether these fluctuations nonetheless exhibit reproducible spatiotemporal structure and systematic relationships that are more consistent with a meaningful neural-dynamical structure than with unconstrained noise (Das et al., 2021; Uddin, 2017, 2020). Accordingly, this thesis does not aim to prove that infra-slow BOLD activity is 100% free of non-neural influences. Instead, it treats physiological contamination as a realistic boundary condition and asks a more tractable question: do infra-slow BOLD signals obey quantifiable constraints in time and space, and do they show cross-state and cross-individual regularities that are consistent with stable neural dynamics?

An important methodological challenge is that neural and physiological contributions to infra-slow BOLD fluctuations cannot be distinguished by frequency alone. Although the fundamental respiratory rhythm (~0.2–0.3 Hz) generally lies above the conventional 0.01–0.1 Hz BOLD range, slower breath-to-breath variations in respiratory depth and rate, together with associated changes in end-tidal CO_2, can generate BOLD fluctuations below 0.1 Hz (Birn et al., 2006; Chang et al., 2009). Similarly, cardiac pulsation itself occurs at a much higher frequency (~1 Hz), but slow fluctuations in cardiac rate and heart-rate variability also occur below 0.1 Hz and can therefore overlap directly with infra-slow BOLD activity (Chang et al., 2009; Shmueli et al., 2007). Consequently, band-pass filtering alone cannot fully separate neural from physiological components within the infra-slow range. More specific separation requires concurrent physiological recordings and model-based correction, including cardiac and respiratory phase regressors, respiratory-volume and cardiac-rate response functions, or peripheral hemodynamic measurements and time-delay mapping (Glover et al., 2000; Y. Tong et al., 2019). Neural and systemic low-frequency signals can also differ in their spatiotemporal properties: neural fluctuations tend to be regionally organized, whereas systemic hemodynamic fluctuations can propagate through the brain with blood-flow-related delays (Y. Tong et al.,

2019). Thus, the present thesis does not assume that BOLD fluctuations within 0.01–0.1 Hz are exclusively neural, but instead treats them as a mixed signal whose neural interpretation requires converging spatial, temporal, behavioral, and physiological evidence.

As mentioned above, much of the existing fMRI literature has approached infra-slow BOLD fluctuations indirectly, through analytical frameworks that emphasize static/single summaries of brain organization. FC analyses typically characterize the average strength of inter-regional coupling over extended time windows (Van Den Heuvel & Hulshoff Pol, 2010), while general linear model (GLM)- or variability- based activation models focus on condition-averaged changes in signal amplitude (Lewis et al., 2016; Monti, 2011). Although extensions such as dynamic FC attempt to introduce temporal variability, these approaches often rely on sliding-window correlations that remain agnostic to the intrinsic time–frequency properties of infra-slow activity itself (Hutchison et al., 2013; Lurie et al., 2020). As a result, they are not designed to directly examine how infra-slow dynamics evolve across time, how variability is distributed across frequencies, or how such dynamics are constrained by underlying neural properties.

These approaches have been invaluable for characterizing large-scale organization, but they do not directly formalize the intrinsic temporal persistence and spectral allocation that define infra-slow dynamics. This motivates articulating a small set of system-level requirements that any structured ISO should satisfy. First, because cognition and behavior unfold over extended and heterogeneous timescales, neural activity must exhibit intrinsic temporal persistence that determines how long information is integrated or segregated over time (e.g. see Wolff et al., 2022). Such temporal persistence cannot be imposed solely by external task structure but must be an intrinsic property of the system itself (Northoff et al., 2020a). Second, because infra-slow dynamics coexist with faster neural processes, their organization must accommodate interactions across multiple timescales without privileging a single characteristic frequency, implying a background structure that governs how variability is distributed across the temporal spectrum. These requirements naturally map onto two complementary constraint dimensions: one in the time domain and one in the frequency domain (Figure 3).

In the time domain, infra-slow dynamics are biased by intrinsic neural timescales (INT, Figure 3) (Çatal et al., 2024; Çatal, Keskin, et al., 2025; Golesorkhi, Gomez-Pilar, Zilio, et al., 2021; Wolff et al., 2022; Wolman et al., 2023), which capture regional differences in temporal persistence and integration and therefore predict systematic variation in how infra-slow activity evolves across its phase cycle (Study 1). In the frequency domain, infra-slow activity is embedded within a spectral organization (scale-freeness, Figure 3) (He, 2011, 2014; He et al., 2010; Klar et al., 2023a, 2023b; Lin et al., 2016; Pei et al., 2023), which provides a background temporal feature that shapes how neural variability is distributed across frequencies and how it links to behavioral variability during sustained attention (Study 2). Finally, to assess whether these organizational principles generalize beyond short cognitive timescales, we examine their systematic reorganization across the adult lifespan, where ISO shows frequency-specific changes and reorganization consistent with spatiotemporal dedifferentiation (Study 3).

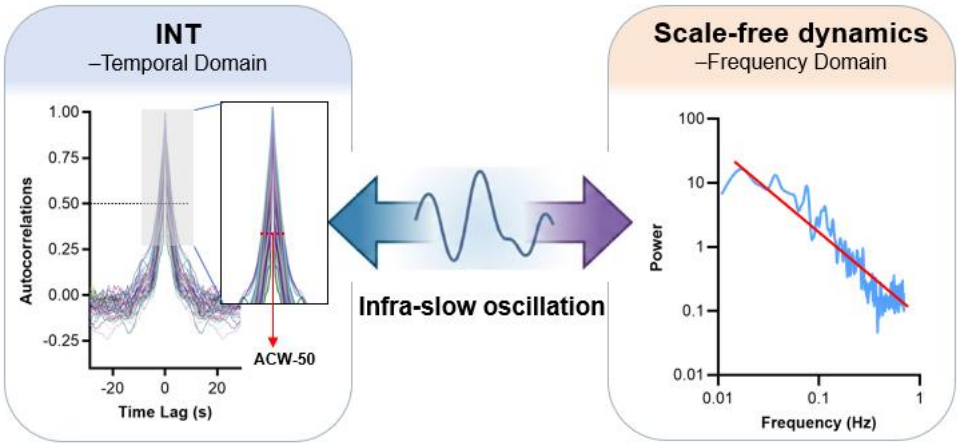

Figure 3. Two complementary characterizations of infra-slow oscillation (ISO). In the temporal domain, ISO is characterized in relation to intrinsic neural timescales (INT), which in this thesis are operationalized using the autocorrelation window (ACW), defined as the first lag at which the autocorrelation reaches zero. In the frequency domain, ISO manifests as scale-free (1/f-like) dynamics, captured by the power spectral density and its log–log slope across low frequencies.

1.2.5 ISO in the Time-Domain—Intrinsic Neural Timescales

Intrinsic neural timescales (INT) refer to the characteristic temporal persistence of neural activity, that is, the duration over which a neural system's current activity remains statistically dependent on its recent past. A longer INT indicates that activity changes more

slowly and information can be integrated over a longer temporal window, whereas a shorter INT reflects faster updating and a shorter window of temporal integration. INT is therefore a general dynamical property rather than a single anatomical or physiological mechanism, and it can be estimated using different time-series measures. In the present thesis, INT is operationalized using the autocorrelation window (ACW), which quantifies the decay of a signal's autocorrelation across successive time lags. Specifically, Study 1 defines ACW as the first lag at which the autocorrelation reaches zero within the 0.01–0.1 Hz BOLD signal. Thus, throughout this thesis, references to longer or shorter INT specifically refer to longer or shorter ACW unless otherwise stated (Golesorkhi, Gomez-Pilar, Tumati, et al., 2021; Golesorkhi, Gomez-Pilar, Zilio, et al., 2021) (see also Figure 3).

INT exhibit a reproducible cortical hierarchy, with shorter timescales in unimodal regions and longer timescales in transmodal association cortex (Golesorkhi, Gomez-Pilar, Tumati, et al., 2021). If infra-slow activity reflects an organized dynamics rather than unconstrained drift, then its evolution should be biased by this hierarchy (Raut et al., 2021). In other words, regions with longer temporal persistence should tend to express slower, more stable infra-slow progression, whereas regions with shorter persistence should exhibit faster updating. This framing treats infra-slow dynamics as embedded within a broader multi-timescale organization of ongoing brain activity.

Importantly, INT are not only biophysical descriptors but also show clear psychological relevance. Evidence suggests that longer INT support extended temporal integration in transmodal regions (e.g., default-mode and dorsolateral prefrontal cortex), linking neural temporal continuity to self-related bias and self-specific experience (Smith et al., 2022; Wolman et al., 2023). More recent cross-species work further indicates that INT track behavioral engagement in a state-dependent manner: in studies combining mouse calcium imaging during spontaneous behavior with human EEG across rest and task, behavioral states could be decoded from INT, and INT reliably lengthened during behavior relative to rest (Çatal et al., 2024). Further evidence shows that INT are positively associated with task-evoked responses (e.g., event-related fields), consistent with a shared biological substrate (intracortical excitatory and inhibitory connectivity) that links resting-state temporal dynamics to

responsiveness under external drive (Çatal, Keskin, et al., 2025). Clinical work also reports reduced INTs in major depressive disorder compared with healthy controls (Djimbouon et al., 2025). Collectively, these results are consistent with the view that INT are dynamically adjustable constraints that connect spontaneous neural continuity to psychologically meaningful state organization.

A related implication is that amplitude-based descriptors alone (e.g., band-limited power, ALFF) are insufficient for mechanistic interpretation (L. Yang et al., 2018). While amplitude captures "how much" infra-slow activity is present, it can conflate multiple generative influences (neural dynamics, vascular gain, global arousal) and is largely remained unclear to how the system moves through its oscillatory cycle (Kropotov, 2022). If infra-slow activity is meaningfully oscillatory or quasi-oscillatory, its defining feature is phase progression: different parts of the cycle (e.g., rising vs falling segments, peaks vs troughs) may correspond to distinct ISO dynamics and INT (Huang et al., 2017).

To quantify the speed of this progression, one can use phase-derived measures such as the temporal derivative of instantaneous phase (i.e., instantaneous frequency, sometimes implemented via frequency sliding) (Cohen, 2014; Hua et al., 2022). This phase-velocity perspective provides a natural bridge to INT: temporal persistence should predict how rapidly a region moves through infra-slow phase space, linking a time-domain constraint (INT) to a dynamic descriptor of infra-slow evolution. Accordingly, a central mechanistic question is whether infra-slow dynamics show phase-structured evolution and whether the rate of phase progression is systematically constrained by regional INT. This question will be investigated in study 1.

1.2.6 ISO in the Frequency-Domain—Scale-Free Dynamics

Neural signals typically exhibit an approximately 1/f-like spectral profile, reflecting a scale-free allocation of energy across frequencies (He, 2014; He et al., 2010) (Figure 3). This background organization is often summarized by the power-law exponent (PLE), which captures the steepness of the spectral decay (Klar et al., 2023a, 2023b). In general, a larger PLE indicates a steeper spectrum with relatively stronger low-frequency contributions and longer

INT, whereas a smaller PLE indicates a flatter spectrum with relatively stronger high-frequency contributions and shorter INT (Frelih et al., 2025; Rosenblum et al., 2022). Importantly, PLE is not simply "how much power" a signal contains; rather, it is a structural parameter describing how slow and fast components are balanced in the background spectrum, and it has been linked to differences in temporal dependency and persistence.

Like INT, PLE exhibits systematic spatial heterogeneity. Transmodal association systems (e.g., default-mode and frontoparietal networks) tend to show steeper aperiodic slopes than unimodal sensory–motor regions, consistent with the idea that higher-order systems integrate information over longer temporal windows, whereas early sensory systems benefit from rapid updating to track a changing environment (Klar et al., 2023b). From this perspective, scale-free spectral organization can be viewed as a background constraint that shapes the temporal feature of different brain systems, effectively defining the spectral context within which slower oscillations and variability unfold.

Across tasks, behavioral domains, and clinical states, evidence suggests that PLE modulates the temporal context in which neural information is integrated and expressed. During cognitively demanding tasks the PLE becomes shallower, implying shortened temporal memory and more efficient information processing, and the exponent varies across network correlating with regional metabolic rates (He, 2014; He et al., 2010). Behaviorally, resting-state scale-free dynamics predict performance only on tasks requiring controlled attention (Pei et al., 2023); individuals with steeper exponents show faster reaction times (Euler et al., 2024), consciousness state (Klar et al., 2023a). And in sensory discrimination tasks, better performance occurs when alpha-band amplitudes exhibit long-range correlations while slow cortical potentials show reduced autocorrelation (Lin et al., 2016). Clinical and pharmacological data further underscore the functional relevance of PLE: a steeper slope accompanies synchronized firing and enhanced inhibitory tone, whereas flatter slopes, observed in major depressive disorder or following serotonergic medication, suggest heightened excitation and noisier neural backgrounds (Rosenblum et al., 2022). Agents that alter arousal or excitatory–inhibitory balance, such as propofol anesthesia, reliably shift the PLE (Klar et al., 2023a; Woods et al., 2024). Because these aperiodic changes can mimic

oscillatory power variations, recent work recommends parameterizing and interpreting PLE separately from rhythmic components (Frelih et al., 2025). Collectively, these findings position PLE as an index of power distribution of neural activity and excitation–inhibition balance, linking ISO to behavioral variability and cognitive function.

Despite this growing literature, an important question is how the spectral organization captured by PLE relates to other measures of neural variability. These measures are related but not mutually exclusive or interchangeable. Standard deviation (SD) quantifies the overall magnitude of temporal fluctuations, whereas sample entropy (SE) characterizes their temporal irregularity or predictability. In contrast, PLE characterizes how signal variance is distributed across frequencies by quantifying the slope of the scale-free power spectrum. Because total time-domain variance is mathematically related to integrated spectral power, PLE and variability measures are not fully independent; however, they are also not redundant, because signals with similar overall variance can differ in their spectral slopes, and signals with similar PLE can differ substantially in fluctuation magnitude. Thus, PLE is treated here as a descriptor of the spectral organization within which neural variability is expressed, rather than as an alternative measure of variability. Study 2 therefore asks whether this spectral organization provides information beyond variability magnitude and complexity and statistically conditions their relationship with behavioral variability (Ao et al., 2025).

1.2.7 ISO across the Lifespan—Spatiotemporal Dedifferentiation

Brain aging is associated with widespread changes in cognition and large-scale neural organization. In the text above, we developed the mechanistic framework that treats ISO as structured dynamics constrained by scale-free spectral organization (how variability is distributed across frequencies). A natural next question is whether this constraint remains stable when the brain is challenged at a much broader timescale—the adult lifespan. In this sense, aging functions as a stress test for the ISO framework: if ISO dynamics reflect genuine organizational principles rather than idiosyncratic drift, then age-related changes of ISO should follow interpretable reorganization in the brain's infra-slow spatiotemporal structure.

A central organizing idea in cognitive aging is dedifferentiation: with increasing age,

neural activity and large-scale network organization become less functionally specific and more broadly shared across regions and systems (Koen & Rugg, 2019). In macroscopic neuroimaging terms, dedifferentiation is most consistently expressed as a shift from a segregated architecture—where networks maintain distinct internal coherence and relatively selective coupling—to a more integrated/common-mode architecture characterized by blurred network boundaries and more homogeneous interactions (Sala-Llonch et al., 2015). This phenomenon has been documented across both resting-state and task contexts and is often interpreted as reflecting reduced selectivity in large-scale coordination, potentially driven by changes in neuromodulatory control, excitation–inhibition regulation, vascular and metabolic constraints, and altered state regulation in late adulthood (C. Hughes et al., 2020). fMRI research has shown that within-network FCs decrease with age, while between-network FCs increase, resulting in more homogeneous connectivity patterns across the entire brain (Damoiseaux, 2017; Malagurski et al., 2020). However, existing evidence has primarily been framed in spatial and connectivity terms, leaving open a critical gap for infra-slow dynamics: does dedifferentiation also manifest in the temporal organization of large-scale fluctuations, particularly in the ISO where global state regulation is most pronounced (Ao et al., 2021)?

If aging reduces the selectivity of large-scale control mechanisms, the consequences should extend beyond where activity is expressed to how it is organized across timescales (Figure 4). Infra-slow fMRI dynamics are frequency-structured and scale-free rather than homogeneous (X.-N. Zuo et al., 2010); distinct infra-slow components can support partially distinct modes of global coordination. Prior work, including our own, suggests that aging is accompanied by systematic changes in the spectral distribution of BOLD variability and in scale-free features of the power spectrum, consistent with altered temporal organization (Ao et al., 2022). What remains unresolved is whether such temporal changes constitute a coherent systems-level phenotype of dedifferentiation, namely, a convergence toward less differentiated global dynamics both across regions/networks (spatial dedifferentiation) and across infra-slow components (temporal/frequency dedifferentiation), which defines the key question of Study 3.

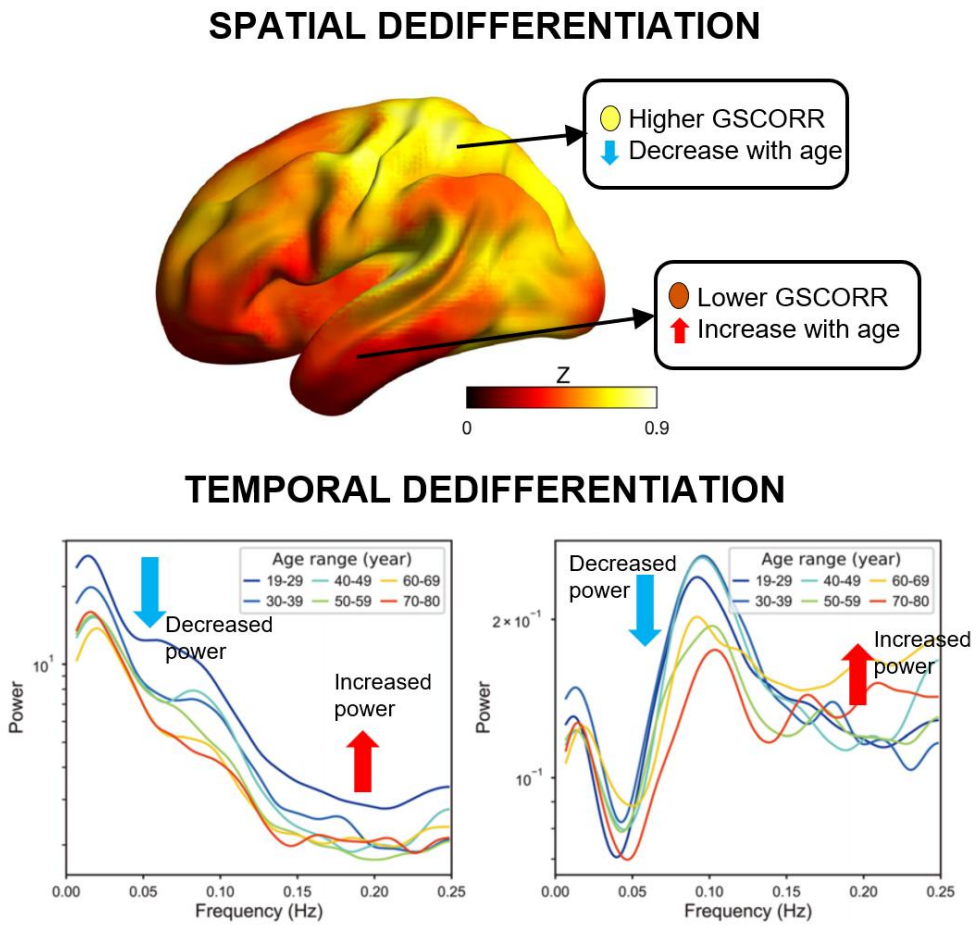

Figure 4. Spatiotemporal dedifferentiation of infra-slow oscillation (ISO) across the adult lifespan. **Top:** Spatial dedifferentiation illustrated by a more homogeneous ISO-related cortical pattern with age—regions showing higher global signal connectivity (GSCORR) values tend to decrease, whereas lower-value regions tend to increase, consistent with reduced regional/network specificity (adapted from Ao et al., 2021). **Bottom:** Temporal (frequency) dedifferentiation shown as an age-related redistribution of infra-slow power, with decreased power in some low-frequency components and increased power in others, indicating altered scale-free spectral organization (adapted from Ao et al., 2022).

1.3 Study Summary

Figure 5 provides a schematic roadmap of the three studies; the following sections describe each study in detail.

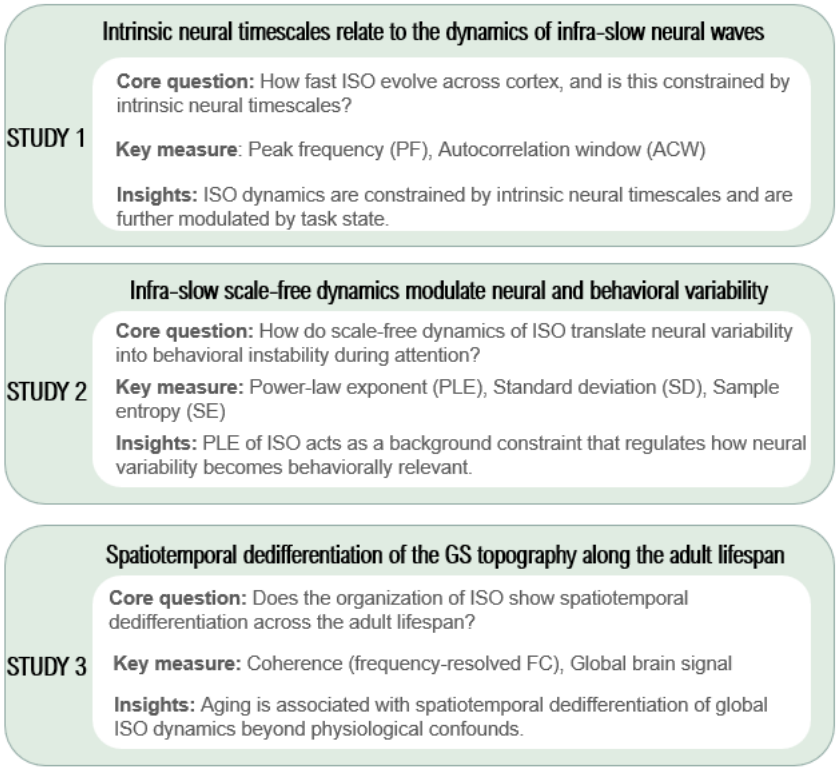

Figure 5. Overview of the three studies and their core questions, measures, and main insights.

1.3.1 Study 1 Summary — Intrinsic neural timescales relate to the dynamics of infra-slow neural waves (Ao et al., 2024)

1.3.1.1 Background

ISO in fMRI were long treated as drift or peripheral physiology. Accumulating evidence suggests, however, that ISO forms a structured spatiotemporal feature, showing reproducible cortical organization and coordinated large-scale dynamics rather than undifferentiated fluctuations (X.-N. Zuo et al., 2010). A central signature of ISO is its wave-like character: the phase of ongoing infra-slow activity (peak, trough, rise, fall) is associated with distinct patterns of activation and coactivation, suggesting that different phase components may correspond to different functional "modes" of global brain organization (Gutierrez-Barragan et al., 2019; Huang et al., 2017; Y. Wang, Huang, et al., 2019). Yet, most fMRI work has emphasized phase-dependent states rather than the dynamics of the wave specifically, whether the speed of infra-slow phase evolution differs across phase components and how such differences map onto cortical topography.

In parallel, neural activity is organized by INT, often quantified by the ACW. ACW exhibits a reproducible cortical hierarchy, with shorter timescales in unimodal regions and longer timescales in transmodal systems (Golesorkhi, Gomez-Pilar, Tumati, et al., 2021). This raises a fundamental cross-scale question: do regions with longer INT also show systematically different dynamics of ongoing wave activity? In EEG/MEG, wave speed can be operationalized using frequency sliding to estimate peak frequency (PF), the instantaneous rate of phase change, and PF has been linked to temporal integration/segregation and task performance (Cohen, 2014; Hua et al., 2022). Whether an analogous coupling between PF and INT exists in the infra-slow fMRI domain remains unresolved. This study therefore asks whether infra-slow waves exhibit structured variation in their instantaneous speed across phases, and whether such dynamics are constrained by INT. Regions with longer INT may favor slower, more stable infra-slow evolution, whereas regions with shorter INT may support faster phase progression.

1.3.1.2 Aim

1. Characterize the Phase Dynamics of ISO: To investigate the dynamic properties of infra-slow (0.01–0.1 Hz) neural waves, specifically mapping how their phase velocity (peak frequency, PF) varies across different cycles (e.g., peak/trough vs. rise/fall) and identifying their topographical distribution across brain regions.

2. Establish the Link Between speed of ISO and INT: To determine if a systematic relationship exists between phase velocity (PF) and the brain's temporal processing windows (measured by ACW), testing the hypothesis that slower phase dynamics correlate with longer INT.

3. Evaluate Rest-Task Modulation of PF and INT: To analyze how these wave dynamics and their relationship with INT are modulated during naturalistic tasks (e.g., movie watching), and to verify if the negative correlation between phase velocity and neural timescales remains stable across different brain states.

1.3.1.3 Hypothesis

1. Infra-slow wave speed is phase-structured: PF will not be constant across the infra-slow cycle. Instead, PF will systematically differ between phase components (e.g.,

peak/trough vs. rise/fall), indicating that ISO dynamics are organized within the oscillatory cycle rather than being a uniform fluctuation.

2. Infra-slow dynamics are constrained by INT: Across regions, PF will relate to INT/ACW such that longer intrinsic timescales are associated with slower infra-slow progression (lower PF), consistent with stronger temporal integration producing more persistent infra-slow states.

3. Task modulates infra-slow dynamics but preserves the core ISO–INT constraint: Movie watching will shift the expression of infra-slow dynamics (e.g., altering PF topography or the strength of phase-dependence), but the coupling between PF and INT will remain detectable, supporting the view that ISO dynamics are anchored by stable intrinsic constraints rather than being state-specific artifacts.

1.3.2 Study 2 Summary — Infra-slow scale-free dynamics modulate the connection of neural and behavioral variability during attention (Ao et al., 2025)

1.3.2.1 Background

If ISO is structured spatiotemporal dynamics, their functional relevance should be expressed not only in mean brain activity but also in how they organize neural variability. This is particularly important for cognition such as sustained attention, which is better characterized by ISO than by stable performance levels. In everyday behavior, attention waxes and wanes, and reaction-time variability often provides a more sensitive index of attentional stability than mean reaction time or accuracy.

A key candidate mechanism for linking ISO organization to variability is the PLE, which characterizes the scale-free temporal structure and long-range temporal dependencies of infra-slow activity. Such scale-free organization may reflect constraints imposed by recurrent circuit dynamics and network-level interactions. Furthermore, neural signals can differ not only in the magnitude of their fluctuations (standard deviation, SD) and the degree of temporal irregularity or complexity (sample entropy, SE), but also in how variability is structured across time even when mean activity is comparable. Therefore, scale-free dynamics can be viewed as a background property that regulates both how strongly variability is expressed (SD) and how

temporally organized that irregularity is (SE).

Although SD, SE, and PLE are often treated as parallel descriptors, they may instead reflect distinct layers of a common dynamical system. In particular, scale-free dynamics may serve as a higher-order constraint that shapes how variability and complexity emerge and, crucially, how they become behaviorally relevant. This framing is especially suited to ISO, which unfolds over long timescales where long-range temporal correlations and scale-free structure are most pronounced. On this basis, Study 2 treats scale-free infra-slow dynamics as a candidate mechanism linking ISO organization to cognitive stability.

1.3.2.2 Aim

1. Investigate Rest-Task Modulation of Infraslow Neural Dynamics: To analyze the spatial distribution and change patterns of three neural dynamic measures (SD, SE, and PLE) within the infra-slow range (0.01–0.1 Hz) across resting and task-based (GradCPT) states.

2. Establish the Connection Between Neural and Behavioral Dynamics: To examine how three measures in specific brain networks (BOLD signal) relate to fluctuations in behavioral performance (such as reaction time variability), revealing how infra-slow activity shapes the dynamic stability of cognitive performance.

3. Reveal the Mediating Role of Scale-Free Dynamics in Hierarchical Organization: To investigate how PLE (as a measure of background constraints) mediates the relationship between neural variability (SD) and complexity (SE), and how it regulates the translation of neural variability into behavioral variability.

1.3.2.3 Hypothesis

1. Rest-to-task changes will not be uniform across the brain: Task engagement will reconfigure across SD, SE, and PLE, but with partially distinct spatial profiles, suggesting that "variability," "complexity," and "scale-free organization" respond differently to attentional demands.

2. Neural variability and behavioral variability are linked, but through differentiated infra-slow features: SD and SE will relate to reaction-time variability,

reflecting that greater neural instability or altered complexity can translate into less stable behavioral output. However, these relationships will not be interchangeable across metrics; instead, each measure will capture a different facet of infra-slow dynamics that supports (or destabilizes) attentional performance.

3. Scale-free infra-slow dynamics provide a background constraint that shapes brain–behavior coupling: PLE will modulate or statistically mediate the relationship between neural variability measures (especially SD) and behavioral variability. Simulations will support the plausibility of this claim by showing that relationships among SD, SE, and behavioral variability are strongest consistent with scale-free dynamics (e.g., pink-noise-like structure), rather than in purely random or regular.

1.3.3 Study 3 Summary — Spatiotemporal dedifferentiation of the global brain signal topography along the adult lifespan (Ao et al., 2023)

1.3.3.1 Background

A central claim of the ISO framework is that infra-slow activity is not merely slow noise, but functional-relevant, and an organized spatiotemporal pattern that constrains large-scale brain states. If so, ISO organization should vary systematically under major biological transitions like aging, which alters neural integration, network specialization, and cognitive stability.

Prominent theories of cognitive aging emphasize dedifferentiation, where functional organization becomes less specialized and regional distinctions weaken. Much of the evidence comes from connectivity and task-evoked analyses, but these approaches often do not directly address a defining feature of infra-slow fMRI dynamics: coordinated fluctuations in global brain activity.

Critically, infra-slow dynamics are frequency-structured, yet prior work often treats global brain activity as broadband. This motivates a central question: does the spatial organization of global infra-slow dynamics become less differentiated across the adult lifespan, and is this reorganization frequency-dependent? In other words, aging may reduce both spatial specialization (regions becoming more similar) and temporal specialization (patterns becoming

more similar across infra-slow frequencies), a process we refer to as spatiotemporal dedifferentiation.

Finally, because aging also affects neurovascular coupling and physiological noise, Study 3 evaluates whether observed dedifferentiation reflects a principled reorganization of global infra-slow dynamics rather than non-neural confounds.

1.3.3.2 Aim

1. Investigating Age-Related correlation of Global Signal (GS) Topography: To analyze how the influence of global brain activity on local regions (GS topography) changes across the adult lifespan using a large-scale cross-sectional dataset.

2. Testing the "Spatiotemporal Dedifferentiation": To examine whether the global signal becomes more uniform across the brain in both spatial (reduced differentiation between regions) and temporal (reduced differentiation across frequency bands) dimensions during aging.

3. Identifying Influencing Physiological Factors: To evaluate the impact of neuro-vascular coupling and physiological noise (such as head motion and non-neuronal signals) on these age-related changes to determine the underlying biological basis of the observed dedifferentiation.

1.3.3.3 Hypothesis

1. Lifespan reorganization of GS topography: The GS topography (the correlation between the global signal and local brain regions) would undergo significant reorganization throughout the adult lifespan, moving away from the distinct spatial patterns observed in younger adults.

2. Spatiotemporal dedifferentiation with aging: Aging is characterized by "dedifferentiation," where the global signal's influence becomes more uniform across the brain. Spatially, this means a reduction in the variability of GS correlations between different regions; temporally, it means a reduction in the differentiation of GS topography across different infra-slow frequency bands.

3. Robustness beyond physiological confounds: While physiological factors (such as head motion and non-neuronal signals) might influence the results, the core pattern of spatiotemporal dedifferentiation in GS topography would remain significant even after rigorous control for these variables, suggesting a primary neural basis for the phenomenon.

2 STUDY 1: Intrinsic neural timescales relate to the dynamics of infraslow neural waves

Ao, Y., Catal, Y., Lechner, S., Hua, J., Northoff, G., 2024. Intrinsic neural timescales relate to the dynamics of infraslow neural waves. NeuroImage 285, 120482. https://doi.org/10.1016/j.neuroimage.2023.120482

ABSTRACT

The human brain is a highly dynamic organ that operates across a variety of timescales, the intrinsic neural timescales (INT). In addition to the INT, the neural waves featured by its phase-related processes including their cycles with peak/trough and rise/fall play a key role in shaping the brain's neural activity. However, the relationship between the brain's ongoing wave dynamics and INT remains yet unclear. In this study, we utilized functional magnetic resonance imaging (fMRI) rest and task data from the Human Connectome Project (HCP) to investigate the relationship of infraslow wave dynamics [as measured in terms of speed by changes in its peak frequency (PF)] with INT. Our findings reveal that: (i) the speed of phase dynamics (PF) is associated with distinct parts of the ongoing phase cycles, namely higher PF in peak/trough and lower PF in rise/fall; (ii) there exists a negative correlation between phase dynamics (PF) and INT such that slower PF relates to longer INT; (iii) exposure to a movie alters both PF and INT across the different phase cycles, yet their negative correlation remains intact. Collectively, our results demonstrate that INT relates to infraslow phase dynamics during both rest and task states.

Keywords: Functional magnetic resonance imaging; Intrinsic neural timescales; Infraslow neural waves; Temporal input processing

2.1 Introduction

Think about being a surfer. You are surfing on a rough ocean. An adept surfer needs to adjust her/his surfboard to the peak, trough, rise, and fall of the ocean's ongoing waves to maintain her/ his balance. This is because the shape and speed of the waves vary across its different part of ongoing phase cycles. Most importantly, the surfer has to adapt her/his movements to the ongoing dynamics of the ocean's wave, that is, especially its speed operating across different timescales (long, medium, short, etc.), in order to align and take advantage of the wave's power to propel the surfboard. Hence, the surfer is confronted with the rather challenging task of adapting her/his movements to the waves' ongoing phase dynamics while, at the same time, integrating the different timescales of the various waves.

Just like the ocean, the brain's neural activity is highly dynamic showing different waves which vary in their phases and timescales (Buzsáki & Draguhn, 2004; Golesorkhi, Gomez-Pilar, Zilio, et al., 2021; S. Palva & Palva, 2018; X.-N. Zuo et al., 2010). This is, for instance, manifest in the variation of its amplitude and its dynamic functional connectivity (FC), including so-called travelling waves, which speak to the spatial blood-oxygen-level-dependent (BOLD) propagation (Garrett et al., 2013; Gu et al., 2021; Raut et al., 2021; Shine et al., 2016). There is strong evidence that the dynamic FC is based on its underlying phases with their distinct positions or angles during the ongoing cycles of the infraslow neural waves, including the peaks, troughs, rises, and falls (Gutierrez-Barragan et al., 2019, 2022; Huang et al., 2017; Scheinost et al., 2016; J. Zhang et al., 2020). At the same time, the brain's neural waves operate on various timescales including shorter and longer ones, the so-called intrinsic neural timescales (INT) (Golesorkhi, Gomez-Pilar, Tumati, et al., 2021; Golesorkhi, Gomez-Pilar, Zilio, et al., 2021; Hasson et al., 2015; Himberger et al., 2018; Ito et al., 2020; Raut et al., 2020; Wolff et al., 2022; Yeshurun et al., 2021). How do the dynamics of the infraslow neural waves with their ongoing phase cycles relate to the INT? Like the surfer, the brain is confronted with the challenge of integrating and connecting the wave dynamics of its ongoing phase cycles with its various timescales, the INT. Hence, addressing this yet open question is the goal of our study. This will provide insights into how two key components of the brain's neural activity, namely phase dynamics and INT, are related to each other and integrate their distinct timescales,

e.g., shorter (phase dynamics) and longer (INT). That, in turn, is key for our understanding of higher-order cognitive features like consciousness (Northoff & Huang, 2017) and self (Wolman et al., 2023) where the integration of different timescales is a core feature.

Previous research on neural waves and their phase cycles predominantly focused on the faster frequency range of 1-80 Hz including so-called Theta (4-8 Hz), Alpha (8-12 Hz), Beta (12-40 Hz), and Gamma (40- Hz) waves in Electroencephalography/Magnetoencephalography (EEG/MEG) studies (Adaikkan et al., 2019; Helfrich et al., 2018; Hua et al., 2022; Klimesch et al., 2007). The ongoing waves' phase dynamics are here measured and operationalized by frequency sliding (Cohen, 2014). As shown in Figure 6, the frequency sliding method calculates the temporal derivative of the phase angle for a filtered signal, thus measuring the sliding of the instantaneous frequency during a given time series, the so-called peak frequency (PF) for each time point (Cohen, 2014). Hence, PF measuring the speed of phase-angle-based changes over time, can, more generally, be conceived as an index of the dynamics of neural waves. Subsequent research has demonstrated PF's predictive ability for visual perception (Samaha & Postle, 2015), its reflection of temporal integration and segregation (Wutz et al., 2018), and its influence on task performance (Benwell et al., 2019) including thoughts (Hua et al., 2022). Moreover, abnormalities in PF have been observed in depression (Wolff et al., 2019). Together, these findings suggest a key role for phase dynamics of waves and specifically their speed in the brain's information processing including its cognition.

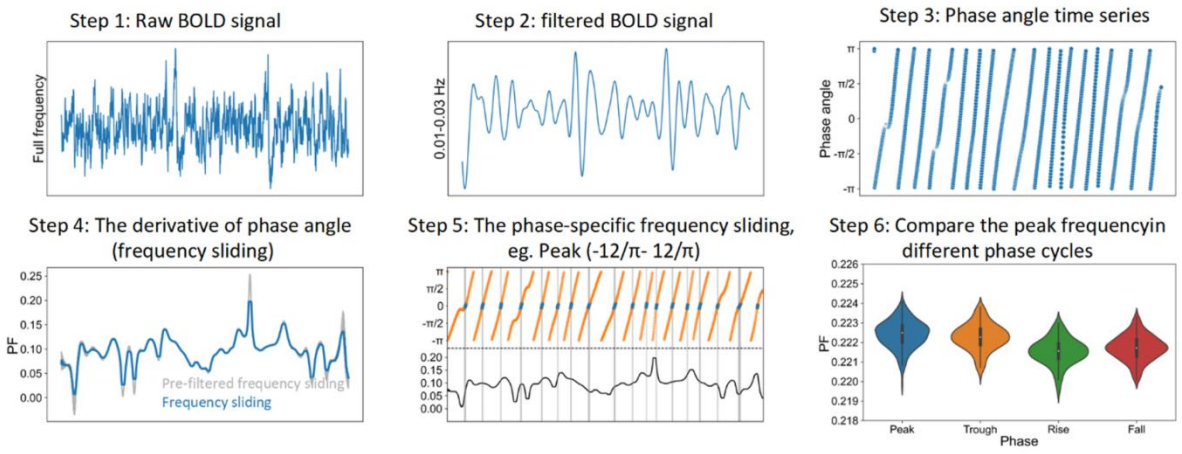

Figure 6. Schematic representation of the frequency sliding method (Cohen, 2014). Step 1: Initiate with the raw BOLD signal. Step 2: Filter the raw data into four narrow bands: 0.01–0.03 Hz, 0.03–0.05 Hz, 0.05–0.07 Hz, and 0.07–0.09 Hz. Step 3: Determine the phase of the filtered data. Step 4: Calculate the

temporal derivative of the phase angle time series, representing peak frequency (PF). Step 5: Extract the PF time series for distinct phases and compute the average of PF within each phase cycle (the Figure exemplifies a "peak" scenario, as the shade shows). Step 6: Conduct statistical comparisons of PF across various phases, including peak, trough, rise, and fall.

The infraslow neural waves, within the 0.01-0.1 Hz range in functional Magnetic Resonance Imaging (fMRI), have increasingly been recognized for their importance in the complex neural stochastic processes of integration and segregation (Golesorkhi, Gomez-Pilar, Zilio, et al., 2021; Wolff et al., 2022). This recognition is evident in various studies (Ao et al., 2022; Doucet et al., 2012; Gong & Zuo, 2023; Thompson & Fransson, 2015), encompassing research on consciousness (Huang et al., 2014), cognitive processes (J. M. Palva & Palva, 2012), and mental disorders (Scalabrini et al., 2020). Unlike in EEG/MEG, fMRI investigations into infraslow neural waves and their phase dynamics have only begun recently (Bolt et al., 2022). Current fMRI studies have underscored the significance of wave-like dynamics featured by its phase as a foundational aspect of understanding the brain's spatiotemporal structure (Pang et al., 2021, 2023; Raut et al., 2021). While other studies demonstrated the modulation of specific brain activation and coactivation patterns during various phases, including peak, trough, rise, and fall in the infraslow frequency domain of fMRI (Gutierrez-Barragan et al., 2019; Huang et al., 2017; Scheinost et al., 2016; Y. Wang, Huang, et al., 2019). Despite these advances, our comprehension of wave dynamics across different phases (peak, trough, rise, fall) in the domain of the brain's infra-slow frequency fluctuations remains somewhat limited. Specifically, the wave dynamics of infraslow frequency fluctuations with potentially differential roles of peak/trough and rise/fall components during the ongoing phase cycles including their topographic distribution remain yet unclear. Hence, our first main aim is to address this gap in our knowledge of the dynamics of neural waves in the infraslow frequency domain of fMRI.

In addition to its phase dynamics, the brain's neural activity can also be characterized by different timescales, the so-called intrinsic neural timescales (INT). Prior research has suggested a hierarchy of INT from short to long as measured by the autocorrelation window (ACW) (Golesorkhi, Gomez-Pilar, Tumati, et al., 2021; Golesorkhi, Gomez-Pilar, Zilio, et al., 2021; Ito et al., 2020; Raut et al., 2020; Wolff et al., 2022). This measure estimates the decay

rate of the autocorrelation function, a signal's correlation with itself at different time lags, and is considered a key mechanism for matching input stochasticity with ongoing temporal statistics (Hasson et al., 2015; Wolff et al., 2022). Given that the phase dynamics may operate at different timescales through its speed (PF), one may want to raise the following question: Are the brain's INT and thus its ACW related to the ongoing wave dynamics, its speed, as measured by PF? Two recent EEG studies demonstrate a correlation of ACW with PF (Buccellato et al., 2023) and inter-trial phase coherence including their breakdown in pathological processes, e.g., schizophrenia (Lechner & Northoff, 2023) and loss of consciousness in anesthesia (Buccellato et al., 2023). This underscores the relevance of the relationship of INT and ACW in the faster frequencies (1 to 80 Hz) of traditional cognitive information processing. Does the same hold for the infraslow frequency domain (0.01 to 0.1Hz) and their topographies in fMRI? Probing the relationship of ACW and PF in the infraslow frequency domain is the second main aim of our study.

In this study, we first analyze the HCP 3T resting-state data to investigate the PF across different phases and to explore how the distinct components during the ongoing phase cycles modulate PF. Previous findings have noted varied brain activations in different phases of peak, trough, rise, and fall, indicating that infraslow wave dynamics vary with phase cycle changes (Huang et al., 2017; Y. Wang, Huang, et al., 2019). We subsequently hypothesize that the magnitude of PF is phase-specific and is modulated by the phase cycle, e.g., peak, trough, rise and fall. Next, we aim to examine the relationship between PF and INT. Based on previous findings (Buccellato et al., 2023; Lechner & Northoff, 2023) of their negative relationship in EEG, we expect the same direction in their correlation in the infraslow frequency domain of fMRI, that is, longer ACW corresponds to slower PF. Lastly, we investigate how PF including its modulation by the ongoing phase cycles and INT change during a movie-watching task. Even though no prior fMRI studies focused on the task-related changes of spontaneous phase dynamics as measured by PF, changes in the dynamics of phase synchrony patterns (Alderson et al., 2020; Stark et al., 2020) and phase-specific performance in peak, trough, rise and fall (Y. Wang, Huang, et al., 2019) have been reported during task states. Thus, we hypothesize that the PF shows phase-specific changes during task states; we especially expect that the task-

related changes in PF occur across the whole brain, e.g., from unimodal to transmodal cortical regions, as the movie stimuli involve both sensory and cognitive functions (Kringelbach et al., 2023; Rajimehr et al., 2022).

2.2 Results

2.2.1 Infraslow phase dynamics (peak frequency/PF) varies in different phase components and frequency bands

Our initial evaluation involved probing the similarity between the EEG-based frequency sliding methods of Cohen (2014) and Lechner & Northoff (2023) in the infraslow frequency range of fMRI. All of the R values obtained for the four frequency bands exceeded 0.9, thereby suggesting that our method can be corroborated by different methodologies (Supplementary Figure 2).

The specific analysis is illustrated in Figure 6, step 5 and 6. To maximize the difference of PF across different phases, we calculated the average PF values across four narrow phase windows with 30° for each, resulting in topographies at the group level for peak (-15°-15°), trough (165°-180° & -180°--165°), rise (-105°--75°), and fall (75°-105°) phases, in line with previous studies (Huang et al., 2017; Y. Wang, Huang, et al., 2019). To quantify the spatial similarity of PF topographies across the four bands, we correlated each region between each pair of bands, as depicted in Figure 7A. A notable observation was the low similarity between the 0.01-0.03 Hz band and higher bands during the phase cycles (r=-0.48~0.16). However, strong within-band and between-phase correlations were evident (r=0.62~0.98). This indicates that the very slow frequency band possesses a unique spatial topography.

We next conducted a 2-way within-subject analysis of variance (ANOVA) for frequency sliding across different phases and bands, as shown in Figure 7. Figure 7B illustrates false discovery rate (FDR)-corrected brain maps with significant F-values ($P<0.05$). The results suggest higher PF during peak and trough phases while lower PF during rise and fall phases were observed across most brain regions (Figure 7C, $F= 820.6$, $P<0.0001$). PF appears to increase with the increase of the frequency band when applying different band passes ($F=1.40e+06$, $P<0.0001$). This is further supported statistically as we detected a robust

interaction (F=250.1, P<0.0001) between phase/PF and bands, characterized by lower phase differences at higher frequencies, as reflected in the decreasing effect size.

In sum, these findings suggest that PF is higher during peak and trough but lower during rise and fall. This effect is most prominent in the 0.01-0.03 Hz band, which displays a unique spatial topography while this effect diminishes in faster frequency bands. These results were consistently replicated using 7T resting-state data, as illustrated in Supplementary Figure 3. In contrast, while the ANOVA result is significant in 0.01-0.03 Hz, low effect size/no significant differences between peak-trough and rise-fall phases were observed in the surrogate data, as shown in Supplementary Figure 4. This further supports the validity of the peak-trough and rise-fall phase differences in terms of their peak frequency as an intrinsic feature of the spontaneous activity's temporal structure.

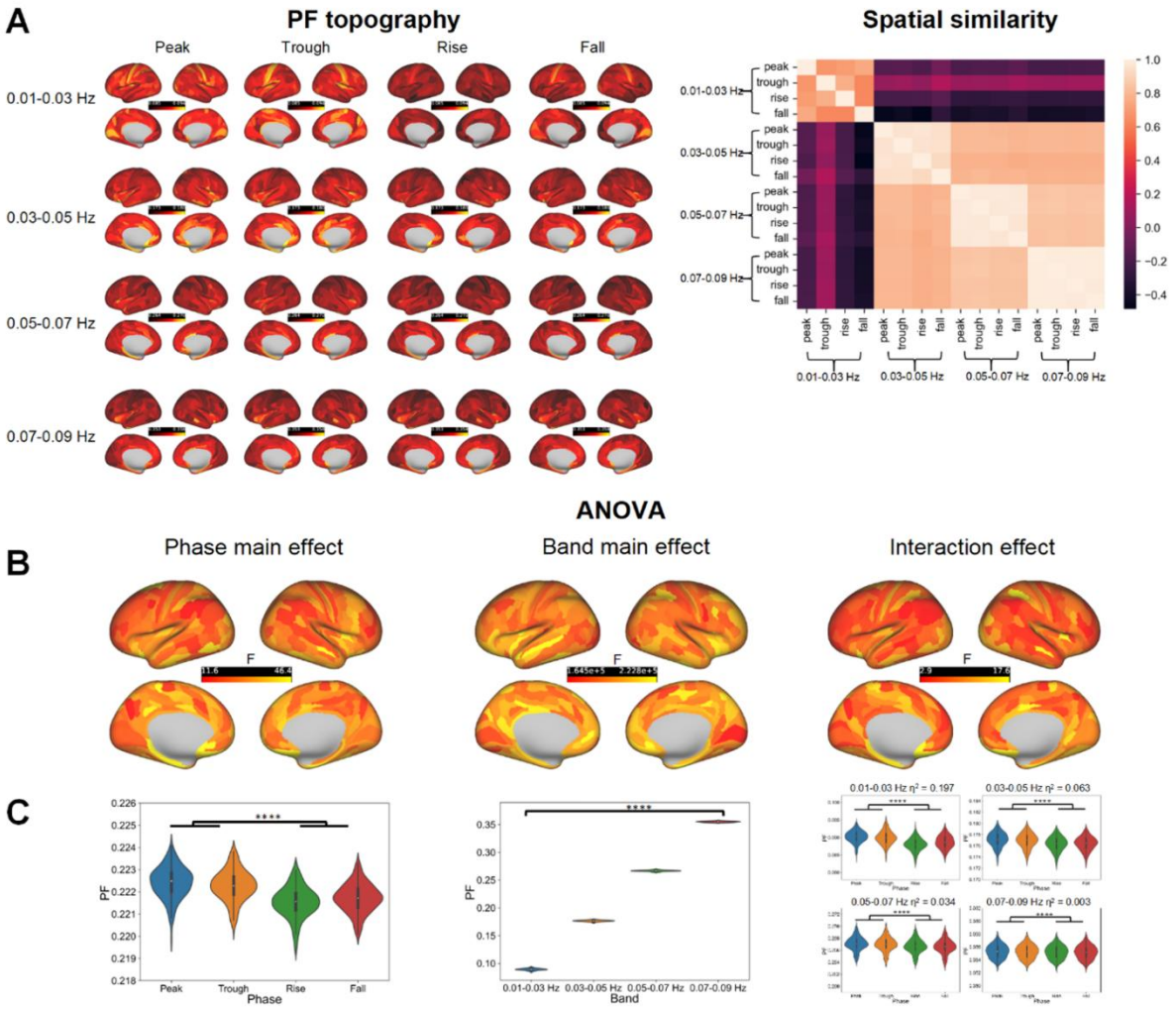

Figure 7. Peak frequency (PF) across four bands and phases. (A) Left: The brain maps of PF within

different filtered bands and phases. Right: Correlation matrix of each pair of topographies (B) The ANOVA outcomes for brain regions in Glasser's atlas. (C) The comprehensive post-hoc analysis was conducted at the whole-brain level.

2.2.2 PF is modulated by the distinct components of the ongoing phase cycles

We have so far demonstrated that PF varies across four phases. To examine the effects of the distinct components of the ongoing phase cycles on PF, we segmented the phase into narrow bins using a window length of 30 degrees and a step length of 1 degree. This process resulted in 360 narrow phase bins (-180~-150, -179~-149, and so on), and we calculated the mean PF in each bin. We computed the normalized Kullback-Leibler (KL) divergence against a uniform distribution, a classical index to measure the modulation effect (Helfrich et al., 2018; Tort et al., 2010), to quantify how strongly the PF distribution was modulated by the different phase components.

In agreement with the results above, the magnitude of PF is higher during the peak and trough phases and lower during the rise and fall phases (Figure 8A). We further applied within-subject ANOVA for each region and the average of them. Interestingly, the ANOVA and post-hoc results show that KL divergence significantly decreases as the frequency of the band increases ($F=657.5$, $P<0.0001$, Figure 8, left), suggesting that the very slow frequency, 0.01-0.03 Hz, exhibits the strongest modulation effect. Topographical analysis reveals that this slow-fast frequency difference is significant in the whole brain (FDR corrected, Figure 8C). This observation is replicated using 7T resting-state data, as shown in Supplementary Figure 5. In contrast, the surrogate data display a much lower modulation index while no similar pattern was observed (Supplementary Figure 4). This supports the assumption that the peak frequency differences between the different phase components are an intrinsic feature of the temporal structure of the brain's spontaneous activity.

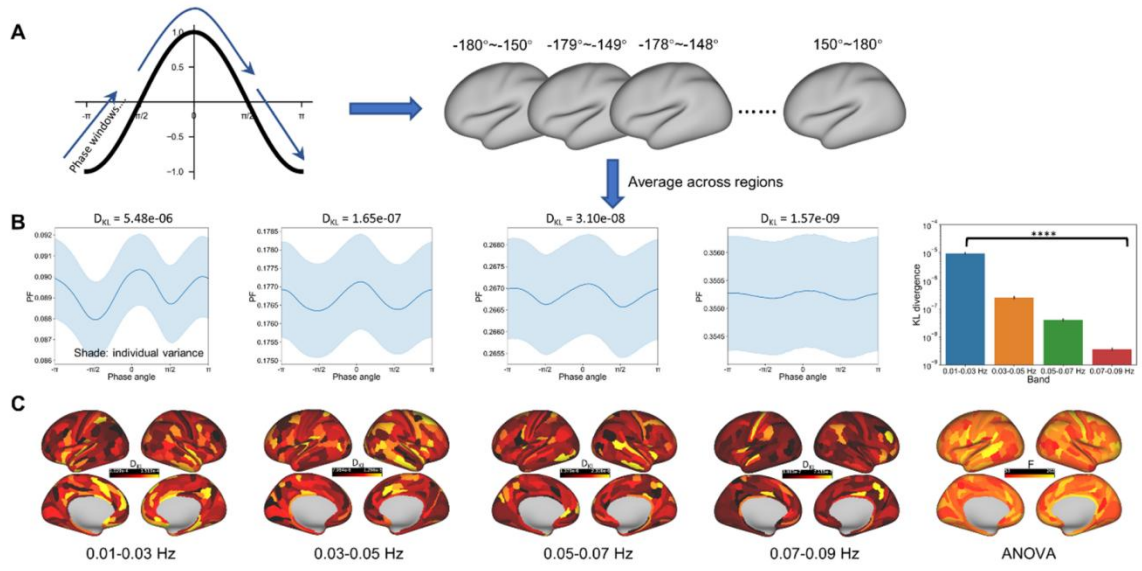

Figure 8. Phase modulation effects on peak frequency (PF). (A) The schematic figure illustrates the method to calculate PF in each phase bin (B) Line charts: The blue line represents PF within the phase cycle, ranging from -π to π, with the shaded area denoting the standard deviation of individual variances. Bar chart: The ANOVA results for KL divergence across the four frequency bands. (C) Topographies of KL-divergence and ANOVA result.

2.2.3 Relationship between phase dynamics (PF) and timescales (ACW)

As delineated in Figure 9A, the ACW is longer in the Default Mode Network (DMN) but shorter in visual and sensorimotor regions. This pattern reflects segregation between unimodal and transmodal regions, an observation that aligns with previous studies (Golesorkhi, Gomez-Pilar, Tumati, et al., 2021; Golesorkhi, Gomez-Pilar, Zilio, et al., 2021; Huntenburg et al., 2018; Margulies et al., 2016).

To investigate the relationship of ACW with PF, we computed the spatial similarity between PF in the four bands (0.01-0.03 Hz, 0.03-0.05 Hz, 0.05-0.07 Hz, and 0.07-0.09 Hz) and ACW for 0.01-0.1 Hz. The correlation analysis between the mean of PF and ACW demonstrated a consistently significant negative trend across all bands (R=-0.22, -0.84, -0.79, -0.76, with all P-values < 0.0001): The longer the INT/ACW, the lower the PF in the same region. These results were replicated using the 7T data, as indicated in Supplementary Figure 6.

We further checked the correlation between frequency power and ACW

(Supplementary Figure 7). The correlations between frequency power and ACW are significantly lower than that between PF and ACW in four bands ($Z = 2.11, 11.49, 8.80, 9.37$, all of P values < 0.05). This suggests that the ACW is, in part, related to specifically the nonlinear component of the signal as reflected in the phase angle of the PF as that is eliminated in frequency power.

In phase-shuffled surrogate data, PF-ACW correlations maintain almost the same with actual data in 0.03-0.05 Hz, 0.05-0.07 Hz, 0.07-0.09 Hz (see Supplementary Figure 8, $Z = -0.24, -0.25, -0.00$, all of P values > 0.05). This is not surprising given that the phase cycles with their distinct components themselves, although temporally randomized in their timing, are essentially preserved in the phase-shuffled surrogate data. This distinguishes the result from the frequency power where the phase components themselves like peak and trough are no longer preserved as the modulus of the Hilbert signal is taken. The fact that only the frequency power but not the phase-shuffled surrogate data impaired the correlation of PF with ACW suggests that the nonlinear phase components themselves like peak and trough, but not so much their exact timing, drive their relationship with ACW.

Note that the correlation between ACW and PF shifts to a positive one in the 0.01-0.03 Hz band ($Z = 5.18$, $P < 0.0001$). Given that our shuffling method, i.e., shuffling the sequency of Fourier phase, specifically eliminated the nonlinearity component of the phase dynamics while preserving the amplitude characteristics, this suggests that the negative relationship of PF and ACW is partly explained by nonlinearity rather than linear features of the signal in the very slow band of 0.01-0.03 Hz but not so much in the more linear features of the faster bands. This is in line with our findings in Figure 7 and previous findings on infraslow neural oscillations (Buzsáki & Draguhn, 2004; X.-N. Zuo et al., 2010), that 0.01-0.03 Hz corresponding to Slow-5 (0.01–0.027 Hz) contains unique feature with a higher frequency corresponding to Slow-4 (0.027–0.073 Hz).

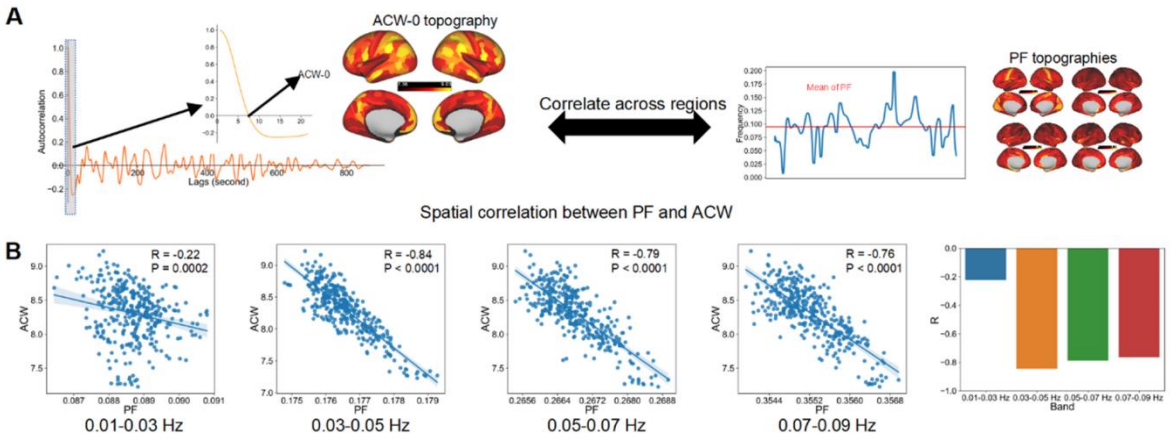

Figure 9. Relationship between peak frequency (PF) and autocorrelation window (ACW). (A) A graphical representation illustrating the process of calculating the correlation between ACW and PF. (B) The regression plot depicts the relationship between ACW and PF across four frequency bands, each dot represents each brain region. The accompanying bar chart highlights the differences in Pearson's correlation coefficients across the four bands.

2.2.4 Effect of band-passing

To mitigate the potential influence of filtering edge effects, we expanded our analysis to replicate the studies using different band-passing filters like 0.005-0.01 Hz as well as 0.01-0.03 Hz as being analyzed within a filtered band of 0.005-0.1 Hz. This supplemental analysis yielded results that concurred with the primary analysis (as delineated in Figures 7-9 and Supplementary Figure 9); this suggests that the outcomes of our study are not merely artifacts of edge effects. Note also the even steeper negative correlation of ACW and PF in this broader bandpass; this is in line with the observation that the length of the ACW is strongly shaped by the slower components of the frequency spectrum (Honey et al., 2012; Zilio et al., 2021).

2.2.5 Task-modulation of infraslow phase dynamics (PF)

The task leads to higher PF in the trough phase than in the peak when compared to the resting state (as shown in Figure 10A, left). The simple effect test indicated that this difference was significant only at 0.01-0.03 Hz ($T=-22.22$, $P<0.0001$, Figure 10A, right). Moreover, the task-state KL divergence in 0.01-0.03 Hz exceeded that observed during the resting state ($T=-6.86$, $P<0.0001$, Figure 10C). Topographical analysis the KL divergence increased mainly in visual, auditory, and sensorimotor cortices which, presumably, are related to the processing of the external sensory stimuli during the movie-watching task.

These findings led us to hypothesize that this increased KL divergence during the task state (compared to rest) is primarily driven by the difference between peak and trough during the task state. To investigate this, we compared PF between resting and task states in different phases at 0.01-0.03 Hz using a paired t-test. We noted a decrease in PF during the task state (compared to rest) across all phases. Topographical analysis shows that this PF decrease is largely present in visual, auditory, and sensorimotor cortices, which is consistent with the KL divergence results. The effect size of the difference between rest and task was greatest in the peak, while it was smallest in the trough. This observation suggests that the increased phase modulation in the task state is primarily driven by the change in the relationship of peak and trough when compared to the resting state (Figure 10A, left).

Several studies have indicated that resting-state and task-related brain activities may be associated with different frequency components beyond the infraslow range (J. E. Chen & Glover, 2015; S. Palva & Palva, 2018). For instance, higher frequencies, such as Slow-3 (0.073-0.198 Hz), have been shown to have specific effects in resting-state and cognitive functions (Ao et al., 2023; Y. Wang, Zou, et al., 2020; H. Zhang et al., 2022). In our study, we further examined the differences in PF during rest and task conditions across a broader frequency range of 0.01-0.2 Hz. As demonstrated in Supplementary Figure 10, we observed frequency-specific effects across various narrow bands. In addition, task modulation was predominantly observed in the 0.01-0.1 Hz range, particularly within the 0.01-0.03 Hz band. This suggests that the infraslow component is particularly significant in the context of a naturalistic continuous task like our movie-watching task.

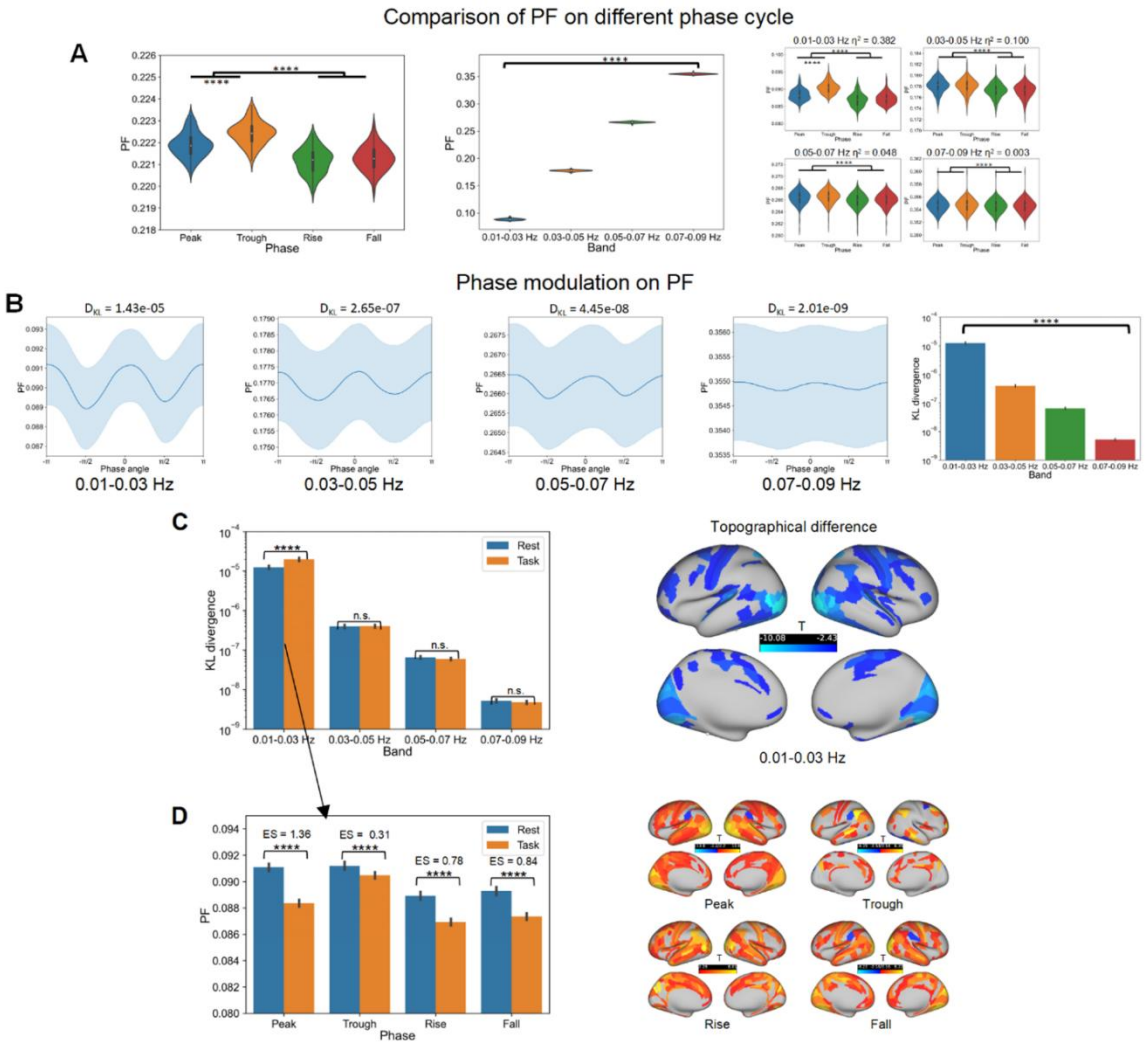

Figure 10. Task-state data analysis. (A) Comparison of peak frequency (PF) on different phase cycles corresponding to Figure 7. (B) Kullback–Leibler (KL) divergence analysis corresponds to Figure 8. (C) Left: Rest-task difference of KL divergence at 4 bands. Right: Rest-task topographical difference of KL divergence at 0.01–0.03 Hz. (D) Left: Rest-task difference of PF in 4 phases at 0.01–0.03 Hz. Right: Rest-task topographical difference of PF at 4 phases.

2.2.6 The relationship between phase dynamics (PF) and INT (ACW) during the task state

We next investigated the relationship between phase dynamics (PF) and INT (ACW) during the task state. First, we correlated PF and INT during the task state. Consistent with the resting-state data, the correlations are significantly negative across all four sub-bands (R=-0.54 ~ -0.20, P<0.0001, Figure 11A). Both decreases and increases in ACW length during the task state were observed relative to the resting state. Specifically, in visual and auditory cortices, regions that play vital roles in processing movie stimuli, we observed an increase in ACW

length during task-related activity compared to the resting state. Conversely, the ACW length in the sensorimotor cortex, the posterior cingulate cortex, and the prefrontal cortex decreased during the task state compared to the resting state (Figure 11B).

Lastly, we calculated the spatial correlation between the unthresholded rest-task difference topographies of PF and ACW. As in the resting state, the correlation consistently shows a negative relationship between PF and ACW, providing yet further evidence that the task modulates the topographies of both PF and ACW in somewhat analogous ways (Figure 11C).\

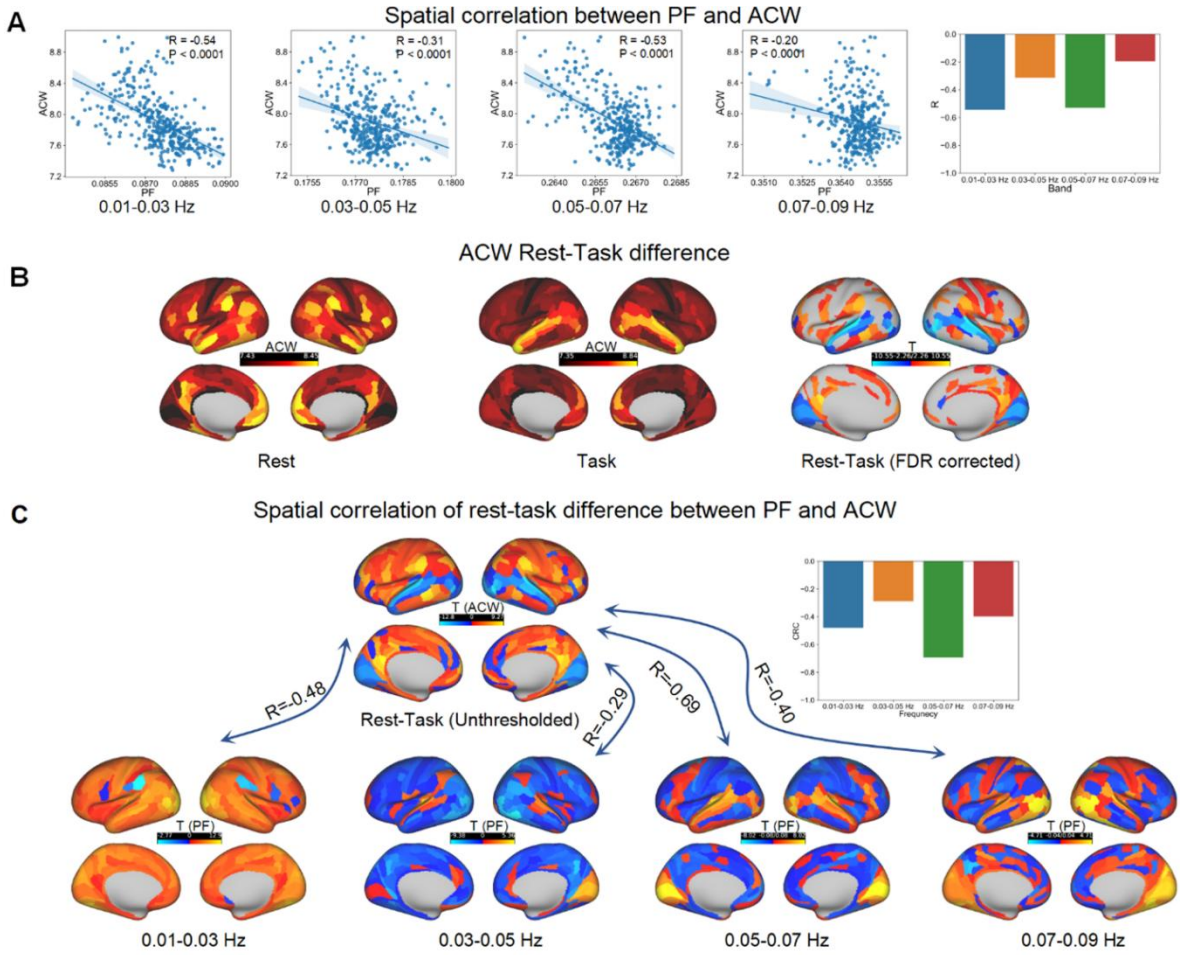

Figure 11. Autocorrelation window (ACW) rest-task difference. (A) Spatial correlation between peak frequency (PF) and ACW in task state. (B) Left: ACW topography in resting state. Middle: ACW topography in task state. Right: T-test topography of rest-task ACW. (C) Top: Unthresholded rest-task difference of ACW. Below: Unthresholded rest-task difference of PF in four bands

2.3 Discussion

Utilizing the Human Connectome Project's (HCP) 3T/7T dataset, we, operating in the infraslow frequency domain, investigated the spontaneous phase dynamics of neural waves, their association with INT, and the subsequent changes during a movie-watching task.

Our first main finding consists of the observation that the speed of the infraslow neural waves, quantified by PF, exhibits higher values at peak/trough and lower values at rise/fall. This modulation of the phase cycle, ranging from -180° to 180°, is clearly illustrated in Figure 8. Significantly, this effect is present within the 0.01-0.03 Hz band, a very slow frequency range, while it is weaker in faster frequency ranges. During the task state, the modulation effect of the phase cycle on PF intensifies within the 0.01-0.03 Hz band. Intriguingly, despite a consistent increase in PF across four phases from rest to task, this stronger modulation effect is primarily driven by a heterogeneous increase in PF at peak and trough positions.

The second main finding consists of the negative correlation between PF and INT, corroborating the findings of the Buccellato et al. (2023) EEG study. While we noted task-related changes in PF and ACW, we also demonstrated the persistence of their negative correlation during the task state. In sum, we demonstrate the major role of the brain's ongoing infraslow wave dynamics including its relation to INT in shaping neural activity during both rest and task states.

2.3.1 Wave dynamics and its task modulation

Neural activities exhibit substantial temporal variations and dynamism (Kringelbach & Deco, 2020). Our research illustrates that PF, a measure of the speed of neural waves, varies concurrently with phase cycle changes. Within resting-state data, we observed higher PF values at peak/troughs and lower PF values during rise/fall across all brain regions. These findings demonstrate the importance of the ongoing phase cycles in shaping the dynamics, that is, the speed of neural activity.

Previous resting-state fMRI studies have identified distinct brain states as configured by the phase of global brain activity during peak, trough, rise, and fall stages (Gutierrez-

Barragan et al., 2019; Scheinost et al., 2016). Yet, the task-related modifications of these phase-dependent brain states remain underexplored. Our study pioneers an examination of wave dynamics in the infraslow frequency domain including task state modulations. We found that PF decreases in the task state, suggesting a slowing of wave speed in response to movie stimuli. The slower speed potentially enables the brain to incorporate and integrate the shorter micro-contents into longer macro content providing psychological continuity, coherence, and unity of the movie in our perception (Himberger et al., 2018). Concurrently, we observed an increase in phase modulation during the task state, suggesting a broader range of timescales operating across different phases which, as we speculate, may be related to the encoding and processing of the movie's different timescales (Golesorkhi, Gomez-Pilar, Tumati, et al., 2021; Wolff et al., 2022). Interestingly, despite a consistent decrease in PF across the ongoing phase cycles, the reduction is most significant at the peak and minimal at the trough, largely maintaining fast speed at the trough. Given that slow PF and longer INT may allow for temporal integration of inputs while faster PF with shorter INT favors their temporal segregation (Hua et al., 2022; Wolff et al., 2022), we suppose that the task-related modulation of PF and INT allows for the concurrent integration and separation of the movie's different timescales: while movie inputs related to each other over longer stretches of time necessitate slower activity (as through the lowering of PF at the peak) for their temporal integration, faster activity (through the preservation of higher PF at the trough) persist in processing the fast-changing movie contents concurrently.

Our results highlight the significant and strongest effect of the 0.01-0.03 Hz band on phase dynamics and task-related changes. The function and role of this frequency band, labeled Slow-5 within the infraslow frequency range (Buzsáki & Draguhn, 2004; Y. Wang, Zou, et al., 2020; X.-N. Zuo et al., 2010), remains poorly understood compared to the higher frequency oscillations, such as theta and alpha bands. Our findings propose that the Slow-5 wave may play a critical role in both spontaneous dynamics and the encoding of external stimuli, corroborating several fMRI studies (Gutierrez-Barragan et al., 2019; Y. Han et al., 2011; Raut et al., 2021). For instance, Gutierrez-Barragan et al. found that the power spectral density of brain coactivation patterns and the global signal peak at approximately 0.02 Hz, suggesting

that brain states are modulated by the ongoing phase dynamics within the 0.01-0.03 Hz range (Gutierrez-Barragan et al., 2019). This may include also body-based physiological modulation as Raut et al. identified a broad peak of coherence at 0.025 Hz between physiological signals (including respiration, heart rate, and pupil size) and network signals (Raut et al., 2021). Collectively, we propose that the 0.01 to 0.03 Hz band may harbor unique and vital information about brain-body coupling that strongly modulates spontaneous brain activity and its temporal encoding of the body's continuous inputs to the brain, a hypothesis that merits further investigation.

2.3.2 Wave dynamics relate to the INT

Our study reveals a negative correlation between the speed of wave dynamics (PF) and the length of INT. This observation aligns with expectations that a slower oscillation corresponds to a longer intrinsic timescale (Honey et al., 2012; Zilio et al., 2021). Such an outcome reaffirms the empirical findings from an EEG study investigating conscious states (Buccellato et al., 2023). Interestingly, that EEG study reported a disruption of the negative PF-ACW correlation in unconscious states. This provides additional evidence for the intrinsic cross-scale temporal organization of wave dynamics and INT. Given that both wave dynamics and INT are known to reflect the brain's inherent capacity to encode inputs (Golesorkhi, Gomez-Pilar, Zilio, et al., 2021; Samaha & Postle, 2015) including their temporal integration and segregation (Wolff et al., 2022; Wutz et al., 2018), we propose that this cross-scale intrinsic temporal relationship may be crucial for processing complex stimuli featured by a variety of different timescales like in a movie.

An interesting observation is the strengthening of the negative correlation between PF and ACW when the low cut-off bandpass is reduced from 0.01 to 0.005. This finding implies that the negative relationship between PF and ACW is predominantly influenced by the very slow frequencies. Although previous research has investigated ACW in both the low-frequency range in fMRI (Ito et al., 2020; Raut et al., 2020) and the high frequency in EEG/MEG (Golesorkhi, Gomez-Pilar, Tumati, et al., 2021; Wolman et al., 2023; Zilio et al., 2021), no study has examined the frequency-sensitivity of ACW. As our study shows that slower to faster PF are associated with distinct components within the ongoing phase cycles, we suggest that

the intrinsic timescales in sub-frequency bands should be considered.

2.3.3 Limitation

Our study primarily utilizes resting-state and movie-watching fMRI data. While movie-watching is a natural continuous stimulus that shows distinct modes of brain function (Demirtaş et al., 2019; Finn, 2021; Huk et al., 2018), it differs from traditional cognitive tasks in its continuous stimulus presentation rather than discontinuous stimuli as in typical event-related paradigms (Huk et al., 2018), for which reason it does not involve behavioral responses. This distinction is important to note, as our findings regarding PF-ACW correlations are derived under this specific condition of a continuous naturalistic task paradigm. Hence, future research on the PF-ACW relationship in more discontinuous typical event-related paradigms is warranted. Moreover, the lack of direct behavioral measures in our dataset limits our ability to draw definitive conclusions about the cognitive functionalities of wave dynamics and INT in more varied or specific cognitive tasks. Future research should aim to include a broader range of cognitive tasks including continuous and discontinuous with corresponding behavioral response data to better understand and apply these findings in cognitive neuroscience.

A further limitation of our study is the use of a dataset from the HCP comprising solely healthy subjects. Given that wave dynamics and ACW reflect the individuals' ability to process inputs, exploring individual differences in pathological or other extreme states could provide valuable insights into future research. Studies should consider including different groups of subjects, such as those experiencing brain aging or mental disorders, to better examine the behavioral and functional relevance of wave dynamics and INT.

Lastly, our analysis was conducted at the conventional infraslow frequency of 0.01-0.1 Hz, primarily to develop a method for studying the dynamics of neural waves in fMRI data. Considering that important neural information is also contained in higher frequencies (>0.1 Hz) (Buzsáki & Draguhn, 2004; J. E. Chen & Glover, 2015; X.-N. Zuo et al., 2010), future research should investigate wave dynamics in higher frequencies using open band passes (Sasai et al., 2021; Y. Wang, Zou, et al., 2020). This would provide a more comprehensive understanding of phase dynamics and INT across the whole frequency spectrum of timescales from longer to

shorter.

2.4 Conclusion

Visualize yourself as a surfer riding the neural waves of the brain. Our findings indicate that the speed of these neural waves varies across their peaks, troughs, rises, and falls, mirroring the changing conditions a surfer faces on the waves of the ocean. Importantly, the length of intrinsic neural timescales requires adaptable responses, similar to a surfer adjusting to the ongoing and continuously changing wave patterns. Furthermore, an adept surfer should always be ready to respond to unexpected changes, analogous to the way the movie task changed both wave dynamics and INT. Based on our research, we propose that wave dynamics and their relationship to the INT play a critical role in organizing the temporal features of the brain's information processing. Future research should further investigate how specific cognitive processes and individual differences influence wave dynamics and INT. Lastly, the development of effective clinical interventions and therapies, aimed at 'mastering the neural waves', should be considered within the context of the temporospatial approach of the brain-mind connection that recently has been introduced, e.g., Spatiotemporal Neuroscience (Northoff et al., 2020b, 2020a).

2.5 Methods

2.5.1 Data acquisition

The study utilized the fMRI dataset from Human Connectome Project (HCP) S1200 release (Van Essen et al., 2013). A total of 179 subjects with comprehensive scan data from both 3T and 7T imaging were incorporated. The 3T dataset was applied for the resting-state analysis, while the 7T data was employed for replication and task analysis. The participants' ages span from 22 to 35 years, with 108 female participants.

The 3T resting-state data collection was performed over two consecutive days. On each day, each participant underwent two 15-minute runs, resulting in four resting-state scans per participant (rfMRI_REST1_LR, rfMRI_REST1_RL, rfMRI_REST2_LR, and rfMRI_REST2_RL). Considering the susceptibility of time-frequency analysis to time samples, the four scans of each participant were amalgamated in the analysis (Honari et al., 2021; Y. Wang, Zou, et al., 2020). The study used surface-based Connectivity Informatics Technology Initiative (CIFTI) resting-state fMRI scans (MSMall registered) that had undergone prior pre-processing with the HCP's independent component analysis (ICA)-based artifact removal process, in order to minimize the effects of spatially structured noise. All brain imaging data were procured on a custom Siemens 3T Skyra at Washington University in St. Louis using a multi-band sequence. Structural images were captured at a 0.7-mm isotropic resolution, while the resting-state fMRI data had a 2-mm isotropic spatial resolution and a repetition time (TR) of 0.72 seconds. Informed consent was obtained from all participants, with all methods conforming to relevant guidelines. The 3T task data were excluded from the analysis due to their limited scan duration (3 to 5 minutes), as the objective was to investigate the very slow frequency bands.

In correspondence with the 3T resting-state data, the 7T resting-state data included four 16-minute scans per participant (rfMRI_REST1_PA, rfMRI_REST2_AP, rfMRI_REST3_PA, and rfMRI_REST4_AP). The 7T task data included movie watching and retinotopy. Movie-watching data was incorporated, given its approximately 15-minute scan duration. Each movie-watching scan consists of several clips with separated by 20-second rest periods (details are

available in WU-Minn HCP S1200 Release Reference Manual). CIFTI fMRI scans that underwent ICA-based artifact removal were utilized, mirroring the 3T data selection. These data were collected at a resolution of 1.6-mm isotropic and 1-second TR, utilizing a multiband acceleration of 5, in-plane acceleration of 2, and 85 slices.

2.5.2 Preprocessing

The data used in this study have already undergone the HCP ICA-based denoising, negating the need for further preprocessing (Bolt et al., 2022; Raut et al., 2021; Van Essen et al., 2013; J. Zhang et al., 2020). For all fMRI scans, the signals from brain regions were extracted using the Human Connectome Project Multi-Modal Parcellation (HCP-MMP) 1.0 template and the activity of vertices inside each of the 360 regions was averaged to get 1 time series per region (Glasser et al., 2016). Subsequently, the signals from each region were filtered to the 0.01-0.1 Hz range using a zero-phase filter ('filtfilt' function in MATLAB), consistent with previous fMRI phase studies (Bolt et al., 2022; Honari et al., 2021).

2.5.3 Peak frequency

The rate of phase change can be characterized as the PF, which can be calculated by the first derivative of the phase angle time series. Higher PF corresponds to faster phase angle variation. This technique was originally developed for measuring the frequency fluctuation of EEG signals by Cohen (2014), who coined the term 'frequency sliding' (Cohen, 2014). We adapt this method to low-frequency fMRI signals as the methodology depicted in Figure 6.

We first applied a zero-phase filter to the raw BOLD signal (step 1) to yield a filtered signal without phase distortion (step 2), as recommended by a prior fMRI study on phase (Honari et al., 2021; Pedersen et al., 2018). Previous fMRI phase studies have advocated narrow-band filtering to satisfy Bedrosian's theorem and generate meaningful envelopes and phases of an analytic signal (Pedersen et al., 2018). In our pursuit to examine frequencies from slow to fast, we divided the signal into four narrow sub-bands: 0.01-0.03 Hz, 0.03-0.05 Hz, 0.05-0.07 Hz, and 0.07-0.09 Hz. We then applied the Hilbert transform to obtain the analytic representation and extract the phase angle time series, as given by the following equation (step 3):

$$z(t) = y(t) + j\tilde{y}(t) = a(t)e^{j\varphi(t)}$$

Where $j = \sqrt{-1}$, $\tilde{y}$ denotes the Hilbert transform of y, $a(t)$ denote amplitudes and $\varphi(t)$ denote phases of signal $z(t)$. Upon calculating the first derivative of the phase angle time series, we applied a median filter using MATLAB's 'medfilt' function to the derivative time series to mitigate large "blips" and negative derivatives due to jumps in the unwrapped phase angle time series. Given that fMRI data comprise fewer time points than EEG data, we increased the median filter order from 10 (used in EEG) to 20 to counteract larger phase jumps in BOLD signal (step 4). To discern phase-specific PF, we calculated the mean PF within a narrow phase window (e.g., a peak is defined from -π/12-π/12 or -15°-15°).

To rule out the edge effect that may be caused by the 0.01-0.03 Hz filtering, the same analysis is done for 0.005-0.01 Hz within 0.005-0.1 Hz band-pass filtering.

2.5.4 Validation on Lechner (2023) method

The Frequency Sliding Method, initially conceived for high-frequency EEG/MEG analysis, is deployed for the first time on fMRI data in this study. In an endeavor to assess its replicability, we explored its congruence with the recently formulated Lechner (2023) method (Lechner & Northoff, 2023). The Lechner (2023) method has been developed to measure the stability of phase dynamics. It designates the -π as the commencement point for each cycle. It computes the time delays from the starting point of a given cycle to the starting points of the successor cycle, subsequently forming a series corresponding to each cycle duration. We further assessed the spatial similarity between the average of PF and cycle duration across the entire time series for each brain region.

2.5.5 Phase cycle modulation on PF

We employed the normalized Kullback-Leibler (KL) divergence of PF distribution P on each phase cycle against a uniform distribution Q to quantify the phase modulation effect on PF. To scrutinize fine-grained phases, phases from -180° to 180° were binned into 360 windows, each with a length of 30° and a step length of 1°. Hence, the cycle of phase is divided into -180° to -150°, -179° to -149°, -178° to -148°, and so forth. As a result, we obtained 360 values

of PF at each phase cycle. The probability distribution of PF is given by the following equation:

$$P_{PF} = \frac{PF(\phi)}{\sum PF(\phi)}$$

Where $PF(\phi)$ represents the value of PF at phase ϕ degree. Subsequently, Shannon entropy was calculated, which reflects the quantity of information for a distribution. If a time series is highly predictable, Shannon entropy will be lower; If a time series is uniformly distributed and hence unpredictable, Shannon entropy is maximal. Shannon entropy of PF is calculated as the equation below:

$$H(P) = -\sum_{j=1}^{N} P_{PF}(j) log P_{PF}(j)$$

Where N is the length of the total phase bins. $Log(N)$ is the maximal entropy of a distribution, corresponding to a uniform distribution. The KL divergence is calculated by the following equation:

$$D_{KL}(P_{PF}, Q) = Log(N) - H(P)$$

Since the uniform distribution is represented by $Log(N)$, we normalized the KL divergence by the following equation:

$$D_{KL\,norm.}(P_{PF}, Q) = \frac{D_{KL}(P_{PF}, Q)}{Log(N)}$$

This definition of normalized KL divergence aligns with previous studies, which used it to examine cross-frequency phase modulation on amplitude (Tort et al., 2010) or behavioral reaction (Helfrich et al., 2018).

2.5.6 Autocorrelation window (ACW)

The autocorrelation functions for time courses of the 360 regions were calculated using MATLAB's "autocorr" function. The ACW value was subsequently defined as the first lag at which the autocorrelation diminishes to zero within the infraslow frequency range (0.01-0.1 Hz), consistent with prior studies (Golesorkhi, Gomez-Pilar, Tumati, et al., 2021; Ito et al., 2020; Raut et al., 2020). It is important to note that we did not assess ACW across the four

narrow bands corresponding to the PF calculations. This decision is grounded in the understanding that ACW represents the neural temporal receptive window, reflecting the duration over which neural activity returns to its baseline (Golesorkhi, Gomez-Pilar, Tumati, et al., 2021). In line with this concept, the INT should encompass a broad spectrum of neural signal timescales, rather than being restricted to a specific frequency band (Golesorkhi, Gomez-Pilar, Zilio, et al., 2021). To maintain data transparency, we have illustrated the ACW topography for these four narrow bands in Supplementary Figure 1. As narrowband filtering imposes a fixed timescale on the neural signal, it revealed topographies with less variability across regions. Moreover, the constrained temporal resolution of fMRI limits the computation of ACW in higher frequency narrow bands due to the scarcity of time samples, leading to a uniform distribution of ACW across different regions (see 0.07-0.09 Hz Supplementary Figure 1).

2.5.7 Spatial similarity

We evaluated the similarity between PF and ACW using spatial correlation. Initially, brain maps of PF and ACW were z-scored on an individual basis. Subsequently, spatial similarity was calculated as a single Pearson's correlation coefficient between PF and ACW topographical maps across brain regions. This calculation was performed after averaging across subjects, thereby generating a single brain per condition (Golesorkhi, Gomez-Pilar, Tumati, et al., 2021; Y. Wang et al., 2018).

We further examined the correlation between ACW and non-phase-based frequency power (Cohen, 2014). The phase information of PF, i.e., its phase angle, captures the non-linear properties of a signal (Cohen, 2014; Glerean et al., 2012; Laird et al., 2002), while these nonlinear properties are eliminated when calculating frequency power (Hua et al., 2022). In the case of frequency power, the analysis paralleled that of PF, with one distinction: frequency power involves extracting the modulus of the Hilbert transform, thereby reflecting the amplitude/power of a frequency band based on its linearity (Cohen, 2014). We calculated the frequency power across our four sub-frequency bands as a linear measurement, and evaluated its correlation with ACW relative to PF, to investigate which metric exhibits greater correlation with INT.

2.5.8 Surrogate data examination

To estimate the influence of phase modulation on PF and the similarity between PF and ACW under the null hypothesis of a linear and Gaussian stationary stochastic process (Chang & Glover, 2010; Liégeois et al., 2019; Zalesky et al., 2014), we employed surrogate data generated by shuffling the Fourier phases. This method manipulates only the phase information of a signal while preserving its amplitude/power spectrum characteristics (Schreiber & Schmitz, 2000). The process begins with the application of a Fourier transform to the time-series data, converting it to the frequency domain. Subsequently, the timings of the signal's phases are randomized independently across each frequency component. Following this phase randomization, an inverse Fourier transform is applied, reconverting the data back to the time domain. In our study, the time series data from various regions, sessions, and individuals in the actual dataset were each shuffled to generate a surrogate dataset that mirrors the original in the phase structure albeit shifted along the time points.

2.5.9 Statistics

Given that the same subjects were included in both the 3T and 7T resting-state and task-state data, we conducted a 4-by-4 within-subject ANOVA for PF in four sub-bands (0.01-0.03 Hz, 0.03-0.05 Hz, 0.05-0.07 Hz, and 0.07-0.09 Hz) and for four phases [peak (-15°-15°), trough (165°-180°&-180°--165°), rise (-105°--75°), and fall (75°-105°)]. A one-way ANOVA was applied for the KL divergence in the four sub-bands. All post-hoc tests were conducted using two-tailed t-tests. Additionally, we assessed the correlations of R values using two-tailed z-tests. Furthermore, all multiple comparisons—including those of brain regions, frequencies, and phases—were corrected using the FDR criterion.

3 STUDY 2: Infra-slow scale-free dynamics modulate the connection of neural and behavioral variability during attention

Ao, Y., Klar, P., Catal, Y., Wang, Y., Northoff, G., 2025. Infra-slow scale-free dynamics modulate the connection of neural and behavioral variability during attention. Communications Biology 8, 1057. https://doi.org/10.1038/s42003-025-08448-3

ABSTRACT

The activities of the human brain vary across different timescales, exhibiting scale-free dynamics. Previous research has highlighted the psychological and physiological significance of brain dynamical fluctuations across the Delta to Gamma bands. However, there has been less focus on infra-slow scale-free dynamics, e.g. power law exponent (PLE), and neural variability, e.g. standard deviation (SD), and sample entropy (SE), in mediating brain-behavior connection during attention. In this study, we recruited 49 participants and recorded functional magnetic resonance imaging (fMRI) resting-state and task data during a sustained attention task paradigm to investigate how the three measures—SD, SE, and PLE—modulate the dynamics of behavioral performance. Our findings demonstrate the following: (i) PLE, SD, and SE exhibit differential topographic distribution with a hierarchical structure from sensory to associative networks, during their rest-task modulation. (ii) PLE, SD, and SE show different topographic extensions from visual cortex to default-mode network in their relationship with behavioral variability. (iii) The relationship between SD and SE is mediated by PLE in the empirical data, which (iv) is further confirmed in simulation. Collectively, our results highlight the topographically- and dynamically-layered mechanisms of distinct neurodynamical features during attention processing: scale-free dynamics modulate neural and behavioral variability.

Keywords: Functional magnetic resonance imaging; Scale-free dynamics; Neural variability; Neural entropy; Visual attention task

3.1 Introduction

3.1.1 Infra-slow dynamics – How do they modulate cognitive function?

The brain is a highly dynamic system. Understanding its neural activity across various timescales is crucial for unraveling its intricate relationship with cognitive functions and disorders (Buzsáki & Draguhn, 2004; Golesorkhi, Gomez-Pilar, Tumati, et al., 2021; Northoff, 2024; S. Palva & Palva, 2018; X.-N. Zuo et al., 2010). Previous research has predominantly focused on faster frequency ranges [e.g., Theta (4-8 Hz), Alpha (8-12 Hz), Beta (12-40 Hz), and Gamma (40- Hz)] in Electroencephalography/Magnetoencephalography (EEG/MEG) studies (Adaikkan et al., 2019; Helfrich et al., 2018; Hua et al., 2022; Klimesch et al., 2007). Recent investigations have shed light on infra-slow oscillations in the blood-oxygen-level-dependent (BOLD) signal (0.01~0.5 Hz). Some work suggests that these infra-slow BOLD fluctuations predominantly reflect the convolution of high-frequency neural activity—including gamma, as well as theta and alpha bands—with the hemodynamic response function (Hacker et al., 2017; Scheeringa et al., 2011). How the infra-slow BOLD fluctuations mediate behavior such performance during an attention task remains yet unclear, though. Addressing this gap in the literature is the goal of our study.

While neuro-vascular effects cannot be excluded (Das et al., 2021), emerging evidence suggest the neural basis of the infra-slow BOLD signals, proposed as the dark brain energy by a recent paper (Gong & Zuo, 2025). For example, significant correlations between infra-slow BOLD signals and infra-slow local field potential (LFP)/EEG correlations indicate that low-frequency neural coordination underlies large-scale BOLD networks implicated in task performance (Hiltunen et al., 2014; Lu et al., 2016; Pan et al., 2013). Furthermore, converging infra-slow electrophysiological, BOLD, and behavioral data reveal that such oscillations across different modalities play a key role in regulating both the integration within and decoupling between concurrently active neuronal communities (J. M. Palva & Palva, 2012). Further support comes from studies showing that the activation of the nucleus basalis of Meynert modulates low-frequency global BOLD signals (Turchi et al., 2018). Collectively, while non-neural factors such as vascular activity and neural-vascular coupling contribute to the BOLD signal (Das et al., 2021), these findings suggest that infra-slow BOLD signals are not merely a

byproduct of high-frequency neural activity. This could be further supported by showing how these intrinsic infra-slow neural processes modulate behavioral and cognitive functions; the mechanisms of such neuro-behavioral modulation remain yet to be explored, though (Ao et al., 2023, 2024; Gutierrez-Barragan et al., 2019; Sasai et al., 2021; H. Zhang et al., 2022).

Relating infra-slow dynamics to cognitive function confronts one with a methodological challenge. Given that high-frequency brain activity can capture specific cognitive processes within milliseconds, it can measure the effects of single trials lasting 100 to 1000 ms (Fiebelkorn & Kastner, 2019; Hanslmayr et al., 2011; S. Palva & Palva, 2018). This is different in the infra-slow frequency band which encompasses several to hundreds of seconds, thus aligning with behavior across a multitude of trials in a temporally more continuous way (Huk et al., 2018). This raises the question how the long durations of the infra-slow dynamics can be linked to the usually shorter durations of the cognitive events or trials, such as for instance during attention. Addressing this challenge is needed to better understand the mechanisms how infra-slow dynamics modulate cognition and behavior; that is the main focus of our paper.

3.1.2 Different facets of infra-slow neural dynamics - Scale-free dynamics and variability

Neural timescale refers to the processing duration, from short to long, over which neural activity fluctuates, capturing the duration and temporal structure of brain signals (Marom, 2010). This broad concept encompasses multiple dynamical properties, such as autocorrelation window (Golesorkhi, Gomez-Pilar, Zilio, et al., 2021; Wolman et al., 2023), power spectrum density (PSD) (Manea et al., 2024), all of which describe different aspects of temporal persistence in neural activity (Northoff, 2024).

A key concept in understanding neural timescales is scale-free dynamics, which can be measured by the power-law exponent (PLE) (Fuscà et al., 2023; He, 2014; Linkenkaer-Hansen et al., 2001; S. Palva & Palva, 2018). This concept of scale-free dynamics describes temporal self-similarity in PSD, where the power distribution of smaller frequency ranges resembles the one of the entire infra-slow frequency ranges. The PLE indicates the distribution of power density/variance across frequencies, e.g. $1/f^{\beta}$: higher PLE (i.e. the value β) reflects more

power/variance in lower frequency components and vice versa (He, 2011, 2014; Y. Wang et al., 2018). Recent studies have shown that the PLE in the infra-slow frequency range is higher in transmodal association cortices like default-mode network (DMN) and lower in unimodal sensory cortex (Golesorkhi et al., 2022; Huntenburg et al., 2018; Klar et al., 2023a, 2023b). Furthermore, infra-slow PLE has been linked to various psychological and physiological functions, including aging (Ao et al., 2022), consciousness (Klar et al., 2023a), task performance (He, 2011; Kasagi et al., 2017), and rest-task modulation (Huang et al., 2017; Scalabrini et al., 2019). While these findings suggest that scale-free dynamics play a role in cognition and behavior, the precise mechanisms through which scale-free dynamics shape behavioral variability remain yet unclear. One possibility, as suggested by studies on scale-free dynamics (Jones et al., 2023; J. M. Palva & Palva, 2014), is that the brain's distribution of slow and fast frequencies may, in a complex corresponding way (Northoff, 2024), be manifest on the behavioral and cognitive level and its own variability. However, a critical question remains: How do the different neural dynamic measures (SD, SE, and PLE) interact with one another and thereby shape behavioral fluctuations?

In this study, we aim to investigate this brain-behavior relationship by examining the inter-dependencies between SD, SE, and PLE across multiple large-scale networks and their links to behavioral variability in an attention task. While our approach is primarily correlational, our findings, supported by mediation models and simulation, suggest a hierarchical structure in which PLE acts as a background constraint that modulates the relationship between neural variability (SD and SE) and behavioral fluctuations. Such layered dynamic organization is in accordance with the recently proposed "Dynamic layer model of brain" (DLB) (Northoff, 2024) that has been supported by both fMRI (Çatal et al., 2022; Wolman, Çatal, et al., 2024) and EEG (Wolman et al., 2023) studies; the present paper aims to show the key relevance of such dynamically layered organization for a specific cognitive process, namely attention.

In addition to its scale-free dynamics, the brain's neural dynamics exhibit significant variability across different timescales (Golesorkhi, Gomez-Pilar, Zilio, et al., 2021; Y. Wang et al., 2018; Wolff et al., 2022). The conception of neural variability describes the degree of change of neural activity across time (Waschke et al., 2021). The simplest and most common

measure of neural variability is the standard deviation (SD), representing the distributional width of a neural time series (Waschke et al., 2021). It has been applied in various functions in neuroimaging studies including cognition (Armbruster-Genç et al., 2016; Guitart-Masip et al., 2016), consciousness (Huang et al., 2016, 2017; Takahashi et al., 2016; Wong et al., 2013, 2016), aging (Ao et al., 2022; Grady & Garrett, 2014), and various other functions and processes (Waschke et al., 2021). This makes neural variability a promising candidate to link neural and behavioral dynamics in the infra-slow frequency range (Armbruster-Genç et al., 2016; Garrett et al., 2011, 2013; Grady & Garrett, 2018; Waschke et al., 2021; W. Xie et al., 2020).

The sample entropy (SE) estimates neural variability and specifically its predictability by analyzing the distribution of temporal patterns based on information theory, i.e., the complexity (Shannon, 1948; Waschke et al., 2021). SE has been validated and effectively used in fMRI studies (Çatal et al., 2022; Omidvarnia et al., 2016; Y. Wang, Ao, et al., 2020; Y. Wang, Wang, et al., 2019). For instance, SE of the BOLD signal was demonstrated to be related to the task performance (Nezafati et al., 2020), aging (Jia et al., 2017), and mental disorders such as attention deficit and hyperactive disorder (ADHD) (Sokunbi et al., 2013). However, the relationship between variance-based SD and information-based SE, and how they are mediated by their underlying scale-free dynamics, as measured by the PLE, remains yet unclear.

3.1.3 From neural to behavioral dynamics – what are the mediating mechanisms?

Like brain dynamics, behavioral dynamics exhibit temporal variability and share temporal patterns with neural activity (Northoff, 2024; Northoff et al., 2020a). For example, Ding and colleagues showed that MEG signals at different timescales concurrently tracked the timescales of different linguistic units such as words, phrases, and sentences (Ding et al., 2016). Evidence supports that both sustained attention and neural activity in the frontoparietal network exhibit theta rhythm (Clayton et al., 2015; Fiebelkorn & Kastner, 2019; Helfrich et al., 2018). The steady-state evoked potential (SSEP) findings revealed that the brain's neural entrainment to rhythmic stimuli, strongly supporting the alignment of brain and behavior (Lakatos et al., 2019; Northoff et al., 2023).

Together, these studies revealed direct brain-behavior connection through entrainment and alignment in the high-frequency range of EEG/MEG. This leaves open the dynamic mechanism of such brain-behavior connection in the infra-slow frequency range. A few individual fMRI studies have begun to explore this question, suggesting a potential direct relationship in this slower frequency domain. For instance, two studies using a simple reaction time task with fixed trial intervals at frequencies of 0.0625 Hz and 0.125 Hz found increased PSD at corresponding frequencies which is known as low-frequency steady-state brain response (lfSSBR) (Y.-F. Wang et al., 2014, 2016). A recent study using an n-back task also revealed that reaction time and working memory capacity are related to BOLD activity at the same frequency as stimuli presentation (Wolman, Çatal, et al., 2024). These studies suggest that behavior, neural activity, and task stimuli share their temporal structure in the infra-slow frequency range—behavior and brain activity may thus share the same infra-slow timescale, e.g., "common currency" (Northoff et al., 2020a) in their fluctuations. Such commonly shared fluctuations allow linking all three levels, external input, internal neural activity, and the subsequently resulting behavior. However, despite these advances, the mechanism through which infra-slow neural dynamics process the temporal features of the input stimuli and how that, in turn, shapes behavior across different timescales, remains yet unclear.

Sustained attention, a fundamental psychological function, exhibits fluctuations ranging from seconds to minutes (Esterman & Rothlein, 2019). These attentional fluctuations occur within the infra-slow frequency range (0.01–0.1 Hz) of neural activity and cognitive performance, highlighting the close interplay between infra-slow neural dynamics and attentional dynamics (Esterman & Rothlein, 2019; J. M. Palva & Palva, 2012; H. Zhang et al., 2022). For example, recent studies have revealed that infra-slow oscillatory transcranial direct current stimulation (tDCS) enhances performance in sustained attention tasks, advancing research on the relationship between neural dynamics and fluctuations of sustained attention (Qiao et al., 2022). Thus, investigating sustained attention fluctuations may provide important insights into the mechanisms of how infra-slow neural dynamics mediates cognitive function, e.g., the dynamical brain-behavior connection.

3.1.4 Aims, hypotheses, and procedures

In this study, we utilized the Gradual-onset Continuous Performance Task (GradCPT) paradigm to measure moment-to-moment attention fluctuations by constantly recording reaction time at intervals of 1200 ms (see Figure 12 top-left) (Esterman et al., 2013). A key advantage of this paradigm is its alignment with the fMRI sampling rate, as the repetition time (TR) of our fMRI acquisition was 800 ms. This results in an approximate ratio of 2 RT values per 3 BOLD volumes, enabling simultaneous exploration of brain and behavioral dynamics within the same infra-slow frequency range (Esterman et al., 2013). Through this approach, we aim to connect neural and behavioral dynamics, with three specific objectives and steps (conceptualized in Figure 12):

Step 1: Investigation of the rest-task modulation in GradCPT paradigm for SD, SE, and PLE in the infra-slow frequency range. We primarily hypothesized that all three measures show task-related modulation in visual and somatomotor networks, the unimodal cortex, which are thought to primarily process visual-motor inputs as required in our task (Golesorkhi, Gomez-Pilar, Zilio, et al., 2021; Margulies et al., 2016). Additionally, we hypothesized that the dorsal and ventral attention networks, important in attentional control functions, will participate in such dynamic task modulation reflecting the cognitive demands of our sustained attention paradigm (Vossel et al., 2014).

Step 2: Investigation of the connection between neural and behavioral dynamics. We hypothesized that SD and SE of the BOLD signal relates to behavioral variance (SD) although in distinct ways in the networks like the visual, somatomotor, and attention networks that are known to mediate the attention task (Vossel et al., 2014). We also suppose that the PLE will mediate the brain-behavior relationship in sensory input regions like the visual network, given its key role in input processing (Golesorkhi et al., 2022; Klar et al., 2023a, 2023b; Linkenkaer-Hansen et al., 2001; J. M. Palva & Palva, 2014).

Step 3: Investigation of the relationship of BOLD signal's SD with SE and PLE. We primarily hypothesized the three measures to reflect different facets or layers of neural dynamics as suggested in the 'Dynamic layer model of brain' (Northoff, 2024). This may be reflected by their topographical differences along for instance lower-order sensorimotor and higher-order cognitive networks (Huntenburg et al., 2018; Klar et al., 2023a, 2023b).

Furthermore, we hypothesize that the PLE, as a more comprehensive and most basic or fundamental measure operating in the neural background (Çatal et al., 2022), mediates the relationship of neural SD and SE in the neural and behavioral foreground. This step involves empirical data analysis and simulated data analysis to assess the mathematical relationship of SD and SE in dependence on varied PLE values.

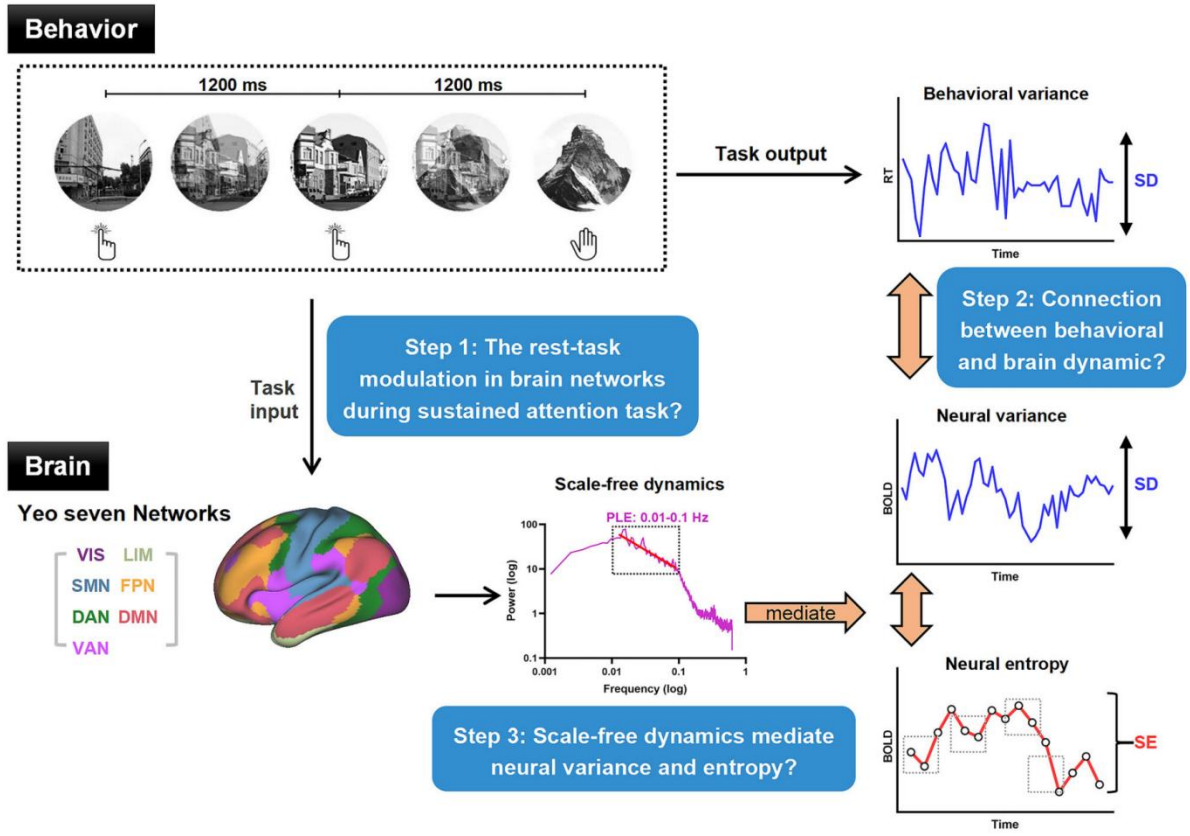

Figure 12. Concept and procedure of the current study. This Figure contains three key steps: (1) Examining the sustained attention task modulation by detecting the rest-task difference in three measures; (2) Investigating the connection between behavioral and brain dynamics by correlating neural and behavioral measures; (3) Conducting mediation analysis to assess power-law exponent (PLE) mediation on the relationship between standard deviation (SD) and sample entropy (SE).

3.2 Results

3.2.1 Differences in neural dynamics between rest and task states occur mainly in sensorimotor and attention-related cortices

This study primarily aimed to examine the differences between rest and task states using three measures of brain dynamics: SD, SE, and PLE. Figure 13A illustrates the topographical

distributions of these measures during both resting and task states. The spatial distributions of SD, SE, and PLE are significantly different from each other. For instance, during the task state, SD and PLE exhibit elevated distributions in frontoparietal network (FPN) but diminished distributions in somatomotor network (SMN) (see Figure 13A, and Supplementary Figure 11 for statistics).

Crucially, the significant t-test differences [n=49, $p<0.05$, false discovery rate (FDR) corrected] between rest and task states in these measures are consistently manifested in and overlap with each other across all three measures within unimodal regions and attention-related networks, specifically the visual network (VIS), SMN, dorsal attention network (DAN), and ventral attention network (VAN) (Figure 13B and 14). Although the changes in SD within DMN are significant, the effect is minimal when compared to the SD changes observed in the unimodal and attention-related cortices. Furthermore, the study found a decrease in the values of SD and PLE from rest to task in those networks, while SE increased in the same regions; this suggests that SE may inversely influence behavioral outcomes during our attention task.

Together, these findings reveal a consistent pattern of rest-to-task changes across all three dynamical measures (SD, SE, and PLE) in unimodal networks. However, in high-order networks such as the default mode network (DMN), only SD exhibits a task-related increase, while SE and PLE follow different patterns (schematized in Figure 13C). Importantly, this pattern was also observed after task regression (Supplementary Table 1), indicating that in unimodal networks the three measures converge in their responses to the task, whereas in higher-order networks (FPN and DMN) their changes diverge. Moreover, it shall be noted that we observed task-related decreases in both PLE and SD, whereas SE exhibited the opposite pattern, showing a task-related increase across all examined networks.

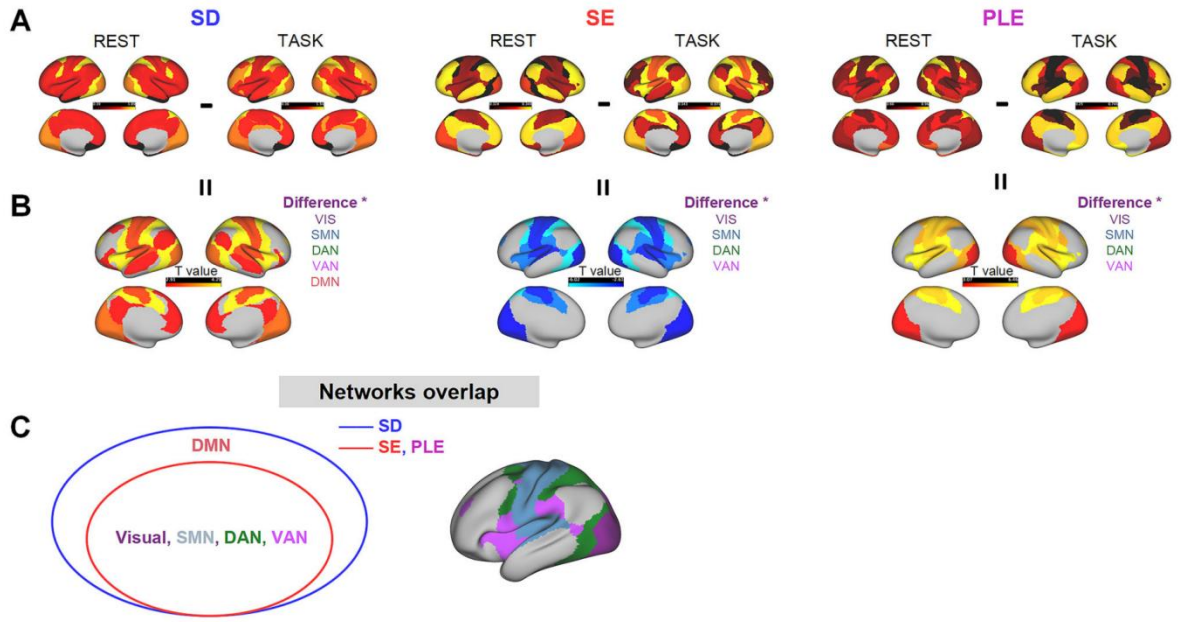

Figure 13. Rest-task difference of standard deviation (SD), sample entropy (SE), and power-law exponent (PLE). A The topographies of SD, SE, and PLE in resting and task states. B: Paired t-test results for rest-task differences within subjects (n = 49, p < 0.05, FDR corrected). C Schematics for the overlapped networks in three measures.

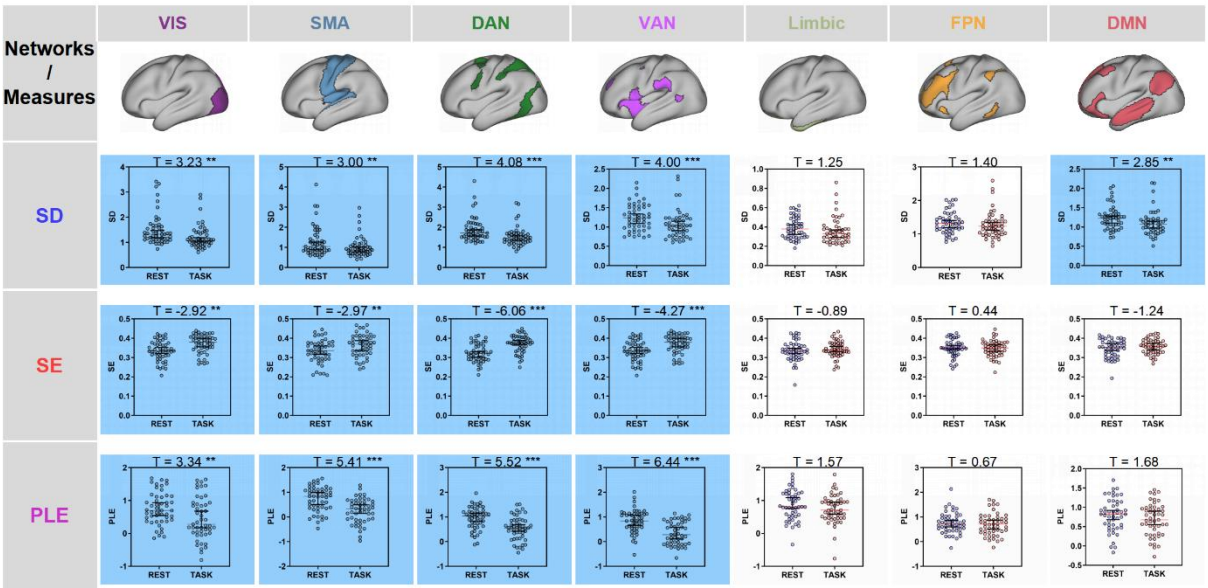

Figure 14. The statistics of rest-task differences for three measures in seven networks. Error bars in dot-plots indicate the median value with 95% confidence interval (CI) of the measure across participants (n = 49). Significance levels are denoted as follows: *p < 0.05, **p < 0.01, ***p < 0.001, ****p < 0.0001.

3.2.2 From neural to behavioral dynamics: the differentiation of brain-behavior relation through the distinct neural dynamics of SD, SE, and PLE

We next explored how the three dynamic measures correlate with behavioral performance as indexed by the SD of the RT. Figure 15A demonstrates the Pearson correlations between the three BOLD measures and RT across the seven networks at the group level (n=49, FDR corrected for 21 comparisons).

Specifically, PLE displayed significant positive correlations exclusively within the VIS, a key network predominantly involved in processing visual stimuli in our attention paradigm. A different pattern was observed in SE, which showed negative brain-behavior correlations in both the sensorimotor cortex and attention-related networks, including VIS, SMN, DAN, and VAN.

Finally, SD of RT positively correlated with BOLD SD in networks overlapping with SE but also in DMN, as shown in Figure 15B. This correlation remained significant in the task-regressed data (Supplementary Table 2). Supplementary Figure 12 shows that the distributions of SD, SE, and PLE values are approximately Gaussian with a wide range, supporting the validity of our correlation analysis. We also calculated Spearman's rank correlations (Supplementary Table 3). Although the Spearman correlations for SD and SE in the VIS and SMN (and for PLE in VIS) were nominally significant (n=49, $p<0.05$), none survived correction for multiple comparisons. This suggests that the RT–BOLD relationship is primarily linear rather than monotonic or non-linear. Moreover, the broad data distributions (Supplementary Figure 12) justify using Pearson's correlation to capture the full variability in the data.

We also examined both Pearson's and Spearman's correlations between the three BOLD measures and additional behavioral metrics, including mean RT, number of commission errors, and number of omission errors (Supplementary Tables 3-9). None of these correlations survived multiple comparison correction, indicating that the variability-based BOLD measures are primarily associated with behavioral variability, rather than with the mean behavioral performance as averaged across the single trials. Overall, we show a linear relationship between the variability of the BOLD signal and the variability of the RT.

Together, these findings suggest a hierarchical topographic-dynamic structure of brain-

behavior connections that extend from PLE to SE and SD, moving from the visual network over attention-related networks to higher-order networks like DMN. This pattern suggests distinct roles of the three measures of the dynamics of BOLD signal in mediating behavioral dynamics.

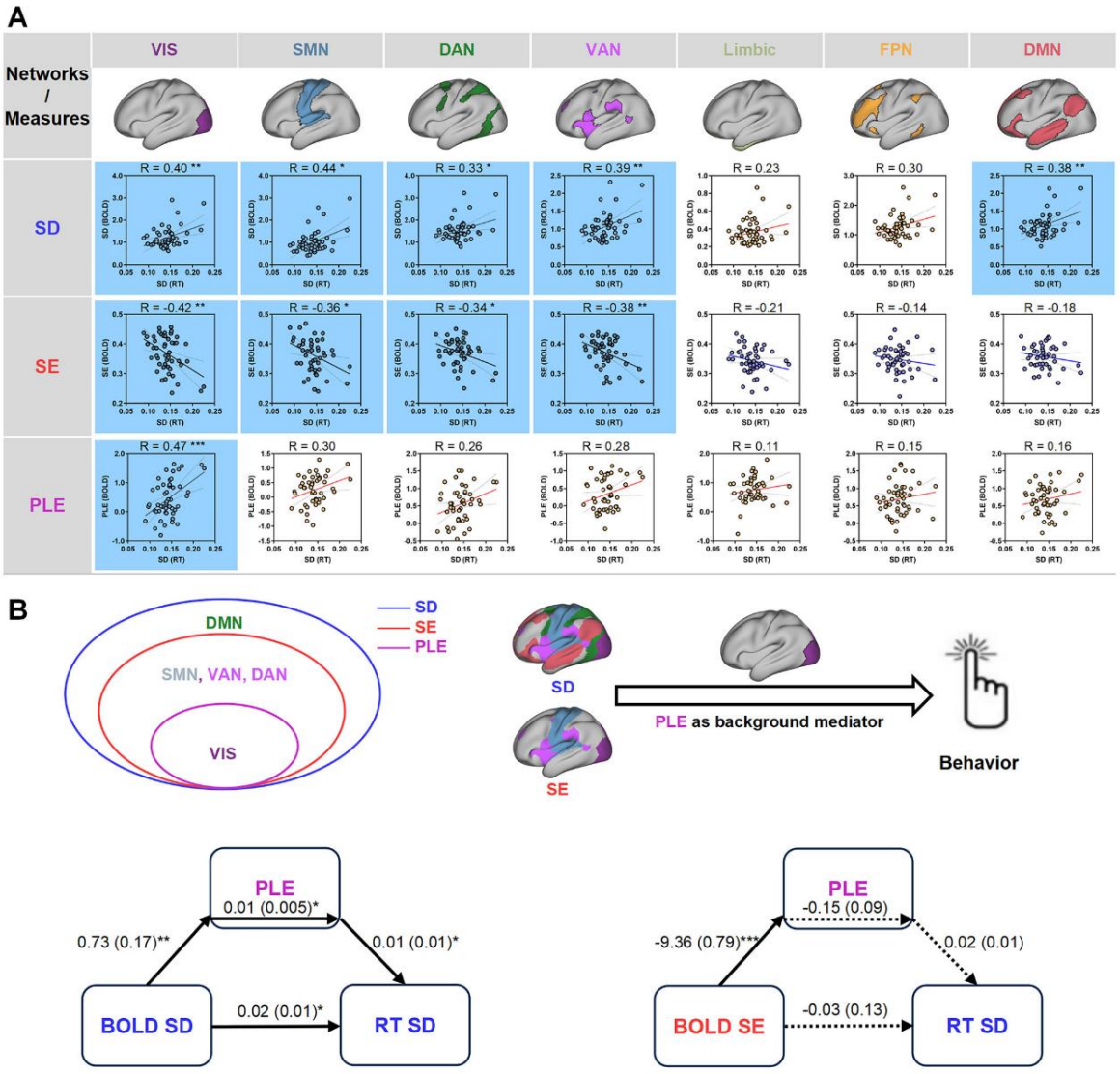

Figure 15. BOLD-RT correlation of standard deviation (SD), sample entropy (SE), and power-law exponent (PLE) at the group level in task state. A Pearson correlations for three measures in seven networks. The regression plots with blue-shaded indicate significant correlation (n = 49, FDR corrected). B The schematics for the hierarchical structure for SD, SE, and PLE. And the mediation model (n = 49) for the relationship between BOLD SD/SE and reaction time (RT) SD in task state. Significance levels are denoted as follows: *p < 0.05, **p < 0.01, ***p < 0.001, ****p < 0.0001.

3.2.3 From the neural background to the connection of neural and behavioral foreground: PLE mediates the relationship between BOLD variability and behavioral variability

Next, we raised the question about the role of PLE in mediating the relationship between neural and behavioral dynamics in VIS, which showed significant correlation between brain and behavior in all our three dynamical BOLD measures. Given that a previous study (Çatal et al., 2022) showed a mediating role of PLE, we first tested whether the relationship between BOLD and behavioral SD was mediated by PLE (Figure 15B). This indeed yielded a partial mediation effect, showing that PLE is a key factor in mediating the transition from neural variability to behavioral variability. In contrast, BOLD SE showed no significant PLE mediation effects with behavioral SD. In the task-regressed data, we found full mediation, further underscoring PLE as a fundamental background linking neural variability to behavioral variability.

Together, these findings demonstrate the key role of scale-free dynamics in operating in the neural background that facilitates the more foreground connection of BOLD variability with behavioral variance.

3.2.4 Scale-free dynamics operate as neural background for neural foreground SD and SE: their relation is strongest in the pink noise regime (empirical and simulated data)

Our findings showed that PLE, as a background index, mediates the relationship from neural variability to behavioral variability (Figure 15). This raises the question of whether PLE also operates in the neural background for the relationship of SE and SD on a purely neuro-dynamical level. To test this hypothesis, we test the relationship between PLE and other dynamical measures such as SD and SE in the seven networks.

As shown in Figure 16A, we first examined the correlations among the three measures in seven networks (n=49). There were consistently negative correlations between SE and the other two measures in every network. The relationship between SD and PLE appeared non-linear in VIS and SMN, showing a second-order polynomial trend, whereas in other networks, the association was more linear but with lower R^2 values. Visual inspection suggested that the observed non-linearity stemmed from an inflection point at PLE = 0 in VIS and SMN for some subjects, indicating a potential transition from blue noise to pink noise. Based on this observation, we hypothesized that the mediation effects of PLE may differ depending on

whether PLE values are above or below zero.

To test this hypothesis, we examined how PLE modulates the correlation between SD and SE within simulated data. For this purpose, we generated time series data with different PLE regimes, corresponding to distinct noise types: white noise (PLE = 0), pink noise (PLE = 1), and blue noise (PLE = -1).

White noise (PLE = 0) is characterized by a flat power spectrum, indicating that all frequencies contribute equally, resulting in a highly unstructured and random signal. Pink noise (PLE = 1), in contrast, follows a 1/f power distribution, meaning that lower frequencies dominate, leading to long-range temporal correlations that are commonly observed in biological and cognitive systems. Blue noise (PLE = -1) exhibits the opposite trend, with power increasing at higher frequencies, generating rapid fluctuations with little persistence over time.

As shown in Figure 16B, in conditions when PLE = -1 (blue noise) or PLE = 0 (white noise), there was no correlation between SD and SE. In contrast, their correlation begins to increase when PLE exceeds 0. Remarkably, this correlation value approaches -1, indicating a fully negative correlation in the presence of pink noise (PLE = 1), which aligns well with our empirical findings.

Together, both empirical data and simulation findings support: 1) the relationship between BOLD SE and SD, and 2) the modulation of their relationship by PLE, which 3) only holds in certain regimes where it relates to pink noise as distinguished from both blue and white noise. This observation underscores the critical role of the PLE in modulating the interaction of BOLD SD and SE, particularly under conditions mimicking biological noise patterns, such as pink noise.

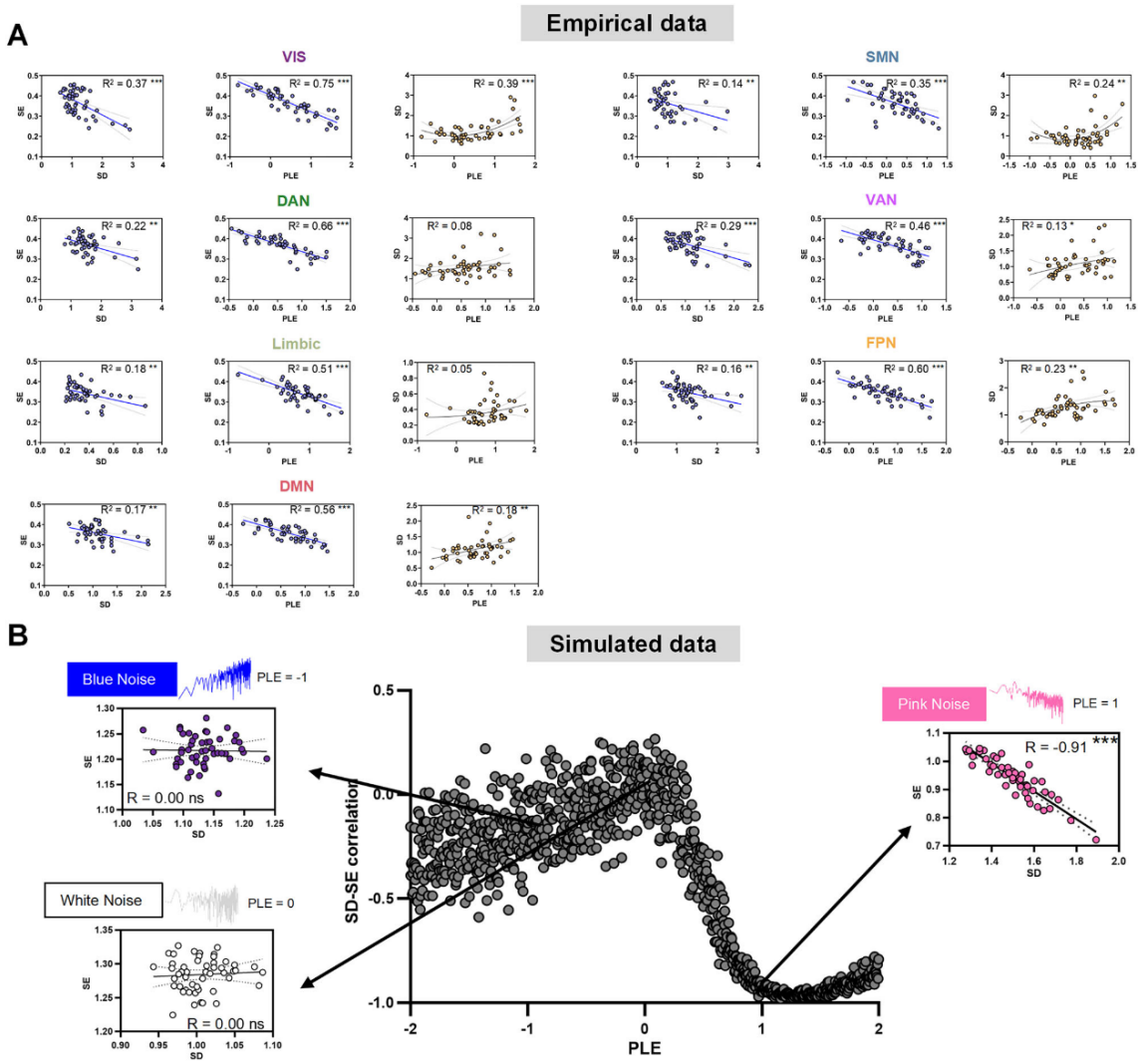

Figure 16. Power-law exponent (PLE) as the mediator for brain-behavior and standard deviation (SD)-sample entropy (SE) relationship. A Correlations between three measures (n = 49). B The relationship between SD and SE mediated by varying PLE in simulated data. Scatter plots depicted the correlations (n = 49) between SD and SE under PLE = -1, 0, and 1.

3.3 Discussion

The brain-behavior connection is a fundamental question in cognitive neuroscience. Previous research has primarily investigated the neural mechanisms of cognitive processes at high frequencies. However, recent advancements have highlighted the importance of infra-slow frequency dynamics in mediating behavior although the exact mechanisms remain yet unclear. In our study, we provide evidence that three neural dynamic measures—SD, SE, and PLE—are related to behavioral variability, the SD of RT, on an infra-slow timescale in the range of 0.01 to 0.1 Hz.

Notably, we also show that PLE, SD and SE take on distinct roles in mediating brain-behavior connection in our sustained attention task. Specifically, showing in both empirical and simulated data, PLE seems to operate in the neural background from where it mediates the more foreground neural connection of SE and SD as well as the latter's dynamic relationship with the dynamics of the behavior, e.g., SD of RT. That is further supported by our simulation showing a mathematical relationship of SD and SE through their mediation by scale-free dynamics (PLE).

Together, we demonstrate the key relevance of infra-slow dynamics and its distinct features, SE, SD and PLE, in mediating behavioral dynamics along a background-foreground distinction. This sheds light on the key role of the brain's infra-slow dynamics for behavior including its mechanisms that mediate cognitive-behavioral dynamics.

3.3.1 The brain-behavior connection in the infra-slow frequency range

Recent cognitive neuroscience research increasingly emphasizes the importance of large-scale networks in understanding the brain mechanisms underlying human attention (Fox et al., 2005; H. Zhang et al., 2022). Many studies have highlighted the significance of the DMN and the FPN in attention, linking them to the inverse attentional processes involved in attention-demanding tasks (Andrews-Hanna et al., 2010; Buckner & DiNicola, 2019; Clayton et al., 2015; Fiebelkorn & Kastner, 2019). Additionally, the GradCPT study revealed the activation of the DMN, the DAN, and regions within the FPN during tasks, associating these networks with changes in attentional capacity (Esterman et al., 2013).

Our current findings align with these observations while also extending previous research. Notably, our study demonstrates consistent modulation of neural dynamics between rest and task states in the VIS, SMN, DAN, and VAN networks, which are associated with the unimodal cortex. In contrast, within transmodal/high-order networks (including the Limbic network, FPN, and DMN), only SD exhibited task-related changes in the DMN. This distinction suggests that while the three dynamic measures (SD, SE, and PLE) follow similar patterns of rest-task modulation in unimodal regions, they diverge in transmodal networks, particularly the DMN.

This divergence may reflect differences in functional specialization between unimodal and transmodal regions. The unimodal cortex primarily processes sensory inputs and motor responses, which are directly engaged by task-related demands, leading to synchronous changes across different measures of neural variability (SD, SE, and PLE). In contrast, transmodal networks, such as the DMN, integrate information across multiple cognitive domains, including internal mentation, memory, and attentional control (Buckner & DiNicola, 2019; Cheng et al., 2020). The fact that only SD exhibited task-related changes in the DMN, while SE and PLE did not, suggests that SD may be more sensitive to cognitive control mechanisms unique to transmodal regions (H. Zhang et al., 2022), whereas SE and PLE may predominantly reflect background neural dynamics that remain stable in these higher-order networks. Thus, our findings do not simply indicate a dynamic characterization of lower-order visual processing. Instead, they highlight how neural variability differentially tracks changes in brain states depending on the functional role of the network for subsequent behavior—being more homogeneous in unimodal networks but more heterogeneous in transmodal regions.

In line with the rest-task modulation findings, our core discovery is the differentiated roles of neural SD, SE, and PLE in their correlation with behavior. All three measures correlate with behavioral performance but differ across brain networks. We found that SD significantly correlates with behavior in the DMN, while SE does not, consistent with the rest-task difference findings. Additionally, the VIS network showed significant correlation with RT SD across all three measures. Importantly, the VIS was the only network where RT SD significantly related to the neural PLE, highlighting its role in processing visual inputs in a visual-demanding task

like ours (Beltramo & Scanziani, 2019; Kastner & Ungerleider, 2000).

Notably, both SD and SE exhibited significant behavioral correlations in the SMN, DAN, and VAN, networks specifically involved in sustained attention tasks. In contrast, PLE did not show significant behavioral correlations in these networks. This divergence between PLE and SD/SE suggests that PLE functions as a topographic and dynamic background measure, which appears to be less sensitive to specific cognitive-attentional task demands. In other words, while SD and SE reflect task-related fluctuations in brain activity that are closely tied to performance in attention-related tasks, PLE operates more as a general and task-unspecific measure of neural dynamics that is not directly influenced by the specific demands of the task. This distinction in the roles of PLE, SD, and SE is further supported by our other findings, indicating that each measure may capture different aspects of brain dynamics.

3.3.2 Scale-free dynamics regulates the SD-SE and brain-behavior relationship: the main contribution of the low-frequency oscillatory component

To investigate the background role of scale-free dynamics and the differential roles of SD and SE, as well as their relationship, we examined the mediation effect of PLE on the correlation between neural variability and behavioral variability as well as its modulating effects on the purely BOLD correlation of SD and SE. First, we found that PLE significantly mediates the relationship between BOLD SD and behavioral SD but not between BOLD SE and behavioral SD. This suggests again a special role for PLE as distinct from both SD and SE in mediating behavioral dynamics. Moreover, it also implies differential roles of SE and SD which again further supports our findings of their subtle differences in the networks of their rest-task modulation. Accordingly, our findings strongly indicate differential roles of PLE, SE and SD in mediating brain-behavior relationship suggesting a layered-like organization of the brain's neural dynamics in mediating behavioral dynamics (Northoff, 2024).

The special role of PLE operating in the neural background is further supported by the purely neuronal, e.g., BOLD relationship of PLE with SE and SD. Our results show that both SD and PLE are negatively correlated with SE, consistent with a previous study (Çatal et al., 2022). A notable finding is the non-linear relationship between SD and PLE, with an inflection

point at approximately PLE = 0. The simulated data further support the results of the non-linear relationship between SD and PLE from real data. During both blue noise (PLE = -1) and white noise (PLE = 0), the correlations between SD and SE are close to zero. In contrast, when PLE increases to 1 (pink noise), the correlation between SD and SE evolves to a nearly full negative correlation in our simulation just as we observe it in our empirical data: as the signal's scale-free dynamics increases moving from white to pink noise, SD and SE start relating to each other.

The underlying idea is that scale-free dynamics, such as those seen in pink noise, provide a temporal background structure in the neural activity that facilitates the more foreground connection between two distinct aspects of neural variability, SD (which reflects the fluctuation magnitude) and SE (which measures the complexity or entropy). These two measures, which operate on different timescales, become more related with each other in the presence of scale-free dynamics. This connection between SD and SE may thus be mediated by the temporal structure of pink noise which, in turn, plays a key role in linking neural dynamics to behavioral outcomes (Çatal et al., 2022).

While we pointed out the differentiation of distinct layers of neural dynamics, e.g., background and foreground, their relationship to physiological and psychological features remains yet unclear. The PLE is measured across the whole frequency range which renders it a perfect candidate to serve as more global (here understood in a temporal sense in terms of the range of frequencies) background measure. In contrast, cognition and behavior require specific frequencies in both high frequency (Busch et al., 2009; Hua et al., 2022) and also within the infra-slow frequency range (Qiao et al., 2022; Y. Wang, Huang, et al., 2019). Together, our findings suggest a topographic-dynamic organization with various layers organized along a gradient from the global brain including all its regions and frequencies/scale-free dynamics (PLE) to more local activity with specific regions and frequencies (SD, SE) specific and restricted regions and frequencies/oscillations (SE, SD) which, in turn, modulates behavior, e.g., SD of RT. That is well in accordance with and supports the recently proposed 'Dynamic layer model of brain' as an integrated dynamic-topographic brain-mind model (Northoff, 2024) (see below for details).

Another though not exclusive perspective is the concept of energy reallocation in PSD, describing the change in the distribution of power in PSD to meet the temporal structure of cognitive tasks (Y. Wang et al., 2018; Y.-F. Wang et al., 2015, 2016). In the current GradCPT task, subjects were required to respond to ever-changing stimuli that demand sustained attention on a faster timescale. Thus, the specific task shifts the brain signal to a faster timescale to meet the fast-changing input, resulting in a loss of low-frequency energy, explaining the decrease in low-frequency power as well as the PSD. This also partly explains the increased SE in the task state: as the ratio of low/high-frequency power decreases, the details/information in a signal increase (Koverda & Skokov, 2012) which is well compatible with our observation of task-related decreases in PLE and SD accompanied by concurrent SE increase.

3.3.3 The Dynamic Layer Model of the Brain: Bridging Neural Activity, Cognition, and Behavior

Together, both our empirical and simulation findings suggest a background-foreground distinction and organization in the brain's neural dynamics which is well in line with other empirical findings (Fuscà et al., 2023; Wolman, Çatal, et al., 2024), and, on a more theoretical level, with the Dynamic layer model of brain (DLB) (Northoff, 2024). Roughly, the DLB characterizes and defines the brain by the dynamic features of its neural activity that are supposed to be organized along different layers featured by their distinct timescales ranging from long to short. This does not mean that the DLB is a purely neural model of the brain, though. The DLB targets a deeper layer of the brain, namely the dynamics of its neural activity and how, that, in turn, modulates its cognitive and behavioral function. Such layered dynamical organization of the brain's neural activity distinguishes the DLB from other brain models like the predictive coding model (Friston, 2010) that, rather than on neural activity itself, focus more on the brain's neural function like its cognitive function, and its underlying computational mechanisms.

The results of the present and others (Chuipka et al., 2025; Wolman, Lechner, et al., 2024; Wolman, Çatal, et al., 2024) demonstrate clearly how such dynamically- and topographically-layered organization modulates both cognition and behavior as indices of the brain's neural function. The rest-task PLE increase in visual cortex suggests that it plays a key

role in the temporal encoding (and processing) of the paradigm's input and its temporal structure, e.g., entrainment (Lakatos et al., 2019) and alignment (Northoff et al., 2023) (see also Klar et al. 2023, Wolman et al. 2024 for similar findings). This presents the deepest dynamic layer of the brain. A next layer allows for temporal integration of the various inputs, e.g., trials of the task, over time as possibly mediated by information complexity as measured by SE. That is complemented by yet another layer of neural variability (SD) which provides temporal feature of the output, e.g., the reaction time and its behavioral variability – this is supported by their correlation.

Together, our findings demonstrate three dynamic layers of the brain's neural activity and their respective mechanisms including (i) scale-free dynamics with temporal input encoding, (ii) information complexity/entropy allowing for temporal input integration; and (iii) neural variability providing temporal feature of the behavioral output and its variability. Reflecting different layers of the brain's neural dynamics, these temporal mechanisms allow connecting input and output through their shared dynamics. This is manifest in the brain's dynamic shaping of its cognition which stands at the very core of what we recently introduced as "Spatiotemporal Neuroscience" (Northoff, 2024; Northoff et al., 2020a, 2020b).

3.3.4 Limitations

Several limitations should be noted. Firstly, our experimental paradigm involved behavioral responses in a highly controlled environment with limited dynamics. The human brain operates on multiple timescales, which need to be investigated in natural environments that provide complex inputs aligning with real-world brain function. For instance, music and movie stimuli have been shown to trigger complex brain responses, including changes in functional connectivity. To our knowledge, no study, including our current one, has explored the complex dynamical relationship between brain and behavior across multiple timescales using natural stimuli. Our study may pave the way for investigating the brain-behavior connection in varied timescales.

A critical aspect of our study is the differentiation between fractal and oscillatory properties in the PSD. We focus exclusively on the former, specifically the PLE. While the

scale-free nature of the background supports cognitive functions—such as attention in our case—oscillations also play a significant role, particularly when considering the timescale in certain frequency points. These oscillations may serve as a stronger indicator of behavioral variability, as suggested by (Wainio-Theberge et al., 2022). To date, only a limited number of fMRI studies have examined the oscillatory component within the infra-slow frequency range, such as in the context of aging (Ao et al., 2022). However, no research has yet explored its cognitive implications. Further investigation is needed to understand the cognitive relevance of this oscillatory component.

Some methodological considerations should be noted. Firstly, we applied the sample entropy calculation with parameters m = 2 and r = 0.5. Although these parameters are commonly used and validated by previous studies (Çatal et al., 2022; McDonough & Nashiro, 2014; Omidvarnia et al., 2021), further methodological research is necessary to explore the impact of different sample entropy parameters. The parameter m is particularly important as it represents the time length of the mode, which is sensitive to the intrinsic timescale of the data. Furthermore, our analysis focused on the conventional infra-slow frequency range of 0.01-0.1 Hz, which is considered to have a higher signal-to-noise ratio and is less influenced by physiological noise. However, many studies have emphasized that important neural information is also contained in higher frequencies (>0.1 Hz) (Buzsáki & Draguhn, 2004; X.-N. Zuo et al., 2010). Future research should investigate these dynamical measures, particularly scale-free dynamics, across a broader frequency range. This approach would provide a more comprehensive understanding of the relationship between brain and behavior across the full spectrum of timescales, from longer to shorter durations.

3.4 Conclusion

In the current study, we demonstrated the direct connection of the behavioral dynamics of task performance during sustained attention with the dynamics of the infra-slow frequency BOLD activity. Based on our research, we propose that the temporal dynamics and their relationship to behavior, and more importantly, the layered structure of SD, SE, and PLE, play an important role in organizing the different temporal features of the brain's task-related processing including its link to behavioral dynamics. This supports the idea that infra-slow

frequency scale-free dynamics with its nested faster timescales as a global component (Buzsáki, 2006; Northoff & Zilio, 2022), like the PLE, provides a "neural background" for cognitive function such as sustained attention, serving as a fundamental function for other cognitive functions operating in the foreground (Esterman & Rothlein, 2019). This is well in line with the recently proposed 'Dynamic layer model of brain' (DLB) (Northoff, 2024) which, briefly, proposes that the brain's dynamically layered neural activity is instrumental in mediating and shaping behavior and cognition.

Together, our findings emphasize the importance of scale-free dynamics and neural timescales, their spatiotemporal structure, in influencing neural and behavioral dynamics, advancing the understanding of fMRI low-frequency activity and its relation to cognitive functions (Northoff et al., 2020b, 2020a). These findings serve as a catalyst for future research, enabling more nuanced dynamic and topographic examinations of infra-slow frequency brain dynamics in brain-behavior connection including its abnormalities in mental disorders.

3.5 Methods

3.5.1 Participants and experiment design

The study recruited 49 healthy adult participants at Sichuan Normal University, comprising 24 males and 25 females (age of 21.15 ± 2.10 years). All participants were confirmed to have no psychiatric disorders and were not taking any psychiatric medications. They were required to abstain from alcohol and caffeine for 24 hours before the experiment and to maintain regular sleep patterns. The experimental procedures received approval from the Ethics Committee of the Institute of Brain and Psychological Sciences at Sichuan Normal University. All ethical regulations relevant to human research participants were followed.

Participants underwent two scanning sessions: the first session was conducted during resting state, followed by the task state. In the resting state, participants were instructed to lie down, eyes open with focus on the cross on the center of the screen, and rest without engaging in specific thought processes for 8 minutes.

The Gradual-onset Continuous Performance Task (GradCPT) paradigm is employed to

assess sustained attention (refer to Figure 12, top-left panel) (M. Rosenberg et al., 2013; M. D. Rosenberg et al., 2016). The GradCPT involved 10 circular grayscale images of urban scenes and an equal number of mountain scenes, standardized in size and grayscale. The task displayed an asymmetrical distribution in GradCPT, with mountain images comprising 10% and urban images 90% of the trials. The sequence of image presentation was randomized to prevent the consecutive display of images from the same category. Transitions between images were achieved by gradually altering their transparency: the outgoing image faded from opaque (0% transparency) to fully transparent (100%), and the incoming image transitioned from fully transparent back to opaque. This fading process lasted for 1200 milliseconds, maintaining constant grayscale and brightness to minimize the potential attentional effects caused by abrupt changes in the stimuli. Participants were tasked with pressing a key using their right thumb when they confidently identified an urban scene and were instructed to refrain from pressing any key upon recognizing a mountain scene. The task comprised 400 trials and spanned 8 minutes, during which response times and errors were recorded.

3.5.2 fMRI data and preprocessing

Imaging data were acquired using the Siemens 3-T connectome-Skyra scanner at the Brain Imaging Center of Sichuan Normal University. The scanning sequence employed was Gradient-echo echo planar imaging (EPI), with a repetition time (TR) of 800 milliseconds, echo time of 38 milliseconds, flip angle of 52 degrees, field of view of 208x180 mm, slice thickness of 2 mm, 72 slices, and a voxel resolution of 2x2x2 mm.

The preprocessing of fMRI data was performed using fMRIPrep version 23.0.2 with default settings (Esteban et al., 2019). The processed data were output in the "fsaverage5" surface format in CIFTI files for subsequent preprocessing and analysis stages. After discarding the initial four time points, we removed artifacts related to six estimated head motion parameters (x, y, z translations and rotations), frame-wise displacement (FD), as well as signals from white matter and cerebrospinal fluid. Finally, we extracted signals corresponding to seven brain networks from the Yeo et al. 2011 template: visual (VIS), somatomotor (SMN), dorsal attention (DAN), ventral attention (VAN), limbic, frontoparietal (FPN), and default-mode (DMN) networks. These signals were then filtered using an ideal filter with a passband of 0.01

Hz to 0.1 Hz.

3.5.3 Behavioral and stimulus confounds control analysis

For each voxel, after performing standard nuisance regression during preprocessing, we applied an additional general linear model (GLM) to account for potential stimulus-related confounds (Fair et al., 2007). In this GLM, each stimulus presentation was modeled as an impulse event, convolved with a canonical hemodynamic response function, and included as regressors for three task-related event types: correct omissions, commission errors, and omission errors. We did not regress out correct commission events (accurate responses to non-target city scenes) because their high frequency effectively defined the continuous "task state." All analyses were then repeated on the residual time series from this regression (the "task-regressed" data), and the results are reported in Supplementary Tables 1-2 and Supplementary Figure 13. This process is consistent with a previous GradCPT study (Fortenbaugh et al., 2018).

3.5.4 Behavioral data and their measures

Response times (RTs) were examined using methods established in previous GradCPT studies (Esterman et al., 2013, 2014; Qiao et al., 2022). In the GradCPT paradigm, each image is gradually revealed over a 1200-ms period until it reaches full clarity. Importantly, the transition to the next image begins immediately once an image is fully presented at 1200 ms. RTs were measured from the onset of each image transition. Thus, an RT of exactly 1200 ms indicated a response at the point of full image clarity, without overlap with the following image. RTs shorter than 1200 ms suggested that the participant responded while the image was still transitioning from the previous one. Conversely, RTs longer than 1200 ms showed responses during the transition to the next image. In cases of significantly aberrant RTs (either before 70% clarity of the current image or after 40% clarity of the subsequent image) or multiple responses, we employed an iterative algorithm to optimize the accuracy of recorded responses. Initially, the algorithm allocated clearly correct responses, leaving a minimal number of ambiguous responses (less than 5% of trials).

Ambiguous responses were reassigned to adjacent trials that lacked a recorded response. When two consecutive trials were missing responses, the ambiguous response was allocated to

the trial closest in time, except if that trial was a no-go—in which case the absence of a response was treated as a correct omission. If multiple responses occurred within a single trial, only the fastest response was considered valid. In instances where two consecutive trials remained without clear reassignment, the missing RTs for city and mountain scenes were imputed using the median RT for each scene type within that run.

Following these adjustments, we computed the standard deviation (SD) of RTs as an index of sustained cognitive performance, instead of mean of RTs, consistent with previous studies (Esterman et al., 2013; M. Rosenberg et al., 2013). A lower SD reflects more stable response patterns, which are associated with higher vigilance and sustained attention in the GradCPT paradigm. In other words, RT variability reflects fluctuations in attentional stability, whereas the mean RT is primarily influenced by the periodic response to the fixed stimulus interval. This metric has been widely used and replicated in prior studies employing GradCPT to assess cognitive performance, vigilance levels, as well as its neural mechanism (Esterman & Rothlein, 2019; Fortenbaugh et al., 2018).

The study did not focus on reaction accuracy where subjects mistakenly responded to mountain images or incorrectly identified city images, as the primary goal was to establish a link between the variability of RT time series and BOLD signals. Hence, error trials were excluded from the time series, and interpolated the missing RT value of these trials by cubic spline interpolation to preserve the time-frequency feature (Qiao et al., 2022). However, to enhance data transparency in brain-behavior correlation analyses, we reported the results for error trials, including commission errors (responses to mountain images), omission errors (missed responses to city images), and the mean RTs (Supplementary Table 4, 5, and 6).

3.5.5 fMRI data measures

SD: SD is a common metric for evaluating signal variance and has been widely used in fMRI studies. It represents the distributional width of BOLD signals (Waschke et al., 2021). Previous studies have shown that SD carries important physiological and psychological significance, not merely signal noise (Dinstein et al., 2015; Stein et al., 2005; Uddin, 2020). In our study, we applied MATLAB's 'std' function to calculate the SD of the BOLD time series

for each network and participant.

SE: Sample entropy (SE) is a measure of complexity or regularity, originally developed to assess the unpredictability of fluctuations in time series data (Richman & Moorman, 2000). Unlike its predecessor, approximate entropy, SE does not include self-matches, resulting in a more consistent discrimination of complex signals (Cieri et al., 2021; Richman & Moorman, 2000). This measure is particularly useful in fMRI studies for evaluating the complexity of neural signals. It functions by identifying repeated patterns; a higher frequency of repetitions indicates more predictable and structured data.

The key parameters used in the calculation of SE were the pattern length m and the similarity factor r. The embedding dimension m was set at 2, which considers pairs of points in constructing the template vectors. The tolerance r, representing the width of the similarity criterion, was set to 0.5 times the standard deviation of the time series.

The formula used for Sample Entropy is:

$$SE(m, r, N) = -\ln(\frac{A}{B})$$

where N is the length of the time series, A is the number of matches for templates of length m + 1 that remain similar for m points, excluding self-matches, and B is the number of matches for templates of length m. Two patterns match if the distance is less than r. The value setting of m and r is consistent with prior fMRI research (Çatal et al., 2022; McDonough & Nashiro, 2014; Omidvarnia et al., 2021). Our SE calculation script is accessible at http://www.georgnorthoff.com/code.

In sum, higher values of SE indicate greater signal complexity, suggesting less predictable neural activity, whereas lower values denote more predictable neural patterns. Although the use of SE in fMRI data can be criticized due to the thermal noise component in the fMRI signal (Liu, 2016), previous studies have confirmed SE's validity and effectiveness in distinguishing between different brain regions and systems, highlighting its ability to mirror the hierarchical structure and functional diversity of brain systems (Çatal et al., 2022; Omidvarnia et al., 2021).

PLE: The power-law exponent, often denoted as the scaling exponent β, is a critical measure in understanding the temporal scaling properties of time series data (He, 2011, 2014). To calculate the PLE, we firstly get a power spectral density (PSD) of a time series. Then the log-log plot of the frequency versus power from the PSD was used to determine the power-law relationship. The PLE, represented by the scaling exponent β, corresponds to the negative slope of this log-log plot, as determined by linear regression in log-log space (Çatal et al., 2022; Klar et al., 2023a, 2023b). This method was utilized, restricting the frequency range to 0.01–0.1 Hz to mitigate interference from scanner drift and physiological noise. Notably, visual inspection (see Figure 12, schematic for PLE) reveals no apparent oscillatory component within the 0.01-0.1 Hz range, suggesting that the PLE calculation is primarily influenced by the 1/f component. This approach aligns with established methodologies, and our script for calculating PLE is also available at http://www.georgnorthoff.com/code.

The value of the power-law exponent β offers insights into the intrinsic timescale of brain activity. A $\beta = 1$ exponent suggests pink noise, which is typical for many biological systems. In contrast, lower values of β (closer to 0) indicate a flatter spectrum, reflecting more transient and unstructured dynamics. This measure has been linked to shifts in attention, arousal, and pathology-related alterations in brain function (He, 2014; Jones et al., 2023; Klar et al., 2023a, 2023b).

3.5.6 Mediation model analysis

To examine whether the power-law exponent (PLE) mediates the relationship between response time variability (RT SD) and brain signal variability, we conducted a mediation analysis using the CANLAB mediation toolbox for MATLAB (Shrout & Bolger, 2002; Wager et al., 2008). Specifically, we tested two mediation models:

1. PLE as a mediator between BOLD signal variability and RT variability:

-The independent variables were the standard deviation (SD) and sample entropy (SE) of BOLD signals during the task.

-The dependent variable was RT SD.

-PLE served as the mediator, allowing us to assess whether neural timescale properties (PLE) explain the link between BOLD signal variability and behavioral variability.

2. PLE as a mediator between different measures of BOLD signal variability:

-The independent variable was the SE of BOLD signals.

-The dependent variable was the SD of BOLD signals.

-PLE was tested as a mediator to evaluate whether infra-slow scale-free dynamics contribute to the relationship between different forms of BOLD variability.

We assessed the significance of direct and indirect effects using a bootstrapping approach with 10,000 resampled iterations, generating 95% confidence intervals. This allowed us to determine whether the mediation effects were statistically robust.

3.5.7 Simulation analysis

To investigate the mathematical relationship between SD and SE under varying PLE, we generated 1000 samples of colored noise consistent with different PLE values. This simulation utilized MATLAB's built-in function "dsp.ColoredNoise," covering PLE values ranging from -2 to 2 at equal intervals. Both SD and SE were calculated in these simulations to explore how PLE influences their relationship.

3.5.8 Statistics and reproducibility

A significance threshold of $p < 0.05$ was applied for all two-sided statistical tests. Sample sizes are reported in the main text. The statistical methods and multiple comparison correction procedures are detailed below.

Difference analysis: We conducted difference analyses using paired t-tests for SD, SE, and PLE of BOLD signals. These analyses encompassed comparisons between rest and task state and the z-scores of the three measures in task state across seven networks.

Behavior-brain correlation analysis: To investigate the relationship between behavioral variability and three BOLD measures, we performed Pearson's correlation analyses: 1) For each subject, we extracted one behavioral measure (RT SD) and three BOLD measures (SD,

SE, and PLE) within each of the seven networks. 2) We then computed Pearson's correlations between RT SD and each of the three BOLD measures within each network, yielding a group-level behavior-brain correlation for each network. 3) Additionally, Pearson's correlations were computed among the three BOLD measures within both empirical data and simulated data (Figure 15).

Three BOLD measures correlations: To assess the relationships between SD, SE, and PLE, we initially computed Pearson's correlations. However, given that visual inspection of scatter plots suggested non-linear trends, particularly in VIS and SMN, we also performed polynomial regression analyses to better capture these relationships. Specifically, we fitted second-order polynomial models and compared their R^2 values to those of linear models. This approach allowed us to determine whether non-linear relationships were more appropriate for specific networks.

Multiple comparison correction: Statistical tests (21 analyses across seven networks and three measures—SD, SE, and PLE; seven networks × three BOLD measures) were corrected for false discovery rate (FDR) using the linear step-up procedure introduced by (Benjamini & Hochberg, 1995).

4 STUDY 3: Spatiotemporal dedifferentiation of the global brain signal topography along the adult lifespan

Ao, Y., Yang, C., Drewes, J., Jiang, M., Huang, L., Jing, X., Northoff, G., Wang, Y., 2023. Spatiotemporal dedifferentiation of the global brain signal topography along the adult lifespan. Human Brain Mapping 44, 5906–5918. https://doi.org/10.1002/hbm.26484

ABSTRACT

Age-related variations in many regions and/or networks of the human brain have been uncovered using resting-state functional magnetic resonance imaging. However, these findings did not account for the dynamical effect the brain's global activity (global signal/GS) causes on local characteristics, which is measured by GS topography, though. To address this gap, we tested GS topography including its correlation with age using a large-scale cross-sectional adult lifespan dataset (n = 492). Both GS topography and its variation with age showed frequency-specific patterns, reflecting the spatiotemporal characteristics of the dynamic change of GS topography with age. A general trend towards dedifferentiation of GS topography with age was observed in both spatial (i.e. less differences of GS between different regions) and temporal (i.e. less differences of GS between different frequencies) dimensions. Further, methodological control analyses suggested that although most age-related dedifferentiation effects remained across different preprocessing strategies, some were triggered by neuro-vascular coupling and physiological noises. Together, these results provide the first evidence for age-related effects on global brain activity and its topographic-dynamic representation in terms of spatiotemporal dedifferentiation.

Keywords: brain aging; fMRI; spatiotemporal dedifferentiation; global signal topography; lifespan.

4.1 Introduction

The human brain is a dynamic system that undergoes continuous change throughout the lifespan (Ferreira & Busatto, 2013; Lou et al., 2019; Vij et al., 2018; Xia et al., 2019), which can be *in vivo* measured by resting-state functional magnetic resonance imaging (rs-fMRI) (Ferreira & Busatto, 2013; Xia et al., 2019; X. N. Zuo et al., 2019). Using rs-fMRI, a host of studies have documented altered functional organization of spontaneous brain activity with age, such as increased or decreased functional connections (FC) in almost all intrinsic functional networks (Ferreira & Busatto, 2013; Tian et al., 2018; Tomasi & Volkow, 2012; Vij et al., 2018). The widespread regional and network changes suggest a global alteration of brain activity in the aging brain.

Global brain activity can be measured by the global signal (GS), which is the mean of the whole brain blood oxygen level dependent (BOLD) signal (Power et al., 2014, 2017). Initially considered to be non-neuronal noise (Power, 2019; Power et al., 2014, 2017), recent studies have demonstrated a close association between GS and neurobiological activities (Fox et al., 2009; Murphy & Fox, 2017) such as local field potentials (Schölvinck et al., 2010). The GS is manifested in different extents across various brain regions, resulting in GS topography, which is defined as the correlation between GS and local signals (GSCORR) (G. J. Yang et al., 2016). Recently, the GS topography has been suggested to be an essential marker of psychopathological symptoms, cognitive tasks, and consciousness states (Tanabe et al., 2020). Given that the aging brain is featured with universal neural and cognitive decline (Koen et al., 2020), GS topography may delineate global changes during brain aging, providing insights into the process of healthy aging and serving as the baseline of geriatric diseases.

In addition, the functional organization of brain networks is constrained by time scales from seconds (De Domenico et al., 2016; Y. Wang, Zou, et al., 2020) to decades (A. C. Yang et al., 2013; L. Yang et al., 2018). In the short time scale, frequency-specific FC has been widely identified to be a core neurophysiological mechanism of brain function (Adaikkan et al., 2019; Buzsáki, 2006; Fiebelkorn & Kastner, 2019; S. Han et al., 2017; Perrault et al., 2019; Y.-F. Wang et al., 2016; Watrous et al., 2013). For example, frequency-specific alteration of the GS topography has been observed in patients with schizophrenia (X. Wang, Liao, et al., 2019). On

the other hand, the human lifespan, as the largest time scale of dynamic brain development, dominates and changes the functional organization of the whole brain (Cao et al., 2014; Vij et al., 2018). Therefore, the frequency characteristics of GS topography across the adult lifespan are of importance for the global dynamics during brain aging.

The dedifferentiation hypothesis is a key theory of brain aging (Sala-Llonch et al., 2015), which proposes a loss of functional specificity of brain regions and more homogeneous neural responses (Koen et al., 2020; Koen & Rugg, 2019; D. C. Park et al., 2004). Research has shown that within-network FCs decrease with age, while between-network FCs increase, resulting in more homogeneous connectivity patterns across the entire brain (Damoiseaux, 2017; Malagurski et al., 2020). The GS topography has been identified as featuring differentiated GSCORR between unimodal and transmodal regions (Ao et al., 2021; G. J. Yang et al., 2016; J. Zhang et al., 2020). Previous research has demonstrated a diminution in the differences in GSCORR between sensory and association regions in individuals with schizophrenia, suggesting a psychiatric-related dedifferentiation (G. J. Yang et al., 2016). However, it remains uncertain whether an analogous spatial and temporal dedifferentiation, marked by reduced local-regional and dynamic frequency differences, can be observed in the GS topography of the aging brain. Such spatiotemporal dedifferentiation of global brain topography would provide further support on the neural level itself for the more cognitive- and function-based dedifferentiation hypothesis (Baltes & Lindenberger, 1997).

Drawing on our previous work (Ao et al., 2022), we aim to expand and bolster the notion of age-related spatiotemporal dedifferentiation by investigating the variation of the spatiotemporal organization of GS topography across the adult lifespan using a large-sample rs-fMRI dataset. In addition to the dedifferentiation across distributed brain regions, we have observed a more homogenous distribution of GS power spectrum density across frequency bands in the aging brain(Ao et al., 2022). We thus hypothesized that the GSCORR would become more homogenous with age in different brain regions and frequency bands. To begin, we calculated the GS topography (GSCORR) using the magnitude-squared coherence, which captures FC in both spatial and temporal/frequency dimensions (De Domenico et al., 2016; Sasai et al., 2021). We then estimated Pearson's correlation between age and GS topography to

elucidate the variability of GS topography with age (GS-TV). To measure the dedifferentiation of GS topography with age, we calculated the Pearson's correlation between GS-TV and GSCORR. If the dedifferentiation of GS topography is genuine, the correlation should be negative, with regions having high GSCORR decreasing with age and regions with low GSCORR increasing with age. On the contrary, the differentiation of GS topography occurs when there is a positive correlation. Given that the physiological factors including head motion, white matter, cerebrospinal fluid signals, and vascular components are frequently contested confounds in detecting BOLD signal in elderly individuals (Fabiani et al., 2014; Tarantini et al., 2017), we aim to investigate the contribution of these physiological factors to our findings. We have demonstrated our results both prior to and following the deconvolution of the hemodynamic response function (HRF) to scrutinize the contributions stemming from neurovascular coupling. Furthermore, we have applied varying control strategies to manage the influence of other physiological signals and have subsequently discussed their outcomes.

4.2 Material and methods

4.2.1 Participants

All subjects in this study came from a public database: the International Data-sharing Initiative (http://fcon_1000.projects.nitrc.org/indi/retro/sald.html). A total of 492 healthy participants (308 females; ages ranged: 19–80 years) were recruited from Southwest University (SWU, Chongqing, China) through leaflets, online advertisements, campus social network and through face-to-face propaganda (Wei et al., 2018). All participants were healthy, and none had a history of psychiatric disorder or substance abuse (including illicit drugs and alcohol), or MRI contraindications. The project was approved by the Research Ethics Committee of the Brain Imaging Center of Southwest University, following the Declaration of Helsinki. Written informed consent was obtained from each participant before the data collection. Participants received payment depending on the time and tasks completed.

4.2.2 Imaging data acquisition

All of the data were obtained from a 3 T Siemens Trio MRI scanner (Siemens Medical, Erlangen, Germany) at the Brain Imaging Center of SWU. During the rs-fMRI scan, subjects

were instructed to lie down, close their eyes, and rest without thinking about anything in particular but to refrain from falling asleep. The 8-min scan of 242 contiguous whole-brain functional images was acquired using T2*-weighted gradient EPI sequence: slices = 32, repetition time/echo time (TR/TE) = 2000/30 ms, flip angle = 90°, field of view = 220 mm × 220 mm, thickness = 3 mm, slice gap = 1 mm, resulting in voxels measuring 3.4 × 3.4 × 4 mm^3.

4.2.3 Data preprocessing

The preprocessing of functional images was conducted using the "Data Processing Assistant for Resting-State fMRI" package (DPARSFA, http://www.restfmri.net) (Yan et al., 2016), according to the steps of previous studies (Fox et al., 2009; X. Wang, Liao, et al., 2019): removal of the first 7 volumes, slice timing, and realignment. The corrected images were normalized to the standard EPI template and resampled to a 3 × 3 × 3 mm^3 voxel size. The linear trend, white matter, and cerebrospinal fluid signals were regressed out from the BOLD signals with default parameters in the DPARSFA software. To minimize the head motion factor, we further linearly regressed out Friston's 24 motion parameters, including 6 head motions, 6 temporal derivatives, and 12 corresponding squares, as well as "bad" time points, with mean framewise displacement (mean FD) greater than 0.2 mm (Jenkinson et al., 2002), following previous studies (Satterthwaite et al., 2013; A. C. Yang et al., 2013). Note that we did not exclude subjects with high levels of mean FD or contaminated volumes, as doing so would introduce a bias in the sample by disproportionately excluding elder participants. Additionally, we noticed an augmentation in head motion correlating with aging ($r=0.35$, $p<0.0001$). We have chosen to document the GS-TV and its dedifferentiation with the individual mean FD regressed. This information is included in the supplementary material for further reference. This decision was made on the basis that the aforementioned increase in head motion could potentially introduce distortions in the post-processed output, particularly after the effects of head motion have been mitigated during preprocessing.

4.2.4 Blind HRF de-convolution

The neurovascular factor is an essential contributor to the BOLD signal, which undergoes change with age (Fabiani et al., 2014; Tarantini et al., 2017). Different HRF has been

observed in brain aging that characterized by increased time-to-peak and decreased peak amplitude with age (West et al., 2019). In addition, the HRF can confound the temporal precedence estimation (G. Wu et al., 2013), which could distort coherence analysis. Hence, we implemented the blind HRF de-convolution in the subject-level, to control the neurovascular factor and test its effect on the GS topography dedifferentiation. This method has demonstrated robustness, feasibility, and efficacy in eliminating neurovascular coupling effects in BOLD time series (Y. Wang et al., 2023; G. Wu et al., 2013; G. R. Wu et al., 2021).

Analogous to our previous studies (Ao et al., 2022; Y.-F. Wang et al., 2014, 2015), the following steps were conducted. After noise regression, a point process analysis was performed to detect spontaneous neural events. BOLD values exceeding the mean plus one standard deviation were extracted and the onsets of neural events were estimated and collected for HRF reconstruction (G. Wu et al., 2013; G. R. Wu et al., 2021). The BOLD signal was matched with the canonical HRF and its time derivative to get the HRF in each voxel. Finally, a Wiener de-convolution was applied to recover signals at the neural level (https://www.nitrc.org/projects/rshrf) (G. Wu et al., 2013; G. R. Wu et al., 2021).

4.2.5 GS topography measurements and its age-related effects

The GS was obtained by averaging BOLD signals over all voxels within the Human Brainnetome Atlas (Fan et al., 2016; Y. Wang, Huang, et al., 2019). The GS topography was defined by the FC between the GS and the time course of each brain region constrained by the Human Brainnetome Atlas. We used the coherence method, which is based on frequency division and temporal correlation, to avoid the limitations of traditional FC (H. Chen et al., 2016; C. W. Wu et al., 2008). First, there is no consensus on the number of bands the low frequency brain signal should be divided into due to insufficient knowledge about its psychophysiological meanings (Baria et al., 2011; Buzsáki & Draguhn, 2004; Krishnan et al., 2018). Furthermore, temporal correlation is sensitive to the phase of brain signals. If there is a fixed phase lag between two signals, an uncorrelated or even anti-correlated relationship may be uncovered by temporal correlation, even though there is information exchange between these signals (Fox et al., 2005; Murphy & Fox, 2017; Y. Wang, Huang, et al., 2019). The coherence method overcomes these limitations by differentiating the full band into narrow

frequency bins and is immune to phase lags when estimating temporal dependence (J. M. Li et al., 2015; Salvador et al., 2008; Y. Wang, Huang, et al., 2019). Consistent with previous studies (De Domenico et al., 2016; Sasai et al., 2021; Y.-F. Wang et al., 2016), we used the coherence coefficients *c* to measure FC across the full frequency band as in equation (1):

$$C(f) = \frac{P_{(roi,gs)}(f)}{\sqrt{P_{roi}(f)} \times \sqrt{P_{gs}(f)}}$$

Where $C(f)$ is the coherence coefficient at frequency *f*. P_{roi} and P_{gs} are power spectral densities (PSD) of local signals and the GS estimated using Welch's fast Fourier transform (FFT) method and $P_{(roi,gs)}$ is the cross-PSD estimation of local signals and the GS. We divided the grey matter into 246 regions of interest (ROIs) defined by the Human Brainnetome Atlas and extracted the mean time course of each ROI to represent the ROI signal. This atlas was established by the FC method and has been demonstrated to show a better performance than several others in a clinical study (Lee et al., 2021). The number of FFT (NFFT) points was set to 512, while $P_{(roi,gs)}$ had a length of 257 calculated by (NFFT+1)/2. Finally, a 246 × 257 *c*-matrix was obtained as the spatiotemporal GS topography for each subject.

The Pearson's correlation between age and each point of the *c*-matrix was calculated with gender as a covariate, obtaining a 246 × 257 matrix of GS-TV. The correlation coefficients were then converted to *z* values using Fisher's *r*-to-*z* transformation.

4.2.6 Spatiotemporal dedifferentiation

Upon visual inspection, we observed an anti-correlation pattern between the GSCORR matrix and GS-TV. Specifically, higher GSCORR tended to get lower with age and vice versa, indicating a more homogeneous GSCORR distribution in the aging brain, i.e. spatiotemporal dedifferentiation. To quantitatively assess this observation, we computed the Pearson's correlation between each pair of *c* and *z*. The same operation was further performed along 246 regions and 257 frequency points to investigate the effect of spatial dedifferentiation and

temporal dedifferentiation, respectively.

4.2.7 Contributors detection for the spatiotemporal dedifferentiation

As suggested in previous studies, the GS is highly susceptible to vascular and physiological noises, which are significant variables in aging (Murphy & Fox, 2017; Power et al., 2017). To investigate these contributions, we incorporated three additional preprocessing protocols targeting head motion, white matter signals, cerebrospinal fluid signals, and neurovascular coupling effects. Detailed parameters for each protocol are outlined in Table 1.

A Z-test was subsequently conducted to compare these dedifferentiation maps with a dedifferentiation map derived from a classical preprocessing strategy, aiming to examine the influence of neurovascular and physiological noises. The methodologies applied in the third protocol are summarized briefly in the following section:

Wavelet-despiking method for head motion: In our study, we calculated the coherence, which reflects the connectivity at each frequency point. This method is also recommended by (Geerligs et al., 2017) to preprocess aging data. Thus, we applied this unsupervised approach to further reduce the influence of head motion over a range of frequencies. This technique identifies and eliminates abnormal events by detecting sequences of anomalous wavelet coefficients within the voxel timeseries. A significant metric employed in this method is the spike percentage. This serves as an indicator of the frequency at which corrections are made using the wavelet-despiking technique, representing the proportion of voxels within each data volume that encompass a spike. Evidently, this method is proficient in eliminating a wide range of motion artifacts, including the effects of spin-history and other high-frequency events. The original paper provides a comprehensive explanation of this approach (Patel et al., 2014).

The component-based noise correction method (CompCor): This approach employs principal component analysis to succinctly characterize the data derived from the signals of noise regions. Subsequently, principal components are integrated as covariates in a general linear model, serving as an approximation of the physiological noise signal space. In line with preceding studies, we executed a regression of the CompCor signals pertaining to both white matter and cerebrospinal fluid. This included their first-order derivatives, their square values,

as well as their squared derivatives (Satterthwaite et al., 2013).

Table 1. Different preprocessing strategies

	Protocol 1 (main results, Fig. 17)	**Protocol 2 (without deconvolution, Fig. 18)**	**Protocol 3 (strict control for physiological factors, Fig. 19)**	**Protocol 4 (no control for physiological factors, Fig. 19)**
Wavelet-despiking	No	No	Yes	No
Classical regression	Yes	Yes	Yes	No
Compcor regression	No	No	Yes	No
Blind HRF deconvolution	Yes	No	Yes	Yes

All of the cortical maps were visualized with the Connectome Workbench (Marcus et al., 2011). Subcortical maps were visualized with the Data Processing & Analysis for (Resting-State) Brain Imaging (DPABI) package (http://www.restfmri.net) (Yan et al., 2016).

4.3 Results

4.3.1 Spatiotemporal dedifferentiation of GS topography

The results obtained from the GSCORR matrix indicated higher values primarily in the posterior sensory cortices, which encompassed regions in the occipital, parietal, and temporal lobes, while the lowest values were observed in the association cortex (e.g., regions in the frontal and temporal lobes belonging to the frontoparietal network and default mode network) and subcortical regions (Figure 17A). These findings were consistent with previous studies (X. Wang, Liao, et al., 2019; G. J. Yang et al., 2016; J. Zhang et al., 2020). The coherence curve showed a bi-peak distribution, which aligned with previous coherence studies (Drew et al., 2008; J. M. Li et al., 2015; Y. Wang, Zou, et al., 2020; Y.-F. Wang et al., 2016). Meanwhile, the correlation between coherence and age showed a reverse trend (refer to line charts in Figure 17A, Supplementary Figure 14A). Specifically, GSCORRs showed higher values around ~0.02 Hz and 0.06~0.1 Hz, but lower at 0.02~0.06 Hz and above 0.1 Hz, whereas GS-TVs displayed the opposite pattern. Overall, the GSCORR appeared to exhibit more homogeneity in the aging brain, as evidenced by the negative correlation between GS-TV and GSCORR (refer to Figure

17A, Supplementary Figure 14B).

As we observed an overall spatiotemporal dedifferentiation, we conducted further analysis to explore its characteristics in temporal and spatial dimensions, respectively. Considering the relatively small effect size of such dedifferentiation ($r^2 = 0.03$), we hypothesized the presence of certain differentiation effects. By averaging the temporal (row) and spatial (column) dimensions of the GSCORR and GS-TV, we detected small dedifferentiation effects in both time ($r^2 = 0.01$) and space ($r^2 = 0.03$). Our results, presented in Figure 17B and Supplementary Figure 14, indicated the temporal dedifferentiation in most brain regions with negative r values (FDR corrected, $q < 0.05$; see also Figure 17B, right), particularly in the association cortex. In contrast, the ventral visual pathway and sensorimotor regions exhibited a trend of temporal differentiation with positive r values (FDR corrected, $q < 0.05$; also refer to Figure 17B, right). Spatial dedifferentiation, as shown in Figure 17C and Supplementary Figure 14D, was found at approximately 0~0.014 Hz and 0.143~0.25 Hz (see also Figure 17C, right). These findings suggest that spatiotemporal dedifferentiation dominates brain aging, although the sensorimotor system showed a trend of temporal differentiation.

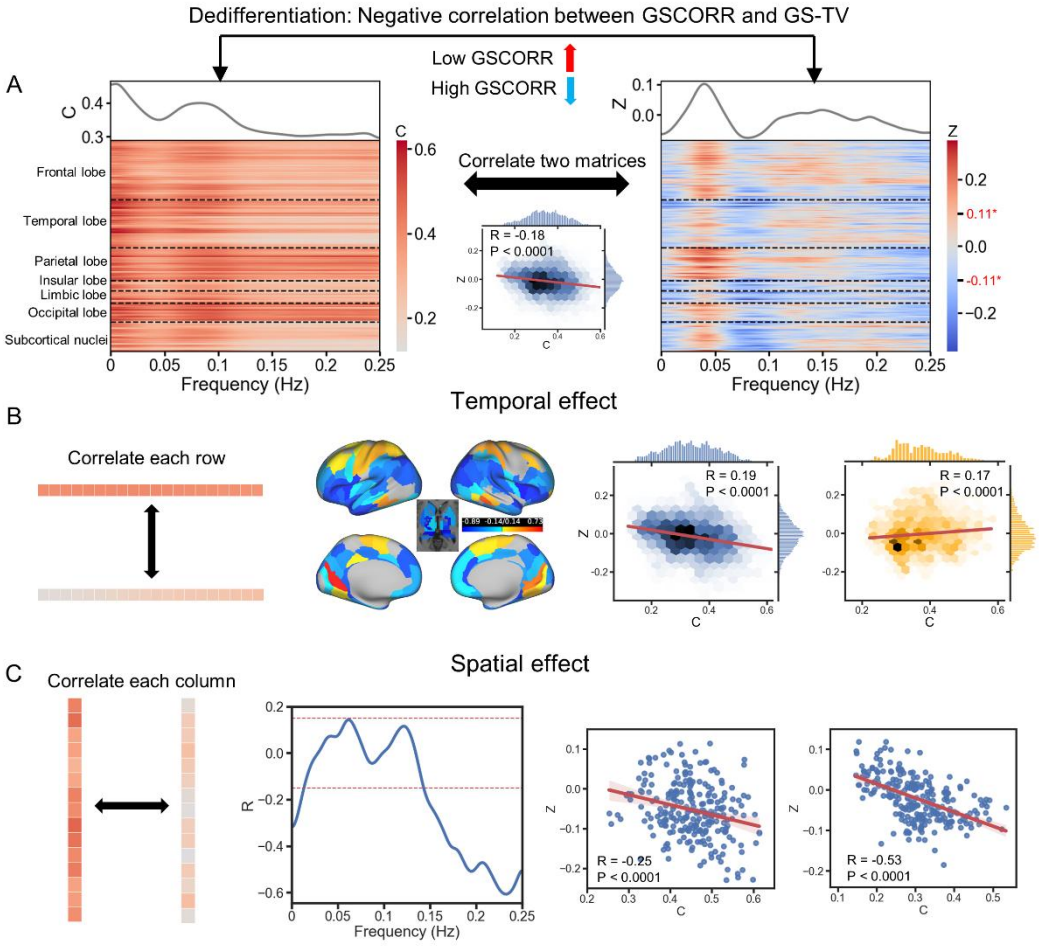

Figure 17. The spatiotemporal distribution of global signal (GS) topography and its spatiotemporal dedifferentiation with age. Panel (A), left: the grand averaged coherence between GS and local signals (GSCORR) of all subjects (thermograph) and the mean coherence across all regions of interest (ROIs) (line chart). Right: correlations between GSCORR and age (thermograph) and the mean correlation coefficient across all ROIs (line chart). The red values on the color bar indicates the threshold of significant z values. Middle: Correlation between GSCORR and GS topography variability with age (GS-TV), i.e. the overall spatiotemporal dedifferentiation of the GS topography with age. Panel (B). Temporal dedifferentiation of each ROI with dedifferentiated (negative) and differentiated (positive) tendencies. Panel (C). Spatial dedifferentiation (negative) of each frequency and the corresponding scatter charts of dedifferentiated bands. Red dotted lines represent the threshold of significant correlations (FDR corrected, $q < 0.05$).

4.3.2 Minimal effects from neuro-vascular coupling

We also examined the GSCORR and GS-TV without HRF de-convolution and found consistent distributions with the HRF de-convolved data, as shown in Figure 18. The overall spatiotemporal dedifferentiation was replicated (Figure 18A, middle), and the temporal dedifferentiated and differentiated regions were similar to those in HRF de-convolved data

(Figure 18B, left), albeit with weakened trends in most regions, as indicated by reduced z values in differentiated regions and increased z values in dedifferentiated regions (Figure 18B, middle). The data without HRF de-convolution raised a trend of spatial differentiation at middle frequency (0.031~0.076 Hz) and remained spatial dedifferentiation at very low (0~0.005 Hz) and fast frequencies (0.141~0.25 Hz) (Figure 18B, right), although no significant difference between the two performances was found at any frequency points. These results suggest that neuro-vascular factors attenuated the trend of spatiotemporal dedifferentiation with age.

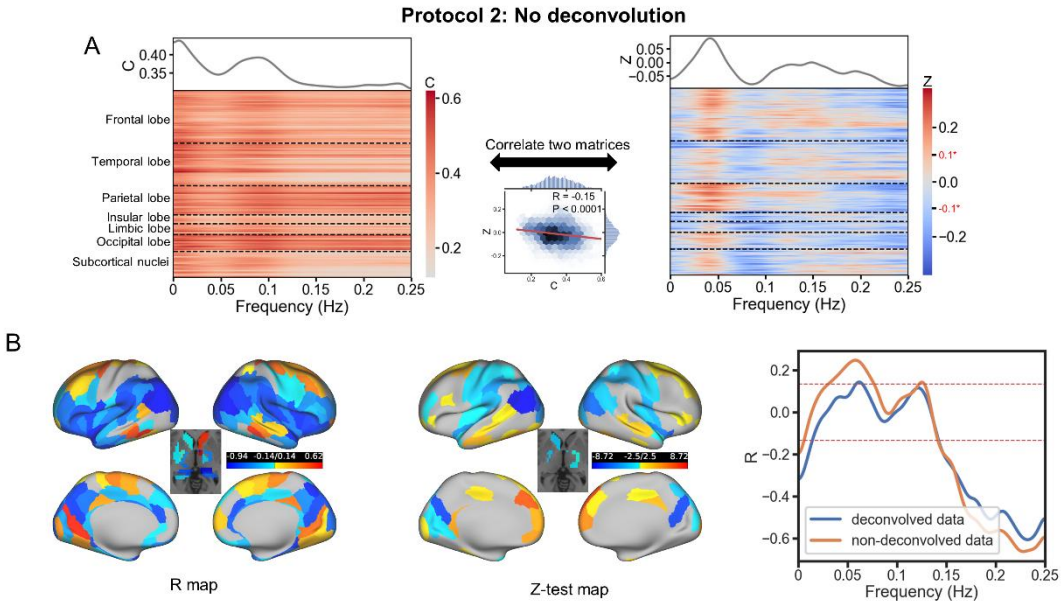

Figure 18. The spatiotemporal dedifferentiation and differentiation during brain aging in data without HRF de-convolution. Panel (A), global signal correlation (GSCORR) map, GS topography variability with age (GS-TV), and overall spatiotemporal dedifferentiation featured by the correlation between GSCORR and GS-TV. Panel (B), left: Temporal dedifferentiation in each ROI. Middle: Difference between HRF deconvolved and no-deconvolved data for temporally dedifferentiation and differentiation in each ROI. Right: Spatial dedifferentiation (negative) of each frequency. Red dotted lines represent the threshold of significant correlations (FDR corrected, $q < 0.05$).

4.3.3 Physiological factors attenuate age-related dedifferentiation

To ascertain the contribution of physiological factors, we applied two distinct preprocessing protocols. In the protocol 3, which employed more stringent regression of these physiological factors, we observed a diminished effect of spatiotemporal dedifferentiation. Conversely, a more pronounced effect of spatiotemporal dedifferentiation was evident in the

absence of noise regression (Figure 19A, C).

The topographic distribution of temporal dedifferentiation effects largely remained consistent, indicating dedifferentiation in transmodal regions and differentiation in unimodal regions. However, the effect of spatial dedifferentiation was attenuated in the protocol 3. In the absence of nuisance regression (protocol 4), temporal dedifferentiation was intensified. In terms of spatial effects, protocol 4 demonstrated trends opposite to those observed in protocol 1, with significantly different trends for spatial dedifferentiation and differentiation at 0-0.027 Hz and 0.143-0.25 Hz, respectively. Significant spatial differentiation was observed at 0-0.035 Hz and 0.127-0.239 Hz (Figure 19B, D).

In summary, the strongest spatiotemporal dedifferentiation was observed in the data without any nuisance control (protocol 4), with moderate dedifferentiation found in the data treated with classical preprocessing (protocol 1). Almost equal effects of dedifferentiation and differentiation were observed in the data subjected to highly rigorous nuisance control (protocol 3). Consequently, these results suggest that physiological factors such as head motion, white matter, and cerebrospinal fluid play substantial roles in causing age-related dedifferentiation.

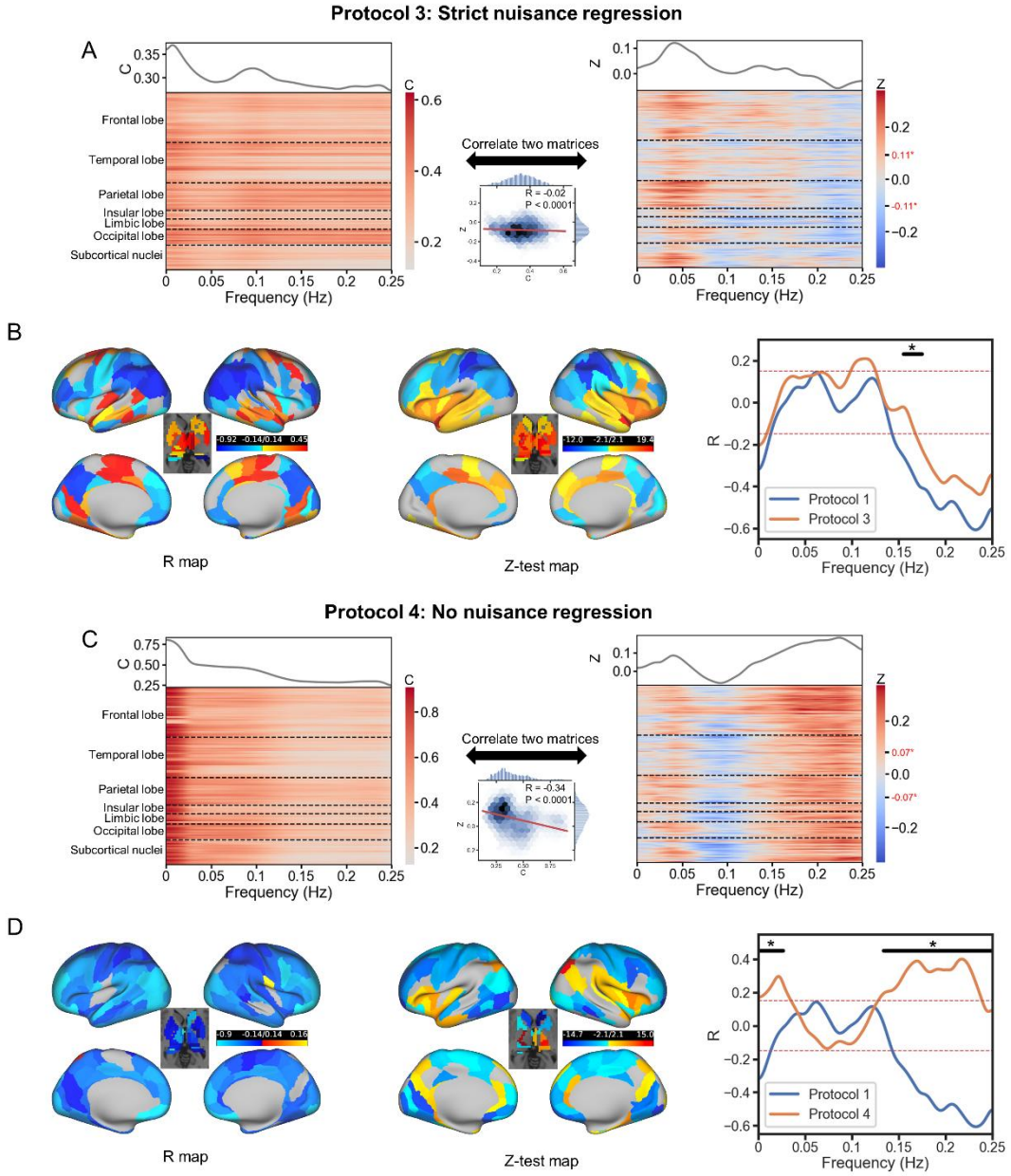

Figure 19. The spatiotemporal dedifferentiation and differentiation during brain aging in data with strict noise regression and without noise regression. Panel (A)(C), global signal correlation (GSCORR) map, GS topography variability with age (GS-TV), and overall spatiotemporal dedifferentiation featured by the correlation between GSCORR and GS-TV. Panel (B)(D), left: Temporal dedifferentiation in each region of interest (ROI). Middle: Difference between HRF deconvolved and no-deconvolved data for temporally dedifferentiation and differentiation in each ROI. Right: Spatial dedifferentiation (negative) of each frequency. Red dotted lines represent the threshold of significant correlations (FDR corrected, $q < 0.05$).

4.4 Discussion

We investigated the spatiotemporal characteristics of GS topography and its age-related

variations during resting-state, in order to provide a baseline for understanding the changes in GS topography in various cognitive tasks and mental disorders. Our findings showed that GS topography dynamically changed at the infra-slow frequency range below 0.25 Hz, as indicated by the bi-peak distribution of coherence, and across the lifespan from 18 to 80 years, as indicated by the age effect. More importantly, the GS topography exhibited an overall trend of spatiotemporal dedifferentiation with age, with dedifferentiation and differentiation tendencies present in both the temporal and spatial dimensions. These tendencies were attenuated by neural-vascular factors and reversed by physiological noises to some extent. To the best of our knowledge, this is the first study to extend the spatial dedifferentiation of brain aging to spatiotemporal dedifferentiation and to delineate dedifferentiation and differentiation at spatial and temporal dimensions, simultaneously.

4.4.1 Spatiotemporal characteristics of GS topography and its age-related changes

We employed the coherence approach to estimate GS topography in spatial (i.e. brain region) and temporal (i.e., infra-slow frequency) dimensions. Coherence is a function of frequency indicating the correspondence of two power spectrum signals. Based on the Parseval's theorem, we have demonstrated that the power spectrum density (PSD) of the brain signal is equivalent to the brain signal variability (BSV) in the corresponding frequency band (Y. Wang et al., 2018). BSV has been linked to the dynamic range of brain function and kinetic energy for the brain to achieve various potential states (Garrett et al., 2013). In this line, both PSD and BSV are considered to reflect the energy consumption of the brain (Y. Wang et al., 2018). Thereby, the magnitude of coherence may reflect the consistency of energy consumption between ROIs in different time scales. Accordingly, the GSCORR reflects the consistency of energy consumption between local regions and the whole brain. The variation of GSCORR with age, in turn, may reflect age-related energy reallocation among functional subsystems and across time scales (Garrett et al., 2011; Y. Wang et al., 2018).

We observed a bi-peak distribution of coherence coefficients, which is consistent with previous findings on coherence among local signals (Drew et al., 2008; J. M. Li et al., 2015; Sasai et al., 2014; Y. Wang, Zou, et al., 2020). This finding suggests that BOLD signal fluctuations may complete particular brain functions through particular oscillating structures,

in line with brain rhythms at traditional EEG frequency ranges. Specifically, distinct GS topographies were captured at two peaks and two troughs of the coherence curve, supporting the "spectral fingerprints theory" which posits the frequency-specific coherence in large-scale functional networks as the 'fingerprints' underlying cognitive processes (Siegel et al., 2012).

In line with the spectral fingerprint theory, we found that age-related variations of GS topography were frequency-specific. Although the psychological mechanisms of multiple low frequency bands remain unclear, many studies have focused on the frequency-specific effects of brain functions. For instance, the GS mainly affects the default mode network at 0.027~0.073 Hz, but also sensory regions at 0.01~0.027 Hz in patients with schizophrenia (X. Wang, Liao, et al., 2019). In addition, recent research by Wang and colleagues has demonstrated the frequency-dependent hub role of the dorsal and ventral anterior insula, highlighting that not only the spatial feature (i.e. dorsal and ventral regions) but also the temporal feature (i.e. multiple frequency bands) underlies compound psychological functions (Y. Wang et al., 2018; Y. Wang, Zou, et al., 2020). These studies suggested that specific psychological functions could be differentiated by different temporal scales of brain activity (S. Palva & Palva, 2018), supporting the spectral fingerprints theory (Siegel et al., 2012). Our findings provided new insight that age-related neural declines are captured by the GS topography in multiple low frequency bands. Overall, these results suggest that the neural functions associated with brain aging may depend on the specific spatiotemporal organization of the GS topography.

4.4.2 The spatiotemporal dedifferentiation during brain aging

The dedifferentiation hypothesis and compensation hypothesis are two widely accepted theories of brain aging. The dedifferentiation hypothesis argues that the aging brain is accompanied by the loss of functional specificity in extensive brain regions engaged in various psychological functions (D. C. Park et al., 2004; Rajah M. & D'Esposito, 2005). On the other hand, the compensation hypothesis posits that elders tend to recruit neural activity in brain regions involved in higher-order cognitive functions to compensate for deficits in other regions (Wingfield & Grossman, 2006). The current results clearly show that the overall spatiotemporal structure of the GS topography becomes more homogeneous with age, supporting that the dedifferentiation as a primary mechanism of age-related variations of GS topography. This

finding extends the dedifferentiation theory from the spatial dimension to the spatiotemporal matrix, suggesting that brain aging is accompanied by homogeneous spatiotemporal structure.

In the temporal dimension, association regions exhibited the phenomenon of dedifferentiation, whereas some sensory and motor regions showed a tendency of differentiation. The different trends of aging in unimodal and multimodal regions are consistent with the intrinsic organization of GS topography (Ao et al., 2021; G. J. Yang et al., 2016) as well as large-scale gradients in cortical organization of the human brain (Huntenburg et al., 2018). Both GS topography and cortical gradients have been demonstrated to correspond well with the principal spatial gene expression pattern, the cortical myelination pattern, and the cortical excitation/inhibition balance (Brown et al., 2022), suggesting the dedifferentiation in multimodal regions and differentiation in sensorimotor regions to be supported by the biological evolvement with age.

Several recent studies have highlighted that the age-related sensory-association segregation in dedifferentiation and differentiation of aging. For instance, Grady and colleagues found that most brain regions showed less BSV with older age whereas a few regions (e.g., the superior frontal gyrus and some subcortical regions) showed increased BSV with age (Grady & Garrett, 2014). In a combined fMRI-EEG study, Kumral and colleagues found that variabilities of BOLD and EEG signals in most frequency bands and brain regions are consistently decreased with aging, but the temporal and sensorimotor regions show an age-related increase of variability of beta EEG oscillations (Kumral et al., 2020). Using longitudinal aging data, Malagurski and colleagues found an age-related decrease of segregation indices in most brain networks but an increase in the limbic network (Malagurski et al., 2020). These findings, combined with our results, suggest that dedifferentiation and differentiation in aging coexist but in different brain regions. However, only the variation of GS topography with age mirrored the intrinsic gradient organization of brain functions.

The spatial dedifferentiation was mainly restricted at the lower and higher ends of the frequency range, suggesting that spatial dedifferentiation is constrained by time scales. However, the spatial dedifferentiation was located at 0~0.014 Hz and 0.143~0.25 Hz which is inconsistent with previous findings of spatial dedifferentiation in the intermediate frequencies

(often at 0.01~0.1Hz) (Chan et al., 2014; Malagurski et al., 2020). Previous studies often examined spatial dedifferentiation with activation, inter-regional FC, or graph theory, while abundant evidence have revealed that GS regression alters resting-state FC within and between networks, suggesting the GS itself contains variability of global connectivity (Scalabrini et al., 2020). Different from GS affecting local activity in higher frequency bands, local activity mainly affects GS at the lowest frequency end (Y. Wang et al., 2023), indicating that the spatial dedifferentiation may be driven by various interactions between GS and local signals at different time scales. Considering that neural oscillations at lower frequency are associated with functions of larger neural networks and higher-order cognition (Buzsáki, 2006), spatial dedifferentiation at the higher frequency end may be driven by more homogeneous local activities while at the lower frequency end may primarily be driven by the GS. This hypothesis warrants further investigation.

4.4.3 Assessment of physiological "noise"

There is abundant non-neural information in the GS and local BOLD signals, which impacts neural activities in complex ways (Birn et al., 2006; Boubela et al., 2013). Therefore, we tested the influence of HRF de-convolution and noise regression on the current findings.

We found that spatiotemporal dedifferentiation was slightly weakened in data that did not undergo HRF de-convolution, which was mainly manifested as weakened temporal dedifferentiation in most brain regions. Furthermore, we observed significant spatial differentiation within 0.031~0.076 Hz. These findings suggest that neurovascular factors tend to preserve the pattern of spatiotemporal differentiation in the elder brain. Although some studies found unchanged neurovascular coupling with normal aging (D'Esposito et al., 1999; Grinband et al., 2017), others have suggested that neurovascular, cardiovascular, and cerebrovascular factors could explain brain aging to a large extent (Fabiani et al., 2014; Tsvetanov et al., 2020). A large number of studies have revealed that cerebral hemodynamic activities at 0.04~0.1 Hz reflect underlying neural information (Auer, 2008; Du et al., 2014; Fox & Raichle, 2007; Ma et al., 2016; Y. Tong & Frederick, 2010; Wright et al., 2017; Y. C. Xie et al., 2016). Yang et al. also revealed cognitive-related frequency and amplitude modulation in aging at 0.045~0.087 Hz (L. Yang et al., 2018), suggesting that neurovascular

factors at this frequency band are cognitive-related. Although the blind de-convolution algorithm cannot fully remove vascular effects, it was shown that neurovascular coupling could be an important protective factor of aging to some extent.

Traditional physiological noises including head motion, white matter, and cerebrospinal fluid signals, strengthened spatiotemporal dedifferentiation in general. However, they preserved spatial differentiation perhaps at the expense of increasing temporal dedifferentiation. The migration of brain signal fluctuations from lower frequencies to higher frequencies were observed during both lifespan development and cognitive tasks (Churchill et al., 2016; He, 2011), resulting in the weakening of scale-free properties and enhancement of temporal dedifferentiation. This temporal reorganization of brain activities was suggested to reflect the brain engaging with more effort on immediate functional networks (He et al., 2010). Although the temporal dedifferentiation of aging has been uncovered (Ao et al., 2022) and been verified here, it is still unknown how these altered temporal structures influence on and interact with the spatial organization of brain function during brain aging. Therefore, the spatiotemporal perspective is valuable for uncovering the dynamic organization of brain function across temporal and spatial dimensions.

In addition, the HRF de-convolution and noise regression exerted distinct effect on different frequencies and regions, suggesting that neural, physiological, and other signals have separable spatiotemporal structures. Considering that physiological networks nicely mirrored neural networks (Cheng et al., 2020), the opposite trend of spatial dedifferentiation between data with and without noise regression suggested that GS topography may serve as an alternative approach to separate neural signal and physiological noises. On the other side, head motion (Zeng et al., 2014), white matter (M. Li et al., 2019), cerebrospinal fluid (Fultz et al., 2019), respiratory (H.-D. Park et al., 2020), and cardiac signals (Mosher et al., 2020) have been demonstrated to contain meaningful physiological and pathological information. This evidence argues that noise plays important roles in brain function (Ghosh et al., 2008; McDonnell & Ward, 2011; Mišić et al., 2010).

Our results demonstrated that the GS topography holds a strong promise to reveal the changes of age-related brain functions. Our findings suggested that it is critical for future

studies to pay caution to “noises” when interpreting their results. As Uddin has argued, “as we continue to embrace the idea that there may be untapped information in spontaneous neural activity, perhaps we should not be so hasty in future efforts to separate brain signal from noise” (Uddin, 2020).

4.4.4 Limitations

Several limitations should be taken into account in our study. First, the precise sources of the age-related dedifferentiation observed here cannot be determined with certainty as the physiological data such as respiratory and cardiac signals were not available in the dataset. While we re-analyzed the data without HRF de-convolution and nuisance regression, future studies should consider collecting simultaneous physiological recordings, given the complex interplay between neural and vascular activities (Das et al., 2021). Moreover, our study did not account for the non-zero lag effects of neurovascular coupling, white matter, and cerebrospinal fluid, which calls for future research on brain aging.

Secondly, the subjects were not uniformly distributed in age (Wei et al., 2018), which may have influenced the correlation between age and GS topography to some extent. Finally, it is important to note that the dedifferentiation theory of aging is primarily associated with cognitive performance. As our study only examined the phenomenon of spontaneous brain activities without cognitive tasks, the findings should be interpreted with caution.

4.5 Conclusion

The GS topography has an intrinsic spatiotemporal architecture and varies with age. Brain aging exhibits spatial and temporal dimensions which are characterized by distinct dedifferentiation and differentiation trends, originating from different signals or “noises”. Our discovery of the spatiotemporal dedifferentiation phenomenon provides novel insights into the spatiotemporal organizational mechanisms underlying brain aging. These findings serve as a catalyst for future research, enabling more nuanced examinations of age-related functional connectivity at both the global and local levels.

5 General Discussion

The present thesis examined whether ISO constitutes structured spatiotemporal brain dynamics rather than nonspecific slow fluctuations or physiological noise. Building on the proposition that ISO is jointly constrained by two complementary organizational axes: intrinsic neural timescales in the time domain and scale-free spectral organization in the frequency domain, three studies tested this framework from converging angles: the time-domain coupling between phase dynamics and intrinsic timescales (Study 1), the frequency-domain role of scale-free dynamics as a background measure for behavioral variability (Study 2), and the systematic reorganization of ISO across the adult lifespan (Study 3).

Study 1 examined the time-domain axis. Infra-slow phase dynamics were not uniform across the oscillatory cycle: peak frequency was systematically structured across phase components and negatively coupled to regional intrinsic neural timescales, such that longer INT predicted slower phase progression. Critically, this PF–INT coupling persisted from rest to naturalistic movie watching, indicating that time-domain constraints on ISO reflect a stable intrinsic property of the system rather than a state-specific feature. Study 2 examined the frequency-domain axis. The PLE, indexing scale-free infra-slow organization, mediated the relationship between BOLD signal standard deviation and reaction-time variability during sustained attention—an effect supported by complementary empirical and simulation evidence. This positions PLE not as a parallel descriptor of variability but as a background measure within which neural variability and complexity acquire behavioral relevance. Study 3 tested whether the regime generalizes beyond short cognitive timescales by examining the adult lifespan. Global signal topography became less differentiated with age across both spatial and frequency dimensions, and this spatiotemporal dedifferentiation survived rigorous control for physiological and vascular confounds, consistent with a systematic reorganization of the ISO regime under aging rather than a degradation toward noise.

Taken together, the three studies support one main conclusion: ISO is not simply a nuisance fluctuation, but part of organized brain dynamics that remain detectable across cognitive states (Studies 1 and 2) and reorganize systematically across the adult lifespan (Study

3). The rest of this discussion considers what these findings mean for the study of infra-slow brain dynamics, and discusses their methodological and possible clinical implications.

5.1 ISO as structured dynamics rather than noise

A reasonable null hypothesis must be confronted before any organizational claim about ISO can be sustained: that infra-slow BOLD fluctuations are predominantly a mixture of scanner drift, vascular and respiratory variation, head motion, and other non-neural sources, and that whatever spatiotemporal structure they appear to carry is either statistical coincidence or an indirect reflection of these confounds (Birn et al., 2006; Chang & Glover, 2009; Liu, 2016). Under this view, infra-slow activity should show three diagnostic features: weak or inconsistent spatial organization across individuals and states, little systematic coupling to known neural properties such as intrinsic timescale or excitation–inhibition balance, and instability under cognitive state changes or biological transitions such as aging (Power et al., 2012; Y. Tong et al., 2019; Tsvetanov et al., 2020). The three studies presented in this thesis were designed, to collectively evaluate whether ISO exhibits these features or whether it instead displays the systematic, multi-scale organization expected of a structured neural activity.

The finding across the three studies is that none of these noise-consistent features are observed. Study 1 demonstrates that infra-slow phase progression is not a featureless drift but is structured across the oscillatory cycle and tightly coupled to a region's intrinsic neural timescale, a property that is biologically grounded in cortical microcircuit organization (Çatal et al., 2024; Çatal, Wolman, et al., 2025; Wolman et al., 2023). Study 2 shows that scale-free infra-slow dynamics do not merely co-occur with neural and behavioral variability but statistically mediate their relationship during sustained attention, a functional role incompatible with a noise interpretation. This finding is consistent with previous studies showing that scale-free infra-slow dynamics systematically differentiate core–periphery brain networks and vary across distinct states of consciousness (Klar et al., 2023a, 2023b). Moreover, study 3 shows that the spatial and frequency-domain organization of global infra-slow activity does not degrade randomly across the adult lifespan but reorganizes systematically, in a manner that aligns with established gradients of cortical hierarchy (Huntenburg et al., 2018; Taylor et al., 2026).

One strong version of the noise hypothesis is that ISO findings could be explained by neurovascular and physiological contamination (Das et al., 2021; Grinband et al., 2017; Tarantini et al., 2017). Study 3 confronted this directly by re-analyzing all lifespan effects with and without hemodynamic response deconvolution and with explicit regression of head motion, white matter, and cerebrospinal fluid signals. Two observations argue against the noise account. First, the core pattern of spatiotemporal dedifferentiation persisted after these controls, indicating that the effect cannot be attributed to physiological confounds alone. Second, and more informatively, attenuating modeled neurovascular and physiological contributions did not eliminate but redistributed the dedifferentiation pattern across frequencies and regions. Neural and vascular infra-slow fluctuations should not, however, be considered fully independent. Neural activity can entrain local vasomotor fluctuations through neurovascular coupling, whereas vascular fluctuations can also arise from intrinsic or systemic hemodynamic processes that are partly independent of local neural activity (Mateo et al., 2017; Y. Tong et al., 2019; Uddin, 2020). Thus, a more productive approach is to ask how distinct neural and physiological sources jointly compose the ISO. The present findings also resonate with broader debates on nuisance regression in neural signals, where removing shared physiological variance may risk "throwing the baby out with the bathwater" (Uddin, 2017).

5.2 From neural variability to behavioral variability

Whether infra-slow neural fluctuations translate into behavioral variability is a question whose framing has shifted substantially over the past decade. Earlier accounts of brain–behavior coupling were predominantly focusing on task-related activation, treating moment-to-moment fluctuations around mean activity as nuisance variance to be modeled out via the general linear model (Monti, 2011). Subsequent work reframed this perspective, demonstrating that signal variability itself carries information about behavioral capacity—often outperforming mean activation in predicting individual differences in cognitive performance (Dinstein et al., 2015; Garrett et al., 2010; Waschke et al., 2021). However, raw variability magnitude has produced inconsistent associations with behavior across tasks, populations, and analytic pipelines (Boylan et al., 2021; Steinberg & King, 2024), suggesting that magnitude alone may not fully capture the functional content of infra-slow fluctuations. The present thesis

advances within this trajectory: the behavioral relevance of infra-slow variability is not determined by its magnitude in isolation but by how that variability is organized across time and frequency. From this perspective, SD, SE, and the PLE do not stand as parallel descriptors of the same underlying instability but as layered features.

Study 2 provided the critical empirical evidence for this view. During a sustained attention task, the relationship between two distinct facets of infra-slow neural variability, including signal magnitude (SD) and temporal complexity (SE), was statistically mediated by PLE, and PLE additionally constrained how these variability measures mapped onto reaction-time variability across cortical networks. The mediation finding is important not because PLE simply explains shared variance—mediation analyses are correlational and cannot resolve causal direction (Shrout & Bolger, 2002). Crucially, the empirical mediation was corroborated by complementary simulations: relationships among SD, SE, and behavioral variability emerged specifically in scale-free property consistent with pink-noise-like dynamics, and were attenuated or absent in signals lacking such structure. Thus, PLE is not interchangeable with SD or SE as an index of neural variability; rather, it indexes the spectral organization within which SD and SE acquire their behavioral relevance.

The explanatory value of the mediation model should be interpreted cautiously. Robustness was assessed using 10,000 bootstrap resamples and by repeating the analysis after regressing out task-evoked effects. However, we did not systematically compare PLE with alternative or multiple mediators. Therefore, PLE should be viewed as explaining a significant component of the brain–behavior relationship, rather than as a unique or complete mechanism.

If PLE provides the spectral background for behavioral relevance, intrinsic neural timescales provide its temporal counterpart. Study 1 demonstrated that infra-slow phase progression (peak frequency) was systematically constrained by regional INT, with longer ACW associated with slower phase progression. This PF–INT coupling was preserved from rest to naturalistic movie watching, indicating that it reflects an intrinsic constraint rather than a state-specific feature. Although Study 1 did not include direct behavioral measures, the inference from these results to behavioral variability is timescale-matched: regions with longer INT sustain infra-slow states over longer windows, and these are precisely the windows over

which behavioral variability—particularly reaction-time variability during sustained tasks—unfolds (Esterman et al., 2013; M. Rosenberg et al., 2013). On this view, INT is not merely a regional label but defines the temporal feature within which neural variability accumulates before it can be translated into behavioral consequence, consistent with studies that demonstrated the relation between INT and brain functions such as working memory (Wolman, Çatal, et al., 2024), event-related activation (Çatal, Keskin, et al., 2025), self (Wolman et al., 2023), and mental disorders (Djimbouon et al., 2025). The two axes are therefore complementary rather than redundant. PLE governs how variability is distributed across frequencies—the spectral allocation that determines which components contribute to ongoing dynamics. INT governs over what duration variability is integrated within a region—the temporal feature over which fluctuations can be coherently expressed.

Taken together, these findings argue for a layered account of how infra-slow dynamics couple to behavior. Two implications follow. First, individual-differences and clinical studies that aim to use infra-slow variability as a marker of cognitive capacity or pathology may benefit from co-indexing variability with measures of its temporal–spectral organization rather than relying on magnitude alone; this is consistent with emerging proposals that scale-free dynamics and intrinsic timescales serve as transdiagnostic markers across affective and neurodegenerative conditions (Djimbouon et al., 2025; Klar et al., 2023a, 2023b; Lechner et al., 2025; Linkenkaer-Hansen et al., 2005; Murai et al., 2024). Second, the present framework resonates with broader proposals from critical brain dynamics and metastability research, in which functional consequence emerges only when neural activity occupies particular dynamics rather than as a monotonic function of fluctuation magnitude (Friston, 2020; Kelso, 2012). If brain–behavior coupling at the infra-slow scale depends on this constraint, a natural follow-up question is whether such constrain itself remains stable when the brain is challenged across cognitive states and across the adult lifespan, which will be discussed in next section.

5.3 Generalization across brain states and the adult lifespan

One framework developed in this thesis is sharpened by the fact that it makes differential predictions about what should and should not be conserved under such perturbations. The expression of the ISO including peak frequency, signal variability

amplitudes, spectral steepness, and global signal topography is allowed to vary across state and age. The framework is therefore falsifiable, and the three studies in this thesis collectively provide the conditions for that falsification test.

Studies 1 and 2 together provide the cross-state evidence for this claim. Expression measures (PF, variability amplitudes, spectral topographies) reconfigured markedly across rest and task, while the organizing constraints (PF–INT coupling and PLE's mediating role) were preserved. This dissociation is precisely what one would expect if INT and PLE are properties of the underlying neural substrate rather than task-imposed features(Northoff et al., 2020b; Wolff et al., 2022).

The second and more demanding generalization test was conducted across the adult lifespan, where aging served as a slow biological perturbation affecting virtually every aspect of brain function. In study 3, we found frequency-resolved global signal topography became less differentiated with age in both spatial and frequency dimensions, yielding a coherent *spatiotemporal* dedifferentiation. Critically, this dedifferentiation followed sensory-to-associative gradients that align with the same cortical hierarchy organizing INT and PLE topographies in Studies 1 and 2. In other words, aging did not dissolve the structure of ISO but reorganizes such dynamics.

Taken together, the cross-state and cross-lifespan evidence supports a stronger claim than either generalization axis would support in isolation. The framework exhibits both signatures expected of an organized spatiotemporal pattern: state dependence under cognitive modulation (Studies 1 and 2) and systematic reorganization along its own axes under biological perturbation (Study 3).

5.4 Broader implications

At a theoretical level, the framework reinforces the broader shift from activation-centric to temporo-spatial accounts of brain function, in which the temporal organization of neural activity is treated as constitutive of cognition, rather than its incidental (Gong & Zuo, 2025; Northoff, 2024; C. Zhang et al., 2023). INT and PLE as temporo-spatial measure in exactly this sense, defining the temporal windows over which prior information can be integrated and

positioning the ISO as a candidate substrate for slow-timescale predictive computation (Gabhart et al., 2025). The same temporo-spatial lens also extends classical accounts of brain aging: dedifferentiation theory has been formulated predominantly in spatial terms: regions becoming less specialized, networks becoming less segregated (Koen & Rugg, 2019; D. C. Park et al., 2004; Sala-Llonch et al., 2015), whereas Study 3 demonstrates that dedifferentiation also occurs along the frequency dimension, yielding a coherent spatiotemporal phenomenon rather than a purely spatial one. Neuromodulatory systems, particularly cholinergic and noradrenergic projections from basal forebrain and locus coeruleus, may regulate this mechanism through gain modulation (Kjaerby et al., 2025; Turchi et al., 2018), offering a generative mechanism for the ISO's expression and reorganization. The central reframing is therefore that the question is no longer what ISO does, but what constraints make ISO behaviorally coherent.

At a practical level, the framework offers potential for several translational lines of work. A growing body of work has documented altered infra-slow dynamics in major depression, schizophrenia, Parkinson's disease, and disorders of consciousness (Godwin et al., 2017; Tanabe et al., 2020; Wolters et al., 2019). Rather than asking simply whether variability or complexity differs between patients and controls, the present framework suggests a more targeted question: whether the organizational measures are preserved or disrupted. This reframes clinical biomarker work from descriptive group contrasts toward comparisons with clearer mechanistic grounding. The cholinergic and noradrenergic systems identified in the neural-substrate review offer direct targets for pharmacological or neuromodulatory testing, a direction that ongoing work is beginning to explore. Finally, the spatiotemporal dedifferentiation characterized in Study 3 is a candidate intermediate phenotype for distinguishing healthy aging from pathological trajectories, though longitudinal validation is still needed (Tsvetanov et al., 2020).

5.5 Limitations and future directions

Several limitations of the three studies have been discussed within their respective chapters. The present section focuses on limitations that arise specifically from the cumulative framework and from the conditions under which it was tested:

One limitation of the present framework is that the evidence derives primarily from neuroimaging data. Although the three studies provide converging evidence that infra-slow activity is spatially organized, temporally structured, and behaviorally relevant, these analyses cannot by themselves establish causality. Mediation analyses in Study 2 clarify the statistical relations among variability, scale-free organization, and behavior, but do not determine causal direction. Fourier-phase-shuffled surrogate testing in Study 1 helps rule out specific null explanations for the observed phase structure, but does not identify the biological mechanisms that generate it. Similarly, simulation evidence supports the generation of the proposed mechanisms under explicit model assumptions, but does not validate those mechanisms directly. Thus, the stronger causal version of the framework requires perturbation evidence. Three classes of perturbation are particularly critical. First, pharmacological probes of the neuromodulator systems implicated by the neural substrate review in this thesis, that is, cholinergic challenges via basal forebrain pathways and noradrenergic challenges via the locus coeruleus, would directly test whether these systems regulate the ISO and its temporo-spatial measures (Kjaerby et al., 2025; Turchi et al., 2018). Second, non-invasive brain stimulation targeted at the ISO (transcranial alternating current stimulation, slow-frequency repetitive transcranial magnetic stimulation (TMS)) offers a complementary perturbation modality, where feasibility has begun to be established (Helfrich et al., 2018; Qiao et al., 2022; Yu et al., 2025).

A second class of limitations concerns the imaging modality itself and the resulting gap between description and generative mechanism. BOLD signals are downstream of multiple neural, vascular, and metabolic processes, and although Study 3 directly examined whether the dedifferentiation pattern survives standard physiological controls, the conclusion that ISO organization is primarily neural in origin remains a relative rather than an absolute claim (Das et al., 2021; Liu, 2016). The candidate generators identified in the neural-substrate revie, such as slow cellular and glial mechanisms, neuromodulatory gain control, and subcortical hub systems, are advanced on the basis of external evidence but are not directly tested within this thesis. A related concern is that the specific operationalizations adopted here (ACW computed at the autocorrelation zero-crossing; PLE fit within 0.01–0.1 Hz) are common in the field but

not unique, and methodological convergence across alternative operationalizations (Donoghue et al., 2020; Golesorkhi, Gomez-Pilar, Zilio, et al., 2021) remains an outstanding project. Two directions of future work address these gaps. Multimodal imaging including concurrent fMRI–EEG, fMRI–MEG, and combined fMRI–near-infrared spectroscopy (NIRS) approaches, would help disentangle the neural and vascular contributions to infra-slow BOLD. Neural-mass and biophysical modeling provides a generative testing ground in which circuit-level parameters and neuromodulatory gain can be systematically varied.

A third class of limitations concerns the scope of conditions under which the framework has been tested and its relationship to adjacent theoretical accounts. The behavioral evidence presented here comes primarily from sustained attention and naturalistic viewing, with the framework's behavioral relevance most directly established for variability-sensitive performance metrics. Whether the ISO measures extend to other cognitive domains like working memory, decision-making, social cognition, remains to be tested. All three studies used healthy adult samples, and the clinical extensions outlined in the previous section are therefore hypotheses rather than validated predictions. The lifespan evidence in Study 3 is cross-sectional, and longitudinal designs are needed to confirm within-individual reorganization along the axes the framework specifies. Beyond these scope issues, the framework offers a partial rather than complete account of large-scale brain organization. The future work implied by these limitations is correspondingly broad: extension to wider cognitive tasks, application to clinical and developmental populations, longitudinal aging designs, and explicit theoretical integration work that maps the framework onto adjacent accounts of brain organization.

6 Supplement materials

6.1 Study 1

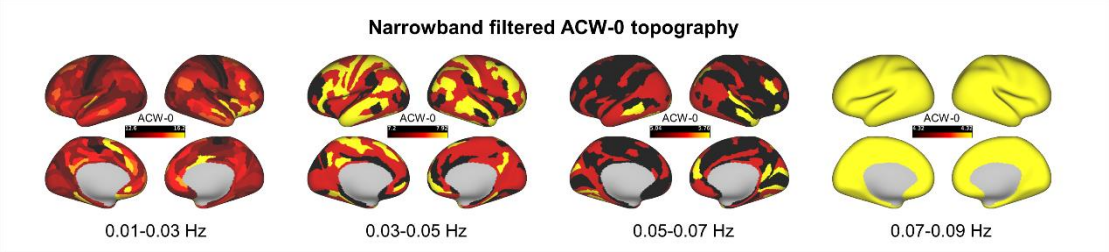

Supplementary Figure 1. ACW topographies in four narrow bands. Note that the narrowband filtered data shows less variance across different brain regions. In 0.07-0.09 Hz, all ACW values are same as the limited temporal resolution in fMRI.

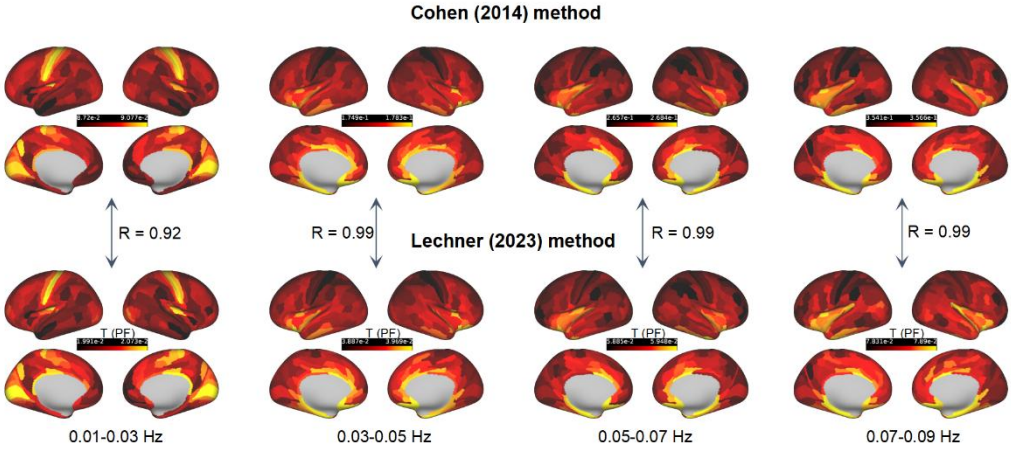

Supplementary Figure 2. Spatial similarity between frequency sliding and Lechner (2023) method.

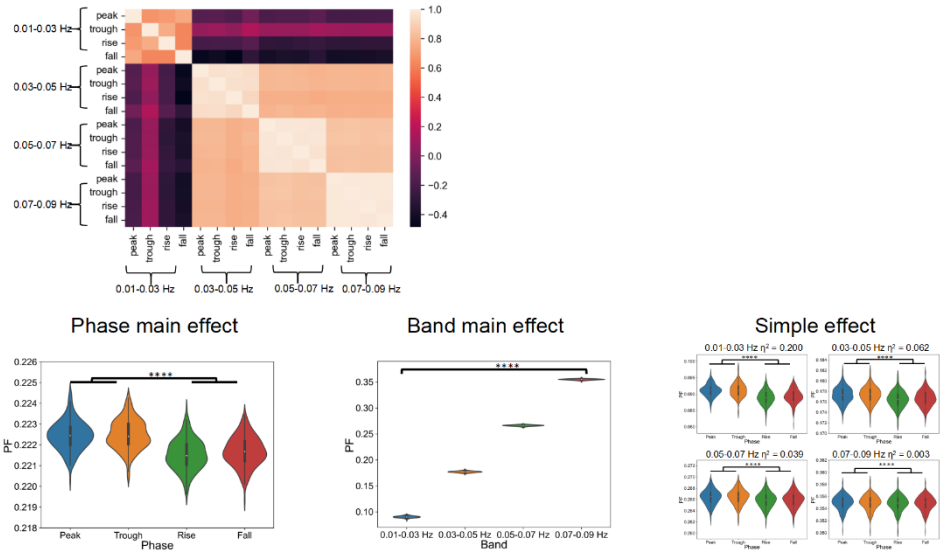

Supplementary Figure 3. PF across four bands and phases in 7T data.

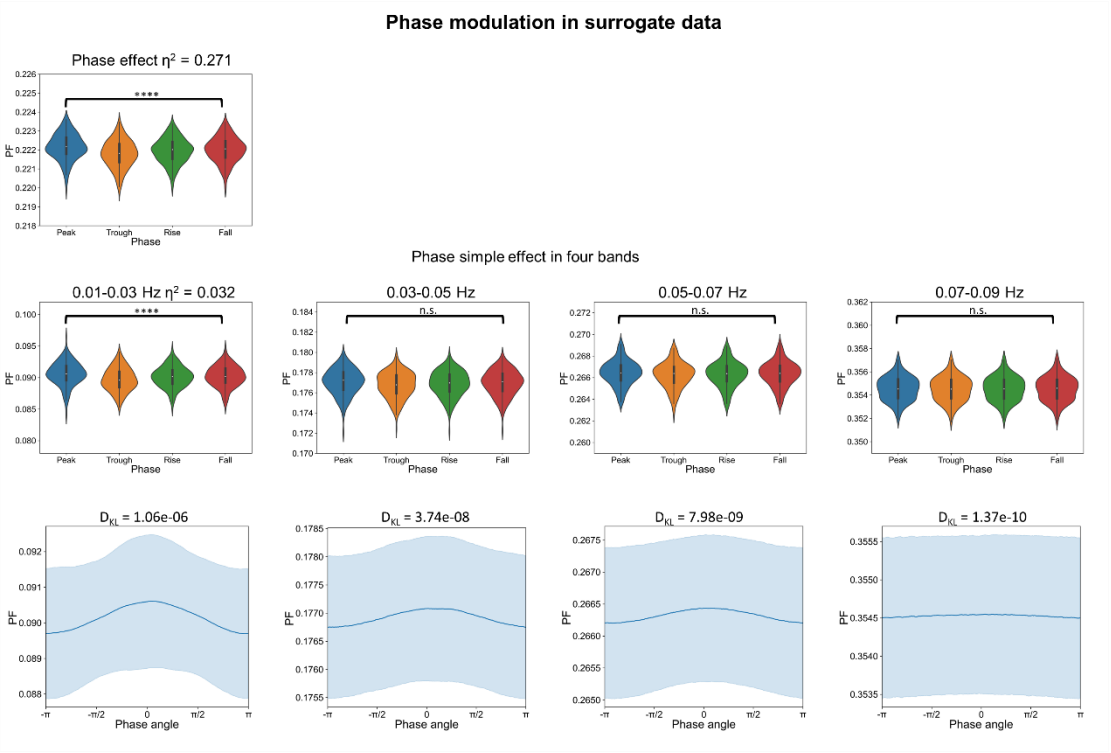

Supplementary Figure 4. Statistics for phase modulation on PF in surrogate data.

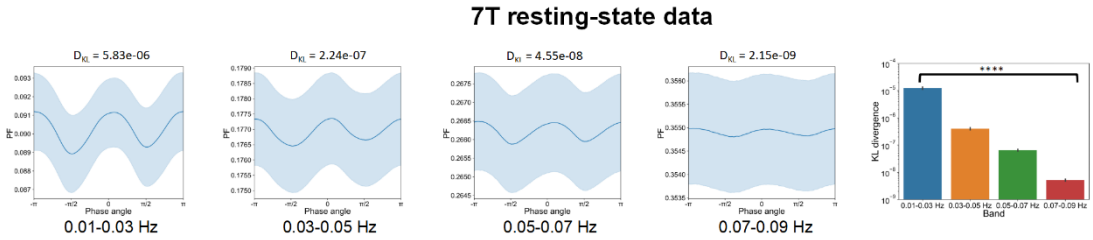

Supplementary Figure 5. Validation in 7T resting-state data.

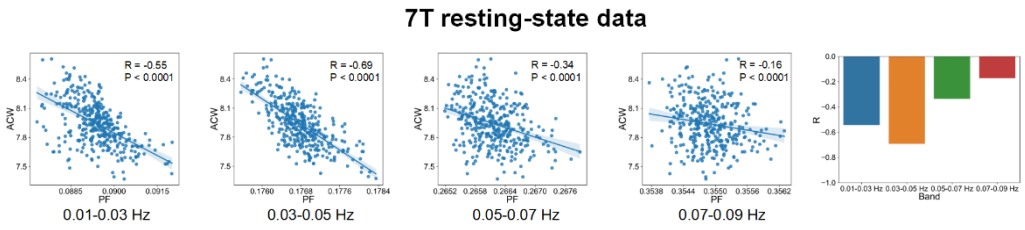

Supplementary Figure 6. Relationship between PF and ACW in 7T resting-state data.

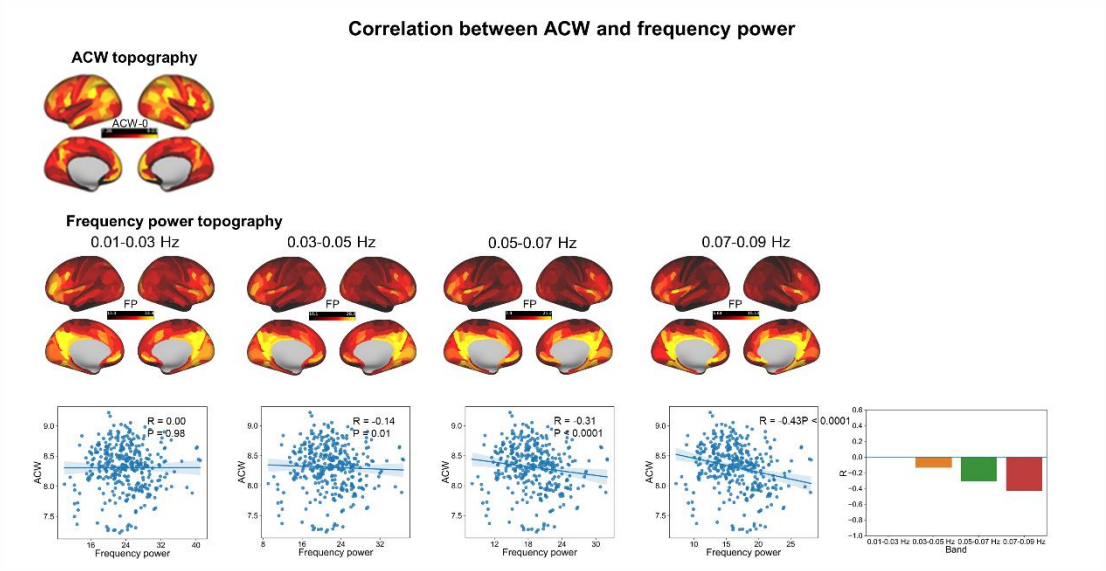

Supplementary Figure 7. Relationship between PF and ACW in surrogate data.

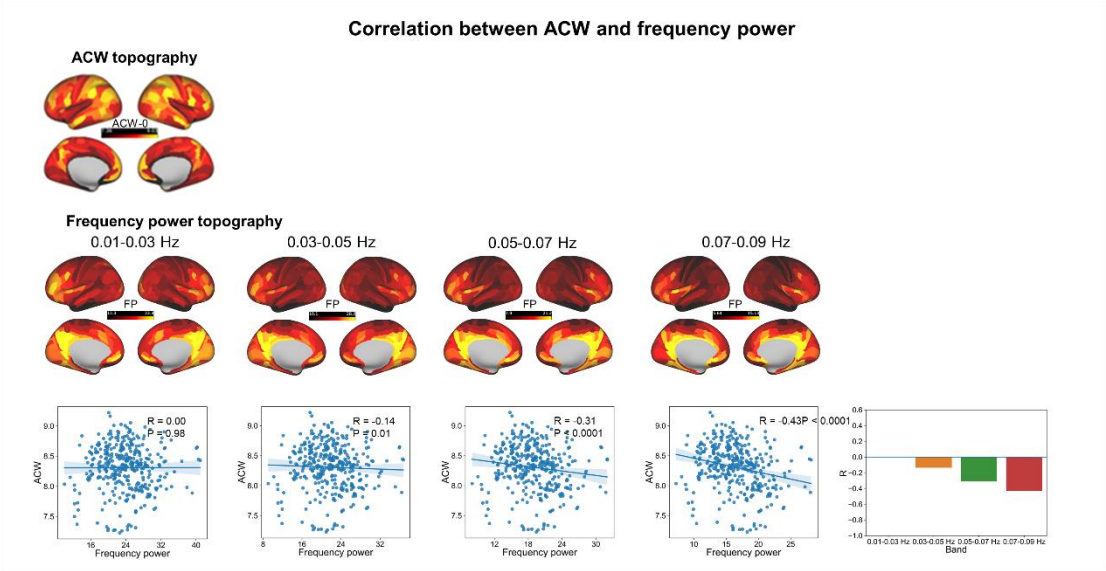

Supplementary Figure 8. Relationship between PF and ACW in surrogate data.

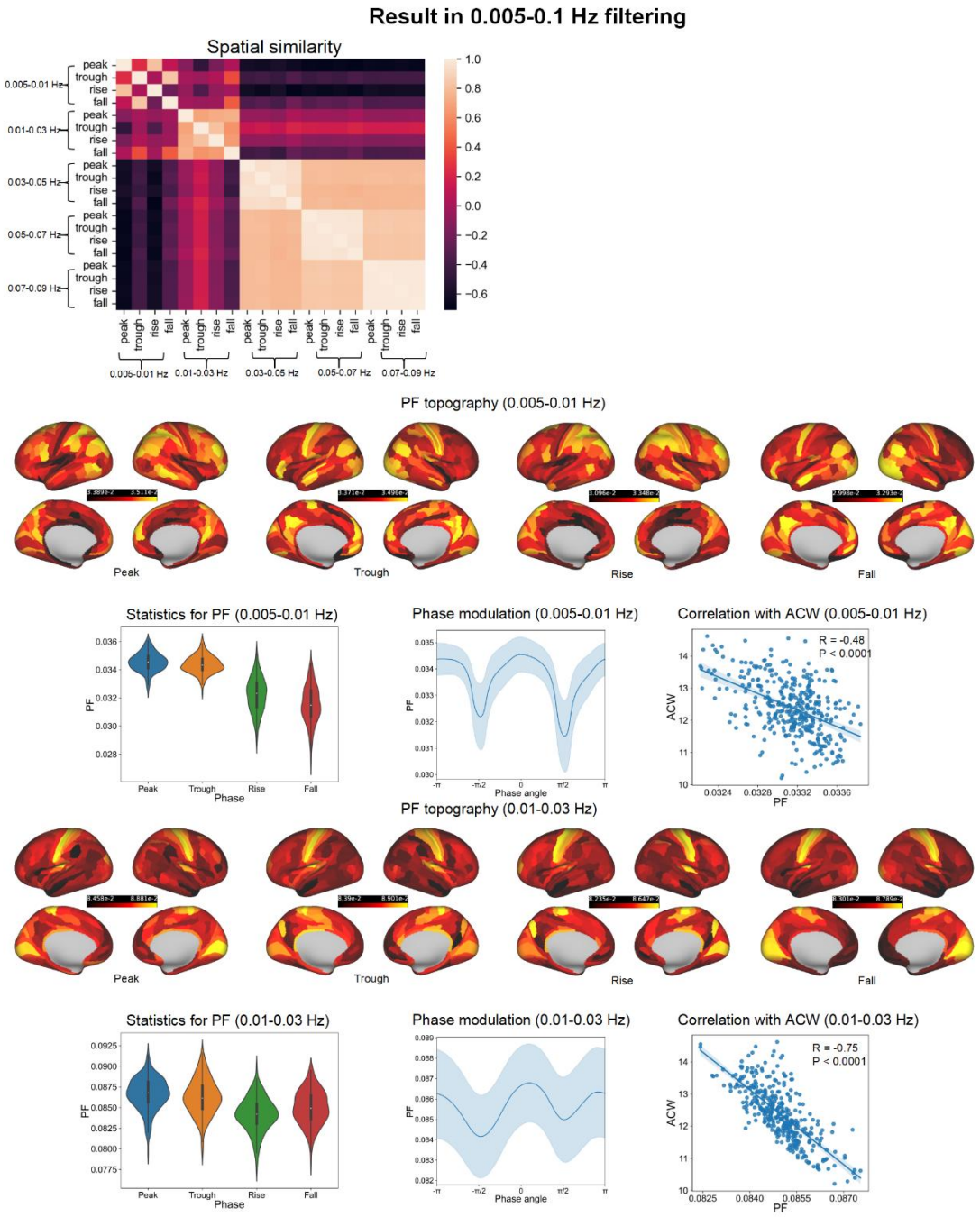

Supplementary Figure 9. Result of 0.005-0.01 Hz to rule out the band-pass edge effect.

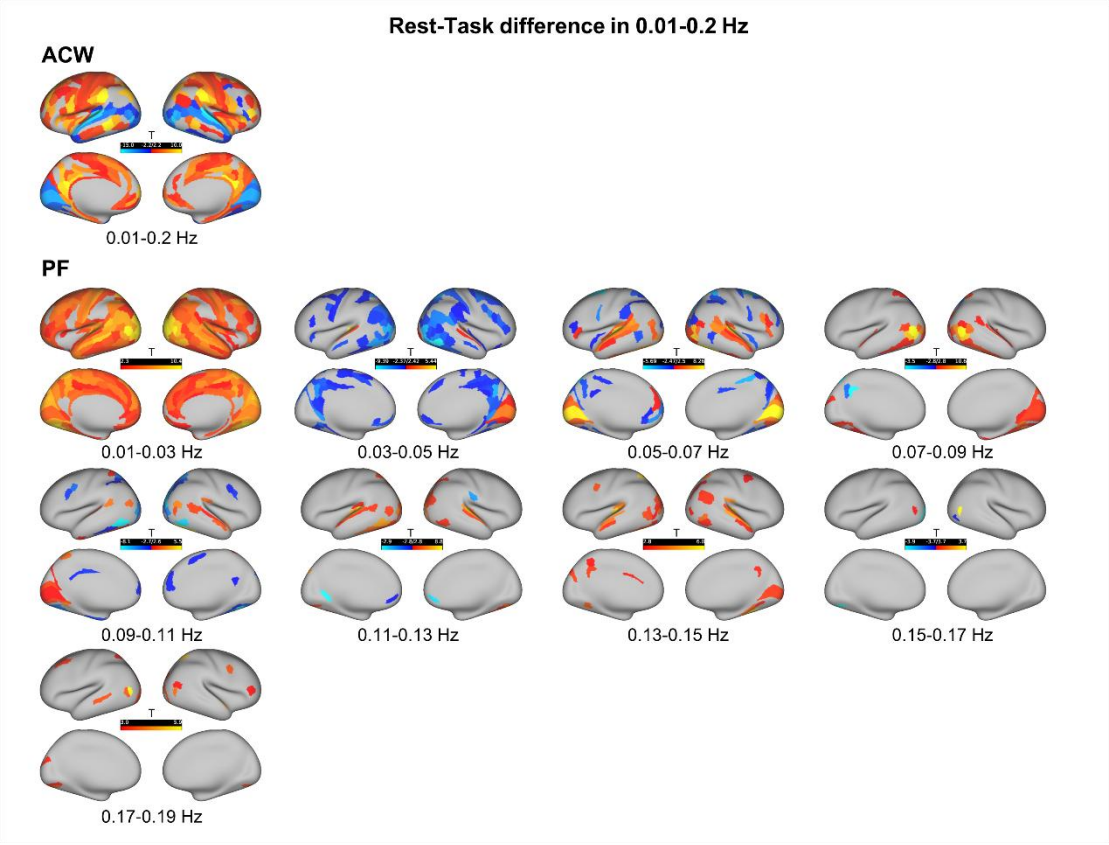

Supplementary Figure 10. Movie-watching task modulation for ACW and PF in 0.01-0.2 Hz.

6.2 Study 2

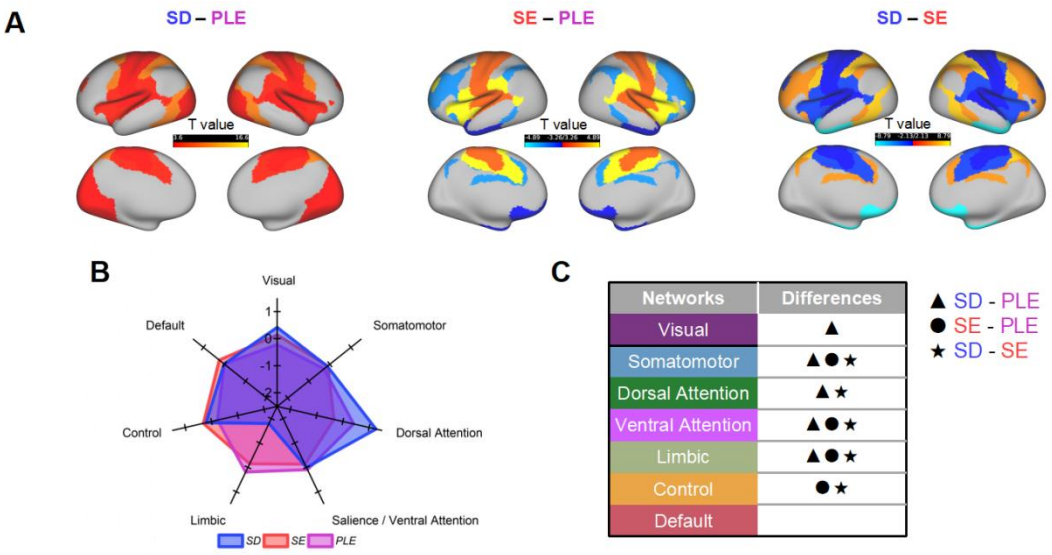

Supplementary Figure 11. Topographical differences between SD, SE, and PLE.

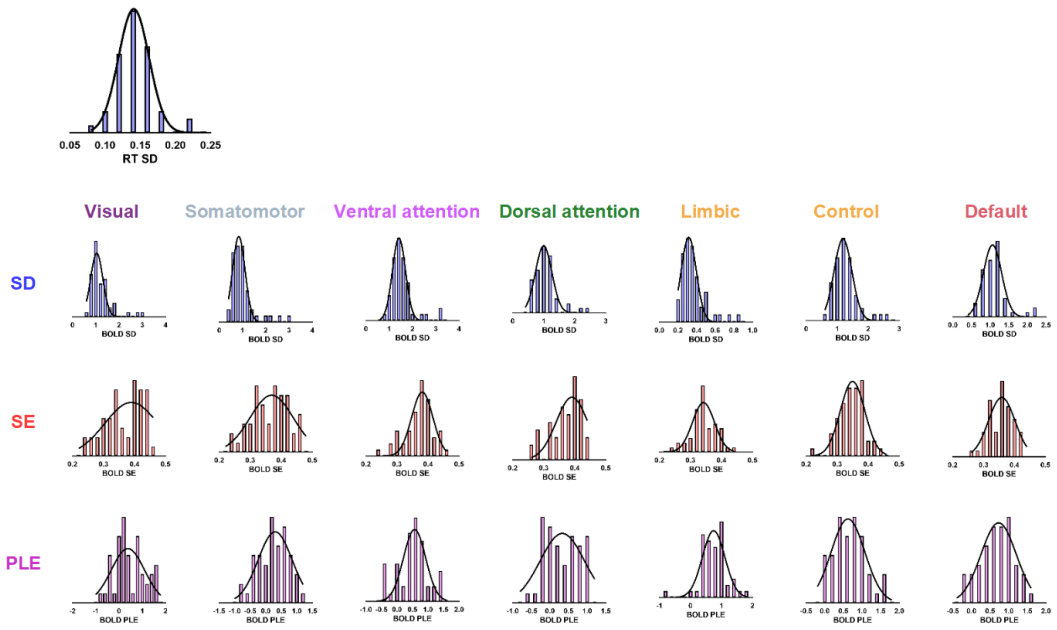

Supplement Figure 12. Distribution of behavioral and neural data.

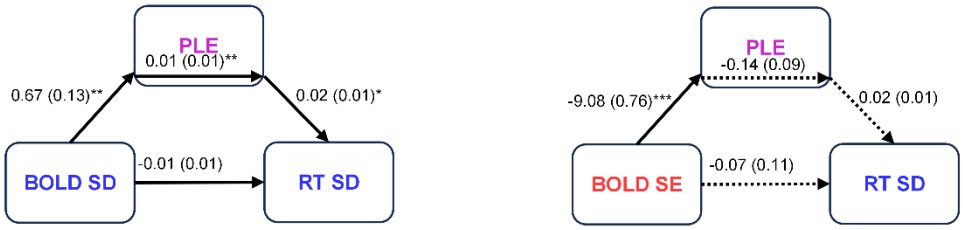

Supplement Figure 13. The mediation model for the relationship between BOLD SD/SE and RT SD in task-effect regression data.

Supplement Table 1. Rest-task difference for three measures in the task-effect regression data (n=49).

	VIS	SMN	DAN	VAN	Limbic	FPN	DMN
T (SD)	3.5***	3.3**	4.8****	5.1***	1.7	2.7**	3.5**
P (SD)	0.00	0.00	0.00	0.00	0.09	0.01	0.00
T (SE)	-3.8***	-3.4**	-6.6****	-4.8****	-1.7	-0.35	-1.8
P (SE)	0.00	0.00	0.00	0.00	0.1	0.73	0.09
T (PLE)	4.00***	6.1****	5.8****	6.2****	2.4	0.92	2.8**
P (PLE)	0.00	0.00	0.00	0.00	0.02	0.36	0.01

Supplement Table 2. Pearson's correlation between RT SD and three BOLD measures in the task-effect regression data (n=49).

	VIS	SMN	DAN	VAN	Limbic	FPN	DMN
R (SD)	0.41**	0.43**	0.3	0.36*	0.19	0.27	0.34*
P (SD)	0.00	0.00	0.04	0.01	0.19	0.06	0.02
R (SE)	-0.46***	-0.37*	-0.38**	-0.35*	-0.22	-0.22	-0.24
P (SE)	0.00	0.01	0.01	0.01	0.14	0.13	0.09

R (PLE)	0.49***	0.36*	0.32	0.28	0.02	0.16	0.2
P (PLE)	0.00	0.01	0.03	0.05	0.87	0.27	0.17

Supplement Table 3. Spearman's correlation between RT SD and three BOLD measures (No significance survive from multiple comparison correction, n=49)

	VIS	**SMN**	**DAN**	**VAN**	**Limbic**	**FPN**	**DMN**
R (SD)	0.29	0.29	0.26	0.36	0.15	0.26	0.26
P (SD)	0.04	0.05	0.07	0.01	0.32	0.07	0.08
R (SE)	-0.32	-0.32	-0.24	-0.28	-0.25	-0.15	-0.10
P (SE)	0.02	0.03	0.10	0.05	0.08	0.31	0.51
R (PLE)	0.40	0.25	0.25	0.26	0.08	0.20	0.09
P (PLE)	0.00	0.08	0.09	0.07	0.56	0.17	0.52

Supplement Table 4. Pearson's correlation between RT mean and three BOLD measures (No significance survive from multiple comparison correction, n=49)

	VIS	**SMN**	**DAN**	**VAN**	**Limbic**	**FPN**	**DMN**
R (SD)	0.23	0.17	0.12	0.1	0.27	0.17	0.25
P (SD)	0.12	0.23	0.4	0.49	0.06	0.24	0.09
R (SE)	-0.17	-0.24	-0.18	-0.09	-0.05	-0.09	-0.19
P (SE)	0.25	0.1	0.23	0.52	0.76	0.55	0.2
R (PLE)	0.16	0.22	0.16	0.24	-0.14	0.04	0.31
P (PLE)	0.26	0.13	0.27	0.09	0.32	0.78	0.03

Supplement Table 5. Pearson's correlation between number of commission errors and three BOLD measures (No significance survive from multiple comparison correction, n=49)

	VIS	**SMN**	**DAN**	**VAN**	**Limbic**	**FPN**	**DMN**
R (SD)	0.33	0.36	0.25	0.34	0.19	0.23	0.29
P (SD)	0.02	0.01	0.08	0.02	0.2	0.12	0.04
R (SE)	-0.35	-0.16	-0.2	-0.21	-0.02	-0.22	-0.2
P (SE)	0.01	0.27	0.17	0.15	0.89	0.13	0.18
R (PLE)	0.38	0.17	0.27	0.19	0.09	0.28	0.2
P (PLE)	0.01	0.23	0.06	0.19	0.54	0.05	0.17

Supplement Table 6. Pearson's correlation between number of omission errors and three BOLD measures (No significance survive from multiple comparison correction, n=49)

	VIS	**SMN**	**DAN**	**VAN**	**Limbic**	**FPN**	**DMN**
R (SD)	0.28	0.35	0.26	0.27	0.08	0.18	0.21
P (SD)	0.05	0.01	0.07	0.07	0.58	0.23	0.15
R (SE)	-0.27	-0.16	-0.13	-0.25	-0.07	-0.04	0.03
P (SE)	0.06	0.27	0.37	0.08	0.63	0.8	0.83
R (PLE)	0.32	0.09	0.12	0.01	0.13	0.04	-0.08
P (PLE)	0.03	0.52	0.43	0.93	0.38	0.76	0.59

Supplement Table 7. Spearman's correlation between RT mean and three BOLD measures (No

significance survive from multiple comparison correction, n=49)

	VIS	SMN	DAN	VAN	Limbic	FPN	DMN
R (SD)	0.31	0.28	0.22	0.19	0.4	0.27	0.34
P (SD)	0.03	0.05	0.12	0.19	0	0.06	0.02
R (SE)	-0.18	-0.26	-0.23	-0.14	0.03	-0.14	-0.2
P (SE)	0.21	0.07	0.12	0.34	0.85	0.35	0.17
R (PLE)	0.18	0.25	0.23	0.31	-0.11	0.11	0.38
P (PLE)	0.21	0.09	0.12	0.03	0.47	0.43	0.01

Supplement Table 8. Spearman's correlation between number of commission errors and three BOLD measures (No significance survive from multiple comparison correction, n=49)

	VIS	SMN	DAN	VAN	Limbic	FPN	DMN
R (SD)	0.29	0.34	0.13	0.31	0.19	0.12	0.26
P (SD)	0.04	0.02	0.36	0.03	0.18	0.4	0.07
R (SE)	-0.38	-0.2	-0.22	-0.25	-0	-0.29	-0.19
P (SE)	0.01	0.17	0.13	0.08	0.99	0.04	0.19
R (PLE)	0.38	0.19	0.29	0.15	-0.02	0.32	0.17
P (PLE)	0.01	0.18	0.04	0.31	0.9	0.03	0.25

Supplement Table 9. Spearman's correlation between number of omission errors and three BOLD measures (No significance survive from multiple comparison correction, n=49)

	VIS	SMN	DAN	VAN	Limbic	FPN	DMN
R (SD)	0.03	0.1	-0.05	0.08	-0.2	-0.05	-0.12
P (SD)	0.81	0.51	0.73	0.57	0.16	0.73	0.4
R (SE)	-0.25	-0.17	-0.03	-0.09	-0.08	0.06	0.18
P (SE)	0.09	0.24	0.86	0.53	0.6	0.67	0.23
R (PLE)	0.28	0.06	0.03	-0.11	0	0.01	-0.26
P (PLE)	0.05	0.69	0.81	0.47	0.97	0.95	0.07

6.3 Study 3

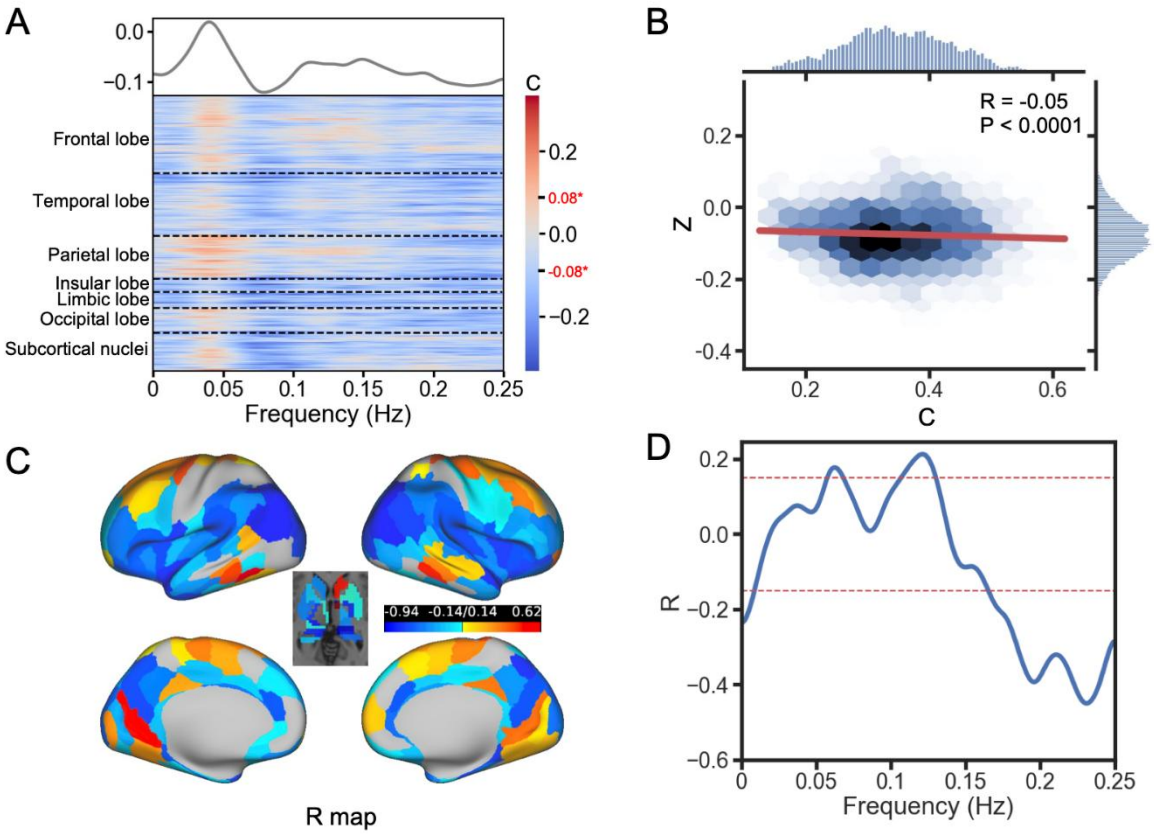

Supplementary Figure 14. The mean FD regressed GS-TV and age-related dedifferentiation correspond to Figure 17B, C. Panel (A): Correlation between GSCORR and age (thermograph) and the mean correlation coefficient across all ROIs (line chart). Panel (B): The overall spatiotemporal dedifferentiation of the GS topography with age. Panel (C): The temporal dedifferentiation. Panel (D): The spatial dedifferentiation.

7 References

Achard, S., Salvador, R., Whitcher, B., Suckling, J., & Bullmore, E. (2006). A Resilient, Low-Frequency, Small-World Human Brain Functional Network with Highly Connected Association Cortical Hubs. *The Journal of Neuroscience*, *26*(1), 63–72. https://doi.org/10.1523/JNEUROSCI.3874-05.2006

Adaikkan, C., Middleton, S. J., Marco, A., Pao, P. C., Mathys, H., Kim, D. N. W., Gao, F., Young, J. Z., Suk, H. J., Boyden, E. S., McHugh, T. J., & Tsai, L. H. (2019). Gamma entrainment binds higher-order brain regions and offers neuroprotection. *Neuron*, *102*(5), 929–943.

Aladjalova, N. A. (1957). Infra-slow rhythmic oscillations of the steady potential of the cerebral cortex. *Nature*, *179*, 957–959. https://doi.org/10.1038/179957a0

Albrecht, D., & Gabriel, S. (1994). Very slow oscillations of activity in geniculate neurones of urethane-anaesthetized rats. *NeuroReport*, *5*(15), 1909.

Alderson, T. H., Bokde, A. L. W., Kelso, J. A. S., Maguire, L., & Coyle, D. (2020). Metastable neural dynamics underlies cognitive performance across multiple behavioural paradigms. *Human Brain Mapping*, *41*(12), 3212–3234. https://doi.org/10.1002/hbm.25009

Andrews-Hanna, J. R., Reidler, J. S., Huang, C., & Buckner, R. L. (2010). Evidence for the default network's role in spontaneous cognition. *Journal of Neurophysiology*, *104*(1), 322–335.

Ao, Y., Catal, Y., Lechner, S., Hua, J., & Northoff, G. (2024). Intrinsic neural timescales relate to the dynamics of infraslow neural waves. *NeuroImage*, *285*, 120482. https://doi.org/10.1016/j.neuroimage.2023.120482

Ao, Y., Klar, P., Catal, Y., Wang, Y., & Northoff, G. (2025). Infra-slow scale-free dynamics modulate the connection of neural and behavioral variability during attention. *Communications Biology*, *8*(1), 1057.

Ao, Y., Kou, J., Yang, C., Wang, Y., Huang, L., Jing, X., Cui, Q., Cai, X., & Chen, J.

(2022). The temporal dedifferentiation of global brain signal fluctuations during human brain ageing. *Scientific Reports*, *12*(1), 3616. https://doi.org/10.1038/s41598-022-07578-6

Ao, Y., Ouyang, Y., Yang, C., & Wang, Y. (2021). Global Signal Topography of the Human Brain: A Novel Framework of Functional Connectivity for Psychological and Pathological Investigations. *Frontiers in Human Neuroscience*, *15*, 644892. https://doi.org/10.3389/fnhum.2021.644892

Ao, Y., Yang, C., Drewes, J., Jiang, M., Huang, L., Jing, X., Northoff, G., & Wang, Y. (2023). Spatiotemporal dedifferentiation of the global brain signal topography along the adult lifespan. *Human Brain Mapping*, *44*(17), 5906–5918. https://doi.org/10.1002/hbm.26484

Armbruster-Genç, D. J., Ueltzhöffer, K., & Fiebach, C. J. (2016). Brain signal variability differentially affects cognitive flexibility and cognitive stability. *Journal of Neuroscience*, *36*(14), 3978–3987.

Auer, D. P. (2008). Spontaneous low-frequency blood oxygenation level-dependent fluctuations and functional connectivity analysis of the “resting” brain. *Journal of Magnetic Resonance Imaging*, *26*(7), 1055–1064. https://doi.org/10.1016/j.mri.2008.05.008

Baltes, P. B., & Lindenberger, U. (1997). Emergence of a powerful connection between sensory and cognitive functions across the adult life span: A new window to the study of cognitive aging? *Psychology and Aging*, *12*(1), 12.

Baria, A. T., Baliki, M. N., Parrish, T., & Apkarian, A. V. (2011). Anatomical and functional assemblies of brain BOLD oscillations. *Journal of Neuroscience*, *31*(21), 7910–7919.

Beltramo, R., & Scanziani, M. (2019). A collicular visual cortex: Neocortical space for an ancient midbrain visual structure. *Science*, *363*(6422), 64–69. https://doi.org/10.1126/science.aau7052

Benjamini, Y., & Hochberg, Y. (1995). Controlling the false discovery rate: A practical and powerful approach to multiple testing. *Journal of the Royal Statistical Society: Series B (Methodological)*, *57*(1), 289–300.

Benwell, C. S. Y., London, R. E., Tagliabue, C. F., Veniero, D., Gross, J., Keitel, C., & Thut, G. (2019). Frequency and power of human alpha oscillations drift systematically with time-on-task. *Neuroimage*, *192*, 101–114. https://doi.org/10.1016/j.neuroimage.2019.02.067

Birn, R. M., Diamond, J. B., Smith, M. A., & Bandettini, P. A. (2006). Separating respiratory-variation-related fluctuations from neuronal-activity-related fluctuations in fMRI. *Neuroimage*, *31*(4), 1536–1548. https://doi.org/10.1016/j.neuroimage.2006.02.048

Biswal, B. B., & Uddin, L. Q. (2025). The history and future of resting-state functional magnetic resonance imaging. *Nature*, *641*(8065), 1121–1131. https://doi.org/10.1038/s41586-025-08953-9

Bolt, T., Nomi, J. S., Bzdok, D., Salas, J. A., Chang, C., Thomas Yeo, B. T., Uddin, L. Q., & Keilholz, S. D. (2022). A parsimonious description of global functional brain organization in three spatiotemporal patterns. *Nature Neuroscience*, *25*(8), 1093–1103. https://doi.org/10.1038/s41593-022-01118-1

Boubela, R. N., Kalcher, K., Huf, W., Kronnerwetter, C., Filzmoser, P., & Moser, E. (2013). Beyond Noise: Using Temporal ICA to Extract Meaningful Information from High-Frequency fMRI Signal Fluctuations during Rest. *Frontiers in Human Neuroscience*, *7*. https://doi.org/10.3389/fnhum.2013.00168

Boylan, M. A., Foster, C. M., Pongpipat, E. E., Webb, C. E., Rodrigue, K. M., & Kennedy, K. M. (2021). Greater BOLD Variability is Associated With Poorer Cognitive Function in an Adult Lifespan Sample. *Cerebral Cortex*, *31*(1), 562–574. https://doi.org/10.1093/cercor/bhaa243

Brown, J. A., Lee, A. J., Pasquini, L., & Seeley, W. W. (2022). A dynamic gradient architecture generates brain activity states. *NeuroImage*, *261*, 119526. https://doi.org/10.1016/j.neuroimage.2022.119526

Buccellato, A., Zang, D., Zilio, F., Gomez-Pilar, J., Wang, Z., Qi, Z., Zheng, R., Xu, Z., Wu, X., & Bisiacchi, P. (2023). Disrupted relationship between intrinsic neural timescales and alpha peak frequency during unconscious states–A high-density EEG study. *Neuroimage*, *265*,

119802. https://doi.org/10.1016/j.neuroimage.2022.119802

Buckner, R. L., & DiNicola, L. M. (2019). The brain's default network: Updated anatomy, physiology and evolving insights. *Nature Review Neuroscience*, *20*(10), 593–608. https://doi.org/10.1038/s41583-019-0212-7

Busch, N. A., Dubois, J., & VanRullen, R. (2009). The Phase of Ongoing EEG Oscillations Predicts Visual Perception. *Journal of Neuroscience*, *29*(24), 7869–7876. https://doi.org/10.1523/Jneurosci.0113-09.2009

Buzsáki, G. (2006). *Rhythms of the Brain*. Oxford university press.

Buzsáki, G. (2025). Time, space, memory and brain–body rhythms. *Nature Reviews Neuroscience*. https://doi.org/10.1038/s41583-025-00987-2

Buzsáki, G., & Draguhn, A. (2004). Neuronal Oscillations in Cortical Networks. *Science*, *304*(5679), 1926–1929. https://doi.org/10.1126/science.1099745

Cao, M., Wang, J., Dai, Z., Cao, X., Jiang, L., Fan, F., Song, X., Xia, M., Shu, N., Dong, Q., Michael P. Milham, F. Xavier Castellanos, Zuo, X., & He, Y. (2014). Topological organization of the human brain functional connectome across the lifespan. *Developmental Cognitive Neuroscience*, *7*(1), 76–93.

Çatal, Y., Gomez-Pilar, J., & Northoff, G. (2022). Intrinsic dynamics and topography of sensory input systems. *Cerebral Cortex*, *32*(20), 4592–4604.

Çatal, Y., Keskin, K., Wolman, A., Buccellato, A., & Northoff, G. (2025). Intrinsic Neural Timescales Relate to Event-Related Activity—Key Role for Intracolumnar Connections. *Journal of Neuroscience*, *45*(48). https://doi.org/10.1523/JNEUROSCI.0896-25.2025

Çatal, Y., Keskin, K., Wolman, A., Klar, P., Smith, D., & Northoff, G. (2024). Flexibility of intrinsic neural timescales during distinct behavioral states. *Communications Biology*, *7*(1), 1667.

Çatal, Y., Wolman, A., Buccellato, A., Keskin, K., & Northoff, G. (2025). *How Intrinsic Neural Timescales Relate To Event-Related Activity – Key Role For Intracolumnar*

Connections. Neuroscience. https://doi.org/10.1101/2025.01.10.632350

Chan, M. Y., Park, D. C., Savalia, N. K., Petersen, S. E., & Wig, G. S. (2014). Decreased segregation of brain systems across the healthy adult lifespan. *Proceedings of the National Academy of Sciences of the United States of America*, *111*(46), E4997-5006. https://doi.org/10.1073/pnas.1415122111

Chang, C., Cunningham, J. P., & Glover, G. H. (2009). Influence of heart rate on the BOLD signal: The cardiac response function. *NeuroImage*, *44*(3), 857–869. https://doi.org/10.1016/j.neuroimage.2008.09.029

Chang, C., & Glover, G. H. (2009). Relationship between respiration, end-tidal CO2, and BOLD signals in resting-state fMRI. *NeuroImage*, *47*(4), 1381–1393. https://doi.org/10.1016/j.neuroimage.2009.04.048

Chang, C., & Glover, G. H. (2010). Time–frequency dynamics of resting-state brain connectivity measured with fMRI. *NeuroImage*, *50*(1), 81–98. https://doi.org/10.1016/j.neuroimage.2009.12.011

Chen, H., Duan, X., Liu, F., Lu, F., Ma, X., Zhang, Y., Uddin, L. Q., & Chen, H. (2016). Multivariate classification of autism spectrum disorder using frequency-specific resting-state functional connectivity-A multi-center study. *Progress in Neuro-Psychopharmacology and Biological Psychiatry*, *64*, 1–9.

Chen, J. E., & Glover, G. H. (2015). BOLD fractional contribution to resting-state functional connectivity above 0.1 Hz. *Neuroimage*, *107*, 207–218.

Cheng, X., Yuan, Y., Wang, Y., & Wang, R. (2020). Neural antagonistic mechanism between default-mode and task-positive networks. *Neurocomputing*, *417*, 74–85. https://doi.org/10.1016/j.neucom.2020.07.079

Chuipka, N., Smy, T., & Northoff, G. (2025). From neural activity to behavioral engagement: Temporal dynamics as their “common currency” during music. *Neuroimage*, 121209.

Churchill, N. W., Spring, R., Grady, C., Cimprich, B., Askren, M. K., Reuter-Lorenz, P. A., Jung, M. S., Peltier, S., Strother, S. C., & Berman, M. G. (2016). The suppression of scale-free fMRI brain dynamics across three different sources of effort: Aging, task novelty and task difficulty. *Scientific Reports*, *6*(1), 30895. https://doi.org/10.1038/srep30895

Cieri, F., Zhuang, X., Caldwell, J. Z., & Cordes, D. (2021). Brain entropy during aging through a free energy principle approach. *Frontiers in Human Neuroscience*, *15*, 647513.

Clayton, M. S., Yeung, N., & Kadosh, R. C. (2015). The roles of cortical oscillations in sustained attention. *Trends in Cognitive Sciences*, *19*(4), 188–195.

Cohen, M. X. (2014). Fluctuations in oscillation frequency control spike timing and coordinate neural networks. *Journal of Neuroscience*, *34*(27), 8988–8998. https://doi.org/10.1523/JNEUROSCI.0261-14.2014

Cooper, C., Parthier, D., Sibille, J., Tukker, J. J., Tritsch, N., & Schmitz, D. (2025). Ultraslow serotonin oscillations in the hippocampus delineate substates across NREM and waking. *eLife*, *13*, RP101105. https://doi.org/10.7554/eLife.101105

Damoiseaux, J. S. (2017). Effects of aging on functional and structural brain connectivity. *Neuroimage*, *160*, 32–40. https://doi.org/10.1016/j.neuroimage.2017.01.077

Das, A., Murphy, K., & Drew, P. J. (2021). Rude mechanicals in brain haemodynamics: Non-neural actors that influence blood flow. *Philosophical Transactions of the Royal Society B: Biological Sciences*, *376*(1815), 20190635. https://doi.org/10.1098/rstb.2019.0635

De Domenico, M., Sasai, S., & Arenas, A. (2016). Mapping Multiplex Hubs in Human Functional Brain Networks. *Frontiers in Neuroscience*, *10*, 326. https://doi.org/10.3389/fnins.2016.00326

Demirtaş, M., Ponce-Alvarez, A., Gilson, M., Hagmann, P., Mantini, D., Betti, V., Romani, G. L., Friston, K., Corbetta, M., & Deco, G. (2019). Distinct modes of functional connectivity induced by movie-watching. *NeuroImage*, *184*, 335–348. https://doi.org/10.1016/j.neuroimage.2018.09.042

D’Esposito, M., Zarahn, E., Aguirre, G. K., & Rypma, B. (1999). The effect of normal aging on the coupling of neural activity to the bold hemodynamic response. *Neuroimage*, *10*(1), 6–14.

Dickey, C. W., Verzhbinsky, I. A., Jiang, X., Rosen, B. Q., Kajfez, S., Stedelin, B., Shih, J. J., Ben-Haim, S., Raslan, A. M., Eskandar, E. N., Gonzalez-Martinez, J., Cash, S. S., & Halgren, E. (2022). Widespread ripples synchronize human cortical activity during sleep, waking, and memory recall. *Proceedings of the National Academy of Sciences*, *119*(28), e2107797119. https://doi.org/10.1073/pnas.2107797119

Ding, N., Melloni, L., Zhang, H., Tian, X., & Poeppel, D. (2016). Cortical tracking of hierarchical linguistic structures in connected speech. *Nat Neurosci*, *19*(1), 158–164. https://doi.org/10.1038/nn.4186

Dinstein, I., Heeger, D. J., & Behrmann, M. (2015). Neural variability: Friend or foe? *Trends Cogn Sci*, *19*(6), 322–328. https://doi.org/10.1016/j.tics.2015.04.005

Djimbouon, F., Stoyanov, D., Çatal, Y., Paunova, R., & Northoff, G. (2025). Reduced intrinsic neural timescales and their relationship to global network connectivity in depression. *Journal of Affective Disorders*, *390*, 119775. https://doi.org/10.1016/j.jad.2025.119775

Dong, Q., He, J., & Chai, Z. (2013). Astrocytic Ca2+ waves mediate activation of extrasynaptic NMDA receptors in hippocampal neurons to aggravate brain damage during ischemia. *Neurobiology of Disease*, *58*, 68–75. https://doi.org/10.1016/j.nbd.2013.05.005

Donoghue, T., Haller, M., Peterson, E. J., Varma, P., Sebastian, P., Gao, R., Noto, T., Lara, A. H., Wallis, J. D., Knight, R. T., Shestyuk, A., & Voytek, B. (2020). Parameterizing neural power spectra into periodic and aperiodic components. *Nature Neuroscience*, *23*(12), 1655–1665. https://doi.org/10.1038/s41593-020-00744-x

Doucet, G., Naveau, M., Petit, L., Zago, L., Crivello, F., Jobard, G., Delcroix, N., Mellet, E., Tzourio-Mazoyer, N., Mazoyer, B., & Joliot, M. (2012). Patterns of hemodynamic low-frequency oscillations in the brain are modulated by the nature of free thought during rest. *NeuroImage*, *59*(4), 3194–3200. https://doi.org/10.1016/j.neuroimage.2011.11.059

Drew, P. J., Duyn, J. H., Golanov, E., & Kleinfeld, D. (2008). Finding coherence in spontaneous oscillations. *Nature Neuroscience*, *11*(9), 991–993.

Du, C., Volkow, N. D., Koretsky, A. P., & Pan, Y. (2014). Low-frequency calcium oscillations accompany deoxyhemoglobin oscillations in rat somatosensory cortex. *Proceedings of the National Academy of Sciences of the United States of America*, *111*(43), E4677-86. https://doi.org/10.1073/pnas.1410800111

Esteban, O., Markiewicz, C. J., Blair, R. W., Moodie, C. A., Isik, A. I., Erramuzpe, A., Kent, J. D., Goncalves, M., DuPre, E., & Snyder, M. (2019). fMRIPrep: A robust preprocessing pipeline for functional MRI. *Nature Methods*, *16*(1), 111–116.

Esterman, M., Noonan, S. K., Rosenberg, M., & DeGutis, J. (2013). In the zone or zoning out? Tracking behavioral and neural fluctuations during sustained attention. *Cerebral Cortex*, *23*(11), 2712–2723.

Esterman, M., Rosenberg, M. D., & Noonan, S. K. (2014). Intrinsic Fluctuations in Sustained Attention and Distractor Processing. *The Journal of Neuroscience*, *34*(5), 1724–1730. https://doi.org/10.1523/JNEUROSCI.2658-13.2014

Esterman, M., & Rothlein, D. (2019). Models of sustained attention. *Current Opinion in Psychology*, *29*, 174–180.

Euler, M. J., Vehar, J. V., Guevara, J. E., Geiger, A. R., Deboeck, P. R., & Lohse, K. R. (2024). Associations between the resting EEG aperiodic slope and broad domains of cognitive ability. *Psychophysiology*, *61*(6), e14543. https://doi.org/10.1111/psyp.14543

Fabiani, M., Gordon, B. A., Maclin, E. L., Pearson, M. A., Brumback-Peltz, C. R., Low, K. A., McAuley, E., Sutton, B. P., Kramer, A. F., & Gratton, G. (2014). Neurovascular coupling in normal aging: A combined optical, ERP and fMRI study. *NeuroImage*, *85*, 592–607. https://doi.org/10.1016/j.neuroimage.2013.04.113

Fair, D. A., Schlaggar, B. L., Cohen, A. L., Miezin, F. M., Dosenbach, N. U., Wenger, K. K., Fox, M. D., Snyder, A. Z., Raichle, M. E., & Petersen, S. E. (2007). A method for using blocked and event-related fMRI data to study "resting state" functional connectivity.

Neuroimage, *35*(1), 396–405. https://doi.org/10.1016/j.neuroimage.2006.11.051

Fan, L., Li, H., Zhuo, J., Zhang, Y., Wang, J., Chen, L., Yang, Z., Chu, C., Xie, S., Laird, A. R., Fox, P. T., Eickhoff, S. B., Yu, C., & Jiang, T. (2016). The Human Brainnetome Atlas: A New Brain Atlas Based on Connectional Architecture. *Cerebral Cortex*, *26*(8), 3508–3526. https://doi.org/10.1093/cercor/bhw157

Ferreira, L. K., & Busatto, G. F. (2013). Resting-state functional connectivity in normal brain aging. *Neuroscience & Biobehavioral Reviews*, *37*(3), 384–400. https://doi.org/10.1016/j.neubiorev.2013.01.017

Fiebelkorn, I. C., & Kastner, S. (2019). A Rhythmic Theory of Attention. *Trends in Cognitive Sciences*, *23*(2), 87–101. https://doi.org/10.1016/j.tics.2018.11.009

Finn, E. S. (2021). Is it time to put rest to rest? *Trends in Cognitive Sciences*, *25*(12), 1021–1032. https://doi.org/10.1016/j.tics.2021.09.005

Fortenbaugh, F. C., Rothlein, D., McGlinchey, R., DeGutis, J., & Esterman, M. (2018). Tracking behavioral and neural fluctuations during sustained attention: A robust replication and extension. *Neuroimage*, *171*, 148–164.

Fox, M. D., & Raichle, M. E. (2007). Spontaneous fluctuations in brain activity observed with functional magnetic resonance imaging. *Nature Review Neuroscience*, *8*(9), 700–711. https://doi.org/10.1038/nrn2201

Fox, M. D., Snyder, A. Z., Vincent, J. L., Corbetta, M., Van Essen, D. C., & Raichle, M. E. (2005). The human brain is intrinsically organized into dynamic, anticorrelated functional networks. *Proceedings of the National Academy of Sciences*, *102*(27), 9673–9678. https://doi.org/10.1073/pnas.0504136102

Fox, M. D., Zhang, D., Snyder, A. Z., & Raichle, M. E. (2009). The global signal and observed anticorrelated resting state brain networks. *J Neurophysiol*, *101*(6), 3270–3283. https://doi.org/10.1152/jn.90777.2008

Frelih, T., Matkovič, A., Mlinarič, T., Bon, J., & Repovš, G. (2025). Modulation of

aperiodic EEG activity provides sensitive index of cognitive state changes during working memory task. *eLife*, *13*, RP101071. https://doi.org/10.7554/eLife.101071

Friston, K. (2010). The free-energy principle: A unified brain theory? *Nature Reviews Neuroscience*, *11*(2), 127–138. https://doi.org/10.1038/nrn2787

Friston, K. (2020). Dynamics versus dualism. *Physics of Life Reviews*, *33*, 70–72. https://doi.org/10.1016/j.plrev.2019.09.002

Fultz, N. E., Bonmassar, G., Setsompop, K., Stickgold, R. A., Rosen, B. R., Polimeni, J. R., & Lewis, L. D. (2019). Coupled electrophysiological, hemodynamic, and cerebrospinal fluid oscillations in human sleep. *Science*, *366*(6465), 628–631. https://doi.org/10.1126/science.aax5440

Fuscà, M., Siebenhühner, F., Wang, S. H., Myrov, V., Arnulfo, G., Nobili, L., Palva, J. M., & Palva, S. (2023). Brain criticality predicts individual levels of inter-areal synchronization in human electrophysiological data. *Nature Communications*, *14*(1), 4736.

Gabhart, K. M., Xiong, Y. (Sophy), & Bastos, A. M. (2025). Predictive coding: A more cognitive process than we thought? *Trends in Cognitive Sciences*, *29*(7), 627–640. https://doi.org/10.1016/j.tics.2025.01.012

Gao, X., Gentile, F., & Rossion, B. (2018). Fast periodic stimulation (FPS): A highly effective approach in fMRI brain mapping. *Brain Structure and Function*, *223*, 2433–2454.

Garrett, D. D., Kovacevic, N., McIntosh, A. R., & Grady, C. L. (2010). Blood oxygen level-dependent signal variability is more than just noise. *The Journal of Neuroscience*, *30*(14), 4914–4921.

Garrett, D. D., Kovacevic, N., McIntosh, A. R., & Grady, C. L. (2011). The importance of being variable. *Journal of Neuroscience*, *31*(12), 4496–4503. https://doi.org/10.1523/JNEUROSCI.5641-10.2011

Garrett, D. D., Samanez-Larkin, G. R., MacDonald, S. W. S., Lindenberger, U., McIntosh, A. R., & Grady, C. L. (2013). Moment-to-moment brain signal variability: A next

frontier in human brain mapping? *Neuroscience & Biobehavioral Reviews*, *37*(4), 610–624. https://doi.org/10.1016/j.neubiorev.2013.02.015

Geerligs, L., Tsvetanov, K. A., & Henson, R. N. (2017). Challenges in measuring individual differences in functional connectivity using fMRI: the case of healthy aging. *Human Brain Mapping*, *38*(8), 4125–4156.

Ghosh, A., Rho, Y., McIntosh, A. R., Kötter, R., & Jirsa, V. K. (2008). Noise during Rest Enables the Exploration of the Brain's Dynamic Repertoire. *PLoS Computational Biology*, *4*(10), e1000196. https://doi.org/10.1371/journal.pcbi.1000196

Glasser, M. F., Coalson, T. S., Robinson, E. C., Hacker, C. D., Harwell, J., Yacoub, E., Ugurbil, K., Andersson, J., Beckmann, C. F., Jenkinson, M., Smith, S. M., & Van Essen, D. C. (2016). A multi-modal parcellation of human cerebral cortex. *Nature*, *536*(7615), 171–178. https://doi.org/10.1038/nature18933

Glerean, E., Salmi, J., Lahnakoski, J. M., Jääskeläinen, I. P., & Sams, M. (2012). Functional magnetic resonance imaging phase synchronization as a measure of dynamic functional connectivity. *Brain Connectivity*, *2*(2), 91–101.

Glover, G. H., Li, T.-Q., & Ress, D. (2000). Image-based method for retrospective correction of physiological motion effects in fMRI: RETROICOR. *Magnetic Resonance in Medicine*, *44*(1), 162–167. https://doi.org/10.1002/1522-2594(200007)44:1%3C162::AID-MRM23%3E3.0.CO;2-E

Godwin, D., Ji, A., Kandala, S., & Mamah, D. (2017). Functional Connectivity of Cognitive Brain Networks in Schizophrenia during a Working Memory Task. *Frontiers in Psychiatry*, *8*, Article 294. https://doi.org/10.3389/fpsyt.2017.00294

Golesorkhi, M., Gomez-Pilar, J., Çatal, Y., Tumati, S., Yagoub, M. C., Stamatakis, E. A., & Northoff, G. (2022). From temporal to spatial topography: Hierarchy of neural dynamics in higher-and lower-order networks shapes their complexity. *Cerebral Cortex*, *32*(24), 5637–5653.

Golesorkhi, M., Gomez-Pilar, J., Tumati, S., Fraser, M., & Northoff, G. (2021).

Temporal hierarchy of intrinsic neural timescales converges with spatial core-periphery organization. *Communications Biology*, *4*(1), 277. https://doi.org/10.1038/s42003-021-01785-z

Golesorkhi, M., Gomez-Pilar, J., Zilio, F., Berberian, N., Wolff, A., Yagoub, M. C. E., & Northoff, G. (2021). The brain and its time: Intrinsic neural timescales are key for input processing. *Communications Biology*, *4*(1), 970. https://doi.org/10.1038/s42003-021-02483-6

Gong, Z.-Q., & Zuo, X.-N. (2023). Connectivity gradients in spontaneous brain activity at multiple frequency bands. *Cerebral Cortex*, *33*(17), 9718–9728. https://doi.org/10.1093/cercor/bhad238

Gong, Z.-Q., & Zuo, X.-N. (2025). Dark Brain Energy: Toward an Integrative Model of Spontaneous Slow Oscillations. *Physics of Life Reviews*.

Grady, C. L., & Garrett, D. D. (2014). Understanding variability in the BOLD signal and why it matters for aging. *Brain Imaging and Behavior*, *8*, 274–283.

Grady, C. L., & Garrett, D. D. (2018). Brain signal variability is modulated as a function of internal and external demand in younger and older adults. *NeuroImage*, *169*, 510–523. https://doi.org/10.1016/j.neuroimage.2017.12.031

Grinband, J., Steffener, J., Razlighi, Q. R., & Stern, Y. (2017). BOLD neurovascular coupling does not change significantly with normal aging. *Human Brain Mapping*, *38*(7), 3538–3551.

Gu, Y., Sainburg, L. E., Kuang, S., Han, F., Williams, J. W., Liu, Y., Zhang, N., Zhang, X., Leopold, D. A., & Liu, X. (2021). Brain Activity Fluctuations Propagate as Waves Traversing the Cortical Hierarchy. *Cerebral Cortex*, *31*(9), 3986–4005. https://doi.org/10.1093/cercor/bhab064

Guitart-Masip, M., Salami, A., Garrett, D., Rieckmann, A., Lindenberger, U., & Bäckman, L. (2016). BOLD variability is related to dopaminergic neurotransmission and cognitive aging. *Cerebral Cortex*, *26*(5), 2074–2083.

Gutierrez-Barragan, D., Basson, M. A., Panzeri, S., & Gozzi, A. (2019). Infraslow State Fluctuations Govern Spontaneous fMRI Network Dynamics. *Current Biology*, *29*(14), 2295-2306.e5. https://doi.org/10.1016/j.cub.2019.06.017

Gutierrez-Barragan, D., Singh, N. A., Alvino, F. G., Coletta, L., Rocchi, F., De Guzman, E., Galbusera, A., Uboldi, M., Panzeri, S., & Gozzi, A. (2022). Unique spatiotemporal fMRI dynamics in the awake mouse brain. *Current Biology*, *32*(3), 631-644.e6. https://doi.org/10.1016/j.cub.2021.12.015

Hacker, C. D., Snyder, A. Z., Pahwa, M., Corbetta, M., & Leuthardt, E. C. (2017). Frequency-specific electrophysiologic correlates of resting state fMRI networks. *Neuroimage*, *149*, 446–457.

Han, S., Zong, X., Hu, M., Yu, Y., Xiao Wang, Long, Z., Wang, Y., Chen, X., & Chen, H. (2017). Frequency-selective alteration in the resting-state corticostriatal-thalamo-cortical circuit correlates with symptoms severity in first-episode drug-naive patients with schizophrenia. *Schizophrenia Research*, *189*, 175–180.

Han, Y., Wang, J., Zhao, Z., Min, B., Lu, J., Li, K., He, Y., & Jia, J. (2011). Frequency-dependent changes in the amplitude of low-frequency fluctuations in amnestic mild cognitive impairment: A resting-state fMRI study. *Neuroimage*, *55*(1), 287–295. https://doi.org/10.1016/j.neuroimage.2010.11.059

Hanslmayr, S., Gross, J., Klimesch, W., & Shapiro, K. L. (2011). The role of alpha oscillations in temporal attention. *Brain Research Reviews*, *67*(1–2), 331–343.

Hasson, U., Chen, J., & Honey, C. J. (2015). Hierarchical process memory: Memory as an integral component of information processing. *Trends in Cognitive Sciences*, *19*(6), 304–313. https://doi.org/10.1016/j.tics.2015.04.006

He, B. J. (2011). Scale-Free Properties of the Functional Magnetic Resonance Imaging Signal during Rest and Task. *The Journal of Neuroscience*, *31*(39), 13786–13795. https://doi.org/10.1523/JNEUROSCI.2111-11.2011

He, B. J. (2014). Scale-free brain activity: Past, present, and future. *Trends in Cognitive*

Sciences, *18*(9), 480–487. https://doi.org/10.1016/j.tics.2014.04.003

He, B. J., Zempel, J. M., Snyder, A. Z., & Raichle, M. E. (2010). The Temporal Structures and Functional Significance of Scale-free Brain Activity. *Neuron*, *66*(3), 353–369. https://doi.org/10.1016/j.neuron.2010.04.020

Helfrich, R. F., Fiebelkorn, I. C., Szczepanski, S. M., Lin, J. J., Parvizi, J., Knight, R. T., & Kastner, S. (2018). Neural Mechanisms of Sustained Attention Are Rhythmic. *Neuron*, *99*(4), 854-865 e5. https://doi.org/10.1016/j.neuron.2018.07.032

Herbst, S. K., & Landau, A. N. (2016). Rhythms for cognition: The case of temporal processing. *Current Opinion in Behavioral Sciences*, *8*, 85–93. https://doi.org/10.1016/j.cobeha.2016.01.014

Hiltunen, T., Kantola, J., Abou Elseoud, A., Lepola, P., Suominen, K., Starck, T., Nikkinen, J., Remes, J., Tervonen, O., & Palva, S. (2014). Infra-slow EEG fluctuations are correlated with resting-state network dynamics in fMRI. *Journal of Neuroscience*, *34*(2), 356–362.

Himberger, K. D., Chien, H.-Y., & Honey, C. J. (2018). Principles of temporal processing across the cortical hierarchy. *Neuroscience*, *389*, 161–174. https://doi.org/10.1016/j.neuroscience.2018.04.030

Honari, H., Choe, A. S., & Lindquist, M. A. (2021). Evaluating phase synchronization methods in fMRI: A comparison study and new approaches. *Neuroimage*, *228*, 117704. https://doi.org/10.1016/j.neuroimage.2020.117704

Honey, C. J., Thesen, T., Donner, T. H., Silbert, L. J., Carlson, C. E., Devinsky, O., Doyle, W. K., Rubin, N., Heeger, D. J., & Hasson, U. (2012). Slow cortical dynamics and the accumulation of information over long timescales. *Neuron*, *76*(2), 423–434. https://doi.org/http://dx.doi.org/10.1016/j.neuron.2012.08.011

Hua, J., Wolff, A., Zhang, J., Yao, L., Zang, Y., Luo, J., Ge, X., Liu, C., & Northoff, G. (2022). Alpha and theta peak frequency track on-and off-thoughts. *Communications Biology*, *5*(1), 209. https://doi.org/10.1038/s42003-022-03146-w

Huang, Z., Dai, R., Wu, X., Yang, Z., Liu, D., Hu, J., Gao, L., Tang, W., Mao, Y., Jin, Y., Wu, X., Liu, B., Zhang, Y., Lu, L., Laureys, S., Weng, X., & Northoff, G. (2014). The self and its resting state in consciousness: An investigation of the vegetative state. *Human Brain Mapping*, *35*(5), 1997–2008. https://doi.org/10.1002/hbm.22308

Huang, Z., Zhang, J., Longtin, A., Dumont, G., Duncan, N. W., Pokorny, J., Qin, P., Dai, R., Ferri, F., Weng, X., & Northoff, G. (2017). Is There a Nonadditive Interaction Between Spontaneous and Evoked Activity? Phase-Dependence and Its Relation to the Temporal Structure of Scale-Free Brain Activity. *Cerebral Cortex*, bhv288. https://doi.org/10.1093/cercor/bhv288

Huang, Z., Zhang, J., Wu, J., Qin, P., Wu, X., Wang, Z., Dai, R., Li, Y., Liang, W., & Mao, Y. (2016). Decoupled temporal variability and signal synchronization of spontaneous brain activity in loss of consciousness: An fMRI study in anesthesia. *Neuroimage*, *124*, 693–703.

Hughes, C., Faskowitz, J., Cassidy, B. S., Sporns, O., & Krendl, A. C. (2020). Aging relates to a disproportionately weaker functional architecture of brain networks during rest and task states. *NeuroImage*, *209*, 116521. https://doi.org/10.1016/j.neuroimage.2020.116521

Hughes, S. W., Lőrincz, M. L., Parri, H. R., & Crunelli, V. (2011). Infraslow (<0.1Hz) oscillations in thalamic relay nuclei. In *Progress in Brain Research* (Vol. 193, pp. 145–162). Elsevier. https://doi.org/10.1016/B978-0-444-53839-0.00010-7

Huk, A., Bonnen, K., & He, B. J. (2018). Beyond trial-based paradigms: Continuous behavior, ongoing neural activity, and natural stimuli. *Journal of Neuroscience*, *38*(35), 7551–7558.

Huntenburg, J. M., Bazin, P. L., & Margulies, D. S. (2018). Large-Scale Gradients in Human Cortical Organization. *Trends in Cognitive Sciences*, *22*(1), 21–31. https://doi.org/10.1016/j.tics.2017.11.002

Hutchison, R. M., Womelsdorf, T., Allen, E. A., Bandettini, P. A., Calhoun, V. D., Corbetta, M., Della Penna, S., Duyn, J. H., Glover, G. H., & Gonzalez-Castillo, J. (2013).

Dynamic functional connectivity: Promise, issues, and interpretations. *Neuroimage*, *80*, 360–378.

Ito, T., Hearne, L. J., & Cole, M. W. (2020). A cortical hierarchy of localized and distributed processes revealed via dissociation of task activations, connectivity changes, and intrinsic timescales. *Neuroimage*, *221*, 117141. https://doi.org/10.1016/j.neuroimage.2020.117141

Jenkinson, M., Bannister, P., Brady, M., & Smith, S. (2002). Improved optimization for the robust and accurate linear registration and motion correction of brain images. *Neuroimage*, *17*(2), 825–841. https://doi.org/10.1016/s1053-8119(02)91132-8

Jia, Y., Gu, H., & Luo, Q. (2017). Sample entropy reveals an age-related reduction in the complexity of dynamic brain. *Scientific Reports*, *7*(1), 7990.

Jones, S. A., Barfield, J. H., Norman, V. K., & Shew, W. L. (2023). Scale-free behavioral dynamics directly linked with scale-free cortical dynamics. *Elife*, *12*, e79950.

Kasagi, M., Huang, Z., Narita, K., Shitara, H., Motegi, T., Suzuki, Y., Fujihara, K., Tanabe, S., Kosaka, H., & Ujita, K. (2017). Association between scale-free brain dynamics and behavioral performance: Functional MRI study in resting state and face processing task. *Behavioural Neurology*, *2017*(1), 2824615.

Kastner, S., & Ungerleider, L. G. (2000). Mechanisms of visual attention in the human cortex. *Annu Rev Neurosci*, *23*, 315–341. https://doi.org/10.1146/annurev.neuro.23.1.315

Kelso, J. A. (2012). Multistability and metastability: Understanding dynamic coordination in the brain. *Philos Trans R Soc Lond B Biol Sci*, *367*(1591), 906–918. https://doi.org/10.1098/rstb.2011.0351

Kjaerby, C., Radovanovic, T., Kovacs, E. R., Bojarowska, Z., Tokarska, K. A., Tsopanidou, A., Nielsen, E. S., Andersen, M., Li, Y., Weikop, P., Untiet, V., & Nedergaard, M. (2025). *Coordinated infraslow cortical oscillations of neuromodulators during NREM sleep*. Neuroscience. https://doi.org/10.64898/2025.12.22.695982

Klar, P., Çatal, Y., Langner, R., Huang, Z., & Northoff, G. (2023a). Scale-free dynamics in the core-periphery topography and task alignment decline from conscious to unconscious states. *Communications Biology*, *6*(1), 499. https://doi.org/10.1038/s42003-023-04879-y

Klar, P., Çatal, Y., Langner, R., Huang, Z., & Northoff, G. (2023b). Scale-free dynamics of core-periphery topography. *Human Brain Mapping*, *44*(5), 1997–2017. https://doi.org/10.1002/hbm.26187

Klimesch, W., Sauseng, P., & Hanslmayr, S. (2007). EEG alpha oscillations: The inhibition-timing hypothesis. *Brain Res Rev*, *53*(1), 63–88. https://doi.org/10.1016/j.brainresrev.2006.06.003

Ko, A. L., Darvas, F., Poliakov, A., Ojemann, J., & Sorensen, L. B. (2011). Quasi-periodic Fluctuations in Default Mode Network Electrophysiology. *The Journal of Neuroscience*, *31*(32), 11728–11732. https://doi.org/10.1523/JNEUROSCI.5730-10.2011

Kobayashi, T., Shimada, Y., Fujiwara, K., & Ikeguchi, T. (2017). Reproducing Infra-Slow Oscillations with Dopaminergic Modulation. *Scientific Reports*, *7*(1), 2411. https://doi.org/10.1038/s41598-017-02366-z

Koen, J. D., & Rugg, M. D. (2019). Neural Dedifferentiation in the Aging Brain. *Trends in Cognitive Sciences*, *23*(7), 547–559. https://doi.org/10.1016/j.tics.2019.04.012

Koen, J. D., Srokova, S., & Rugg, M. D. (2020). Age-related neural dedifferentiation and cognition. *Curr Opin Behav Sci*, *32*, 7–14. https://doi.org/10.1016/j.cobeha.2020.01.006

Koverda, V. P., & Skokov, V. N. (2012). Maximum entropy in a nonlinear system with a 1/f power spectrum. *Physica A: Statistical Mechanics and Its Applications*, *391*(1–2), 21–28.

Kringelbach, M. L., & Deco, G. (2020). Brain States and Transitions: Insights from Computational Neuroscience. *Cell Reports*, *32*(10), 108128. https://doi.org/10.1016/j.celrep.2020.108128

Kringelbach, M. L., Perl, Y. S., Tagliazucchi, E., & Deco, G. (2023). Toward naturalistic neuroscience: Mechanisms underlying the flattening of brain hierarchy in movie-watching

compared to rest and task. *Science Advances*, *9*(2), eade6049.

Krishnan, G. P., González, O. C., & Bazhenov, M. (2018). Origin of slow spontaneous resting-state neuronal fluctuations in brain networks. *Proceedings of the National Academy of Sciences*, *115*(26), 6858–6863. https://doi.org/10.1073/pnas.1715841115

Kropotov, J. D. (2022). The enigma of infra-slow fluctuations in the human EEG. *Frontiers in Human Neuroscience*, *16*, 928410. https://doi.org/10.3389/fnhum.2022.928410

Kuga, N., Sasaki, T., Takahara, Y., Matsuki, N., & Ikegaya, Y. (2011). Large-Scale Calcium Waves Traveling through Astrocytic Networks *In Vivo*. *The Journal of Neuroscience*, *31*(7), 2607–2614. https://doi.org/10.1523/JNEUROSCI.5319-10.2011

Kumral, D., Şansal, F., Cesnaite, E., Mahjoory, K., Al, E., Gaebler, M., Nikulin, V. V., & Villringer, A. (2020). BOLD and EEG signal variability at rest differently relate to aging in the human brain. *NeuroImage*, *207*, 116373. https://doi.org/10.1016/j.neuroimage.2019.116373

Kuroda, T., Matsuda, N., Ishibashi, Y., & Suzuki, I. (2023). Detection of astrocytic slow oscillatory activity and response to seizurogenic compounds using planar microelectrode array. *Frontiers in Neuroscience*, *16*, 1050150. https://doi.org/10.3389/fnins.2022.1050150

Kwak, Y., Peltier, S. J., Bohnen, N. I., Müller, M. L. T. M., Dayalu, P., & Seidler, R. D. (2012). L-DOPA changes spontaneous low-frequency BOLD signal oscillations in Parkinson's disease: A resting state fMRI study. *Frontiers in Systems Neuroscience*, *6*. https://doi.org/10.3389/fnsys.2012.00052

Laird, A. R., Rogers, B. P., Carew, J. D., Arfanakis, K., Moritz, C. H., & Meyerand, M. E. (2002). Characterizing instantaneous phase relationships in whole-brain fMRI activation data. *Human Brain Mapping*, *16*(2), 71–80. https://doi.org/10.1002/hbm.10027

Lakatos, P., Gross, J., & Thut, G. (2019). A new unifying account of the roles of neuronal entrainment. *Current Biology*, *29*(18), R890–R905.

Lechner, S., Hsieh, M. H., Lin, Y.-T., Liu, C.-M., Chen, I.-F., Liu, C.-C., Chien, Y.-L.,

Hwang, T.-J., Hwu, H.-G., & Northoff, G. (2025). Temporal imprecision and its dynamics in schizophrenia. *Translational Psychiatry*, *15*(1), 279. https://doi.org/10.1038/s41398-025-03510-4

Lechner, S., & Northoff, G. (2023). Temporal imprecision and phase instability in schizophrenia resting state EEG. *Asian Journal of Psychiatry*, *86*, 103654. https://doi.org/10.1016/j.ajp.2023.103654

Lee, J. J., Kim, H. J., Ceko, M., Park, B. Y., Lee, S. A., Park, H., Roy, M., Kim, S. G., Wager, T. D., & Woo, C. W. (2021). A neuroimaging biomarker for sustained experimental and clinical pain. *Nature Medicine*, *27*(1), 174–182. https://doi.org/10.1038/s41591-020-1142-7

Leopold, D. A., Murayama, Y., & Logothetis, N. K. (2003). Very Slow Activity Fluctuations in Monkey Visual Cortex: Implications for Functional Brain Imaging. *Cerebral Cortex*, *13*(4), 422–433. https://doi.org/10.1093/cercor/13.4.422

Lewis, L. D., Setsompop, K., Rosen, B. R., & Polimeni, J. R. (2016). Fast fMRI can detect oscillatory neural activity in humans. *Proceedings of the National Academy of Sciences*, *113*(43), E6679–E6685.

Li, J. M., Bentley, W. J., Snyder, A. Z., Raichle, M. E., & Snyder, L. H. (2015). Functional connectivity arises from a slow rhythmic mechanism. *Proceedings of the National Academy of Sciences of the United States of America*, *112*(19), E2527–E2535. https://doi.org/10.1073/pnas.1419837112

Li, M., Newton, A. T., Anderson, A. W., Ding, Z., & Gore, J. C. (2019). Characterization of the hemodynamic response function in white matter tracts for event-related fMRI. *Nature Communications*, *10*(1), 1140. https://doi.org/10.1038/s41467-019-09076-2

Liégeois, R., Li, J., Kong, R., Orban, C., Van De Ville, D., Ge, T., Sabuncu, M. R., & Yeo, B. T. T. (2019). Resting brain dynamics at different timescales capture distinct aspects of human behavior. *Nature Communications*, *10*(1), 2317. https://doi.org/10.1038/s41467-019-10317-7

Lin, A., Maniscalco, B., & He, B. J. (2016). Scale-Free Neural and Physiological

Dynamics in Naturalistic Stimuli Processing. *Eneuro*, *3*(5), ENEURO.0191-16.2016. https://doi.org/10.1523/ENEURO.0191-16.2016

Linkenkaer-Hansen, K., Monto, S., Rytsälä, H., Suominen, K., Isometsä, E., & Kähkönen, S. (2005). Breakdown of Long-Range Temporal Correlations in Theta Oscillations in Patients with Major Depressive Disorder. *The Journal of Neuroscience*, *25*(44), 10131–10137. https://doi.org/10.1523/JNEUROSCI.3244-05.2005

Linkenkaer-Hansen, K., Nikouline, V. V., Palva, J. M., & Ilmoniemi, R. J. (2001). Long-range temporal correlations and scaling behavior in human brain oscillations. *Journal of Neuroscience*, *21*(4), 1370–1377.

Liu, T. T. (2016). Noise contributions to the fMRI signal: An overview. *Neuroimage*, *143*, 141–151.

Liu, T. T., & Falahpour, M. (2020). Vigilance Effects in Resting-State fMRI. *Frontiers in Neuroscience*, *14*, 321. https://doi.org/10.3389/fnins.2020.00321

Lőrincz, M. L., Geall, F., Bao, Y., Crunelli, V., & Hughes, S. W. (2009). ATP-Dependent Infra-Slow (<0.1 Hz) Oscillations in Thalamic Networks. *PLoS ONE*, *4*(2), e4447. https://doi.org/10.1371/journal.pone.0004447

Lou, W., Wang, D., Wong, A., Chu, W. C. W., Mok, V. C. T., & Shi, L. (2019). Frequency-specific age-related decreased brain network diversity in cognitively healthy elderly: A whole-brain data-driven analysis. *Human Brain Mapping*, *40*(1), 340–351. https://doi.org/10.1002/hbm.24376

Lu, H., Wang, L., Rea, W. W., Brynildsen, J. K., Jaime, S., Zuo, Y., Stein, E. A., & Yang, Y. (2016). Low- but Not High-Frequency LFP Correlates with Spontaneous BOLD Fluctuations in Rat Whisker Barrel Cortex. *Cerebral Cortex*, *26*(2), 683–694. https://doi.org/10.1093/cercor/bhu248

Luo, Q., Deng, Z., Qin, J., Wei, D., Cun, L., Qiu, J., Hitchman, G., & Xie, P. (2015). Frequency dependant topological alterations of intrinsic functional connectome in major depressive disorder. *Scientific Reports*, *5*(1), 9710.

Lurie, D. J., Kessler, D., Bassett, D. S., Betzel, R. F., Breakspear, M., Kheilholz, S., Kucyi, A., Liégeois, R., Lindquist, M. A., McIntosh, A. R., Poldrack, R. A., Shine, J. M., Thompson, W. H., Bielczyk, N. Z., Douw, L., Kraft, D., Miller, R. L., Muthuraman, M., Pasquini, L., … Calhoun, V. D. (2020). Questions and controversies in the study of time-varying functional connectivity in resting fMRI. *Network Neuroscience*, *4*(1), 30–69. https://doi.org/10.1162/netn_a_00116

Ma, Y., Shaik, M. A., Kozberg, M. G., Kim, S. H., Portes, J. P., Timerman, D., & Hillman, E. M. (2016). Resting-state hemodynamics are spatiotemporally coupled to synchronized and symmetric neural activity in excitatory neurons. *Proceedings of the National Academy of Sciences of the United States of America*, *113*(52), E8463–E8471. https://doi.org/10.1073/pnas.1525369113

Malagurski, B., Liem, F., Oschwald, J., Merillat, S., & Jancke, L. (2020). Functional dedifferentiation of associative resting state networks in older adults? A longitudinal study. *Neuroimage*, *214*. https://doi.org/ARTN%20116680%2010.1016/j.neuroimage.2020.116680

Manea, A. M., Maisson, D. J.-N., Voloh, B., Zilverstand, A., Hayden, B., & Zimmermann, J. (2024). Neural timescales reflect behavioral demands in freely moving rhesus macaques. *Nature Communications*, *15*(1), 2151.

Marcus, D. S., Harwell, J., Olsen, T., Hodge, M., Glasser, M. F., Prior, F., Jenkinson, M., Laumann, T., Curtiss, S. W., & Van Essen, D. C. (2011). Informatics and data mining tools and strategies for the human connectome project. *Front Neuroinform*, *5*, 4. https://doi.org/10.3389/fninf.2011.00004

Margulies, D. S., Ghosh, S. S., Goulas, A., Falkiewicz, M., Huntenburg, J. M., Langs, G., Bezgin, G., Eickhoff, S. B., Castellanos, F. X., Petrides, M., Jefferies, E., & Smallwood, J. (2016). Situating the default-mode network along a principal gradient of macroscale cortical organization. *Proceedings of the National Academy of Sciences*, *113*(44), 12574–12579. https://doi.org/10.1073/pnas.1608282113

Maris, E., Fries, P., & van Ede, F. (2016). Diverse phase relations among neuronal

rhythms and their potential function. *Trends in Neurosciences*, *39*(2), 86–99.

Marom, S. (2010). Neural timescales or lack thereof. *Progress in Neurobiology*, *90*(1), 16–28.

Mateo, C., Knutsen, P. M., Tsai, P. S., Shih, A. Y., & Kleinfeld, D. (2017). Entrainment of Arteriole Vasomotor Fluctuations by Neural Activity Is a Basis of Blood-Oxygenation-Level-Dependent "Resting-State" Connectivity. *Neuron*, *96*(4), 936-948.e3. https://doi.org/10.1016/j.neuron.2017.10.012

McCabe, C., & Mishor, Z. (2011). Antidepressant medications reduce subcortical–cortical resting-state functional connectivity in healthy volunteers. *NeuroImage*, *57*(4), 1317–1323. https://doi.org/10.1016/j.neuroimage.2011.05.051

McDonnell, M. D., & Ward, L. M. (2011). The benefits of noise in neural systems: Bridging theory and experiment. *Nature Reviews Neuroscience*, *12*(7), 415–425. https://doi.org/10.1038/nrn3061

McDonough, I. M., & Nashiro, K. (2014). Network complexity as a measure of information processing across resting-state networks: Evidence from the Human Connectome Project. *Frontiers in Human Neuroscience*, *8*, 409.

Mieling, M., Göttlich, M., Yousuf, M., & Bunzeck, N. (2023). Basal forebrain activity predicts functional degeneration in the entorhinal cortex in Alzheimer's disease. *Brain Communications*, *5*(5), fcad262. https://doi.org/10.1093/braincomms/fcad262

Mišić, B., Mills, T., Taylor, M. J., & McIntosh, A. R. (2010). Brain Noise Is Task Dependent and Region Specific. *Journal of Neurophysiology*, *104*(5), 2667–2676. https://doi.org/10.1152/jn.00648.2010

Mitra, A., Kraft, A., Wright, P., Acland, B., Snyder, A. Z., Rosenthal, Z., Czerniewski, L., Bauer, A., Snyder, L., Culver, J., Lee, J.-M., & Raichle, M. E. (2018). Spontaneous Infra-slow Brain Activity Has Unique Spatiotemporal Dynamics and Laminar Structure. *Neuron*, *98*(2), 297-305.e6. https://doi.org/10.1016/j.neuron.2018.03.015

Monti, M. (2011). Statistical Analysis of fMRI Time-Series: A Critical Review of the GLM Approach. *Frontiers in Human Neuroscience*, *5*. https://doi.org/10.3389/fnhum.2011.00028

Monto, S., Palva, S., Voipio, J., & Palva, J. M. (2008). Very Slow EEG Fluctuations Predict the Dynamics of Stimulus Detection and Oscillation Amplitudes in Humans. *The Journal of Neuroscience*, *28*(33), 8268–8272. https://doi.org/10.1523/JNEUROSCI.1910-08.2008

Mosher, C. P., Wei, Y., Kamiński, J., Nandi, A., Mamelak, A. N., Anastassiou, C. A., & Rutishauser, U. (2020). Cellular Classes in the Human Brain Revealed In Vivo by Heartbeat-Related Modulation of the Extracellular Action Potential Waveform. *Cell Reports*, *30*(10), 3536-3551.e6. https://doi.org/10.1016/j.celrep.2020.02.027

Murai, S. A., Mano, T., Sanes, J. N., & Watanabe, T. (2024). Atypical intrinsic neural timescale in the left angular gyrus in Alzheimer's disease. *Brain Communications*, *6*(4), fcae199. https://doi.org/10.1093/braincomms/fcae199

Murphy, K., & Fox, M. D. (2017). Towards a consensus regarding global signal regression for resting state functional connectivity MRI. *NeuroImage*, *154*, 169–173. https://doi.org/10.1016/j.neuroimage.2016.11.052

Neske, G. T. (2016). The Slow Oscillation in Cortical and Thalamic Networks: Mechanisms and Functions. *Frontiers in Neural Circuits*, *9*. https://doi.org/10.3389/fncir.2015.00088

Nezafati, M., Temmar, H., & Keilholz, S. D. (2020). Functional MRI signal complexity analysis using sample entropy. *Frontiers in Neuroscience*, *14*, 700.

Northoff, G. (2017). "Paradox of slow frequencies" – Are slow frequencies in upper cortical layers a neural predisposition of the level/state of consciousness (NPC)? *Consciousness and Cognition*, *54*, 20–35. https://doi.org/10.1016/j.concog.2017.03.006

Northoff, G. (2024). *From brain dynamics to the mind: Spatiotemporal neuroscience*. Elsevier. https://doi.org/10.1016/C2019-0-04628-6

Northoff, G., & Huang, Z. (2017). How do the brain's time and space mediate consciousness and its different dimensions? Temporo-spatial theory of consciousness (TTC). *Neuroscience & Biobehavioral Reviews*, *80*, 630–645. https://doi.org/10.1016/j.neubiorev.2017.07.013

Northoff, G., Klar, P., Bein, M., & Safron, A. (2023). As without, so within: How the brain's temporo-spatial alignment to the environment shapes consciousness. *Interface Focus*, *13*(3), 20220076.

Northoff, G., Wainio-Theberge, S., & Evers, K. (2020a). Is temporo-spatial dynamics the "common currency" of brain and mind? In Quest of "Spatiotemporal Neuroscience." *Physics of Life Reviews*, *33*, 34–54. https://doi.org/10.1016/j.plrev.2019.05.002

Northoff, G., Wainio-Theberge, S., & Evers, K. (2020b). Spatiotemporal neuroscience – what is it and why we need it. *Physics of Life Reviews*, *33*, 78–87. https://doi.org/10.1016/j.plrev.2020.06.005

Northoff, G., & Zilio, F. (2022). Temporo-spatial Theory of Consciousness (TTC) – Bridging the gap of neuronal activity and phenomenal states. *Behavioural Brain Research*, *424*, 113788. https://doi.org/10.1016/j.bbr.2022.113788

Norton, S., & Jewett, R. E. (1965). Frequencies of slow potential oscillations in the cortex of cats. *Electroencephalography and Clinical Neurophysiology*, *19*(4), 377–386. https://doi.org/10.1016/0013-4694(65)90162-8

Omidvarnia, A., Pedersen, M., Walz, J. M., Vaughan, D. N., Abbott, D. F., & Jackson, G. D. (2016). Dynamic regional phase synchrony (DRePS): An instantaneous measure of local fMRI connectivity within spatially clustered brain areas. *Human Brain Mapping*, *37*(5), 1970–1985.

Omidvarnia, A., Zalesky, A., Van De Ville, D., Jackson, G. D., & Pedersen, M. (2021). Temporal complexity of fMRI is reproducible and correlates with higher order cognition. *Neuroimage*, *230*, 117760.

Palva, J. M., & Palva, S. (2012). Infra-slow fluctuations in electrophysiological

recordings, blood-oxygenation-level-dependent signals, and psychophysical time series. *Neuroimage*, *62*(4), 2201–2211.

Palva, J. M., & Palva, S. (2014). The Correlation of the Neuronal Long-Range Temporal Correlations, Avalanche Dynamics with the Behavioral Scaling Laws and Interindividual Variability. *Criticality in Neural Systems*, 105–126.

Palva, S., & Palva, J. M. (2018). Roles of Brain Criticality and Multiscale Oscillations in Temporal Predictions for Sensorimotor Processing. *Trends in Neurosciences*, *41*(10), 729–743. https://doi.org/10.1016/j.tins.2018.08.008

Pan, W.-J., Thompson, G. J., Magnuson, M. E., Jaeger, D., & Keilholz, S. (2013). Infraslow LFP correlates to resting-state fMRI BOLD signals. *Neuroimage*, *74*, 288–297.

Pang, J. C., Aquino, K. M., Oldehinkel, M., Robinson, P. A., Fulcher, B. D., Breakspear, M., & Fornito, A. (2023). Geometric constraints on human brain function. *Nature*, 1–9. https://doi.org/10.1038/s41586-023-06098-1

Pang, J. C., Gollo, L. L., & Roberts, J. A. (2021). Stochastic synchronization of dynamics on the human connectome. *NeuroImage*, *229*, 117738. https://doi.org/10.1016/j.neuroimage.2021.117738

Park, D. C., Polk, T. A., Park, R., Minear, M., Savage, A., & Smith, M. R. (2004). Aging reduces neural specialization in ventral visual cortex. *Proceedings of the National Academy of Sciences of the United States of America*, *101*(35), 13091–13095. https://doi.org/10.1073/pnas.0405148101

Park, H.-D., Barnoud, C., Trang, H., Kannape, O. A., Schaller, K., & Blanke, O. (2020). Breathing is coupled with voluntary action and the cortical readiness potential. *Nature Communications*, *11*(1), 289. https://doi.org/10.1038/s41467-019-13967-9

Patel, A. X., Kundu, P., Rubinov, M., Jones, P. S., Vértes, P. E., Ersche, K. D., Suckling, J., & Bullmore, E. T. (2014). A wavelet method for modeling and despiking motion artifacts from resting-state fMRI time series. *Neuroimage*, *95*, 287–304.

Pedersen, M., Omidvarnia, A., Zalesky, A., & Jackson, G. D. (2018). On the relationship between instantaneous phase synchrony and correlation-based sliding windows for time-resolved fMRI connectivity analysis. *Neuroimage*, *181*, 85–94. https://doi.org/10.1016/j.neuroimage.2018.06.020

Pei, L., Zhou, X., Leung, F. K. S., & Ouyang, G. (2023). Differential associations between scale-free neural dynamics and different levels of cognitive ability. *Psychophysiology*, *60*(6), e14259. https://doi.org/10.1111/psyp.14259

Penttonen, M., Nurminen, N., Miettinen, R., Sirviö, J., Henze, D. A., Csicsvári, J., & Buzsáki, G. (1999). Ultra-slow oscillation (0.025 Hz) triggers hippocampal afterdischarges in Wistar rats. *Neuroscience*, *94*(3), 735–743. https://doi.org/10.1016/S0306-4522(99)00367-X

Perrault, A. A., Khani, A., Quairiaux, C., Kompotis, K., Franken, P., Muhlethaler, M., Schwartz, S., & Bayer, L. (2019). Whole-Night Continuous Rocking Entrains Spontaneous Neural Oscillations with Benefits for Sleep and Memory. *Current Biology*, *29*(3), 402-411.e3. https://doi.org/10.1016/j.cub.2018.12.028

Pirttimaki, T. M., Sims, R. E., Saunders, G., Antonio, S. A., Codadu, N. K., & Parri, H. R. (2017). Astrocyte-Mediated Neuronal Synchronization Properties Revealed by False Gliotransmitter Release. *The Journal of Neuroscience*, *37*(41), 9859–9870. https://doi.org/10.1523/JNEUROSCI.2761-16.2017

Power, J. D. (2019). Temporal ICA has not properly separated global fMRI signals: A comment on Glasser et al. (2018). *NeuroImage*, *197*, 650–651. https://doi.org/10.1016/j.neuroimage.2018.12.051

Power, J. D., Barnes, K. A., Snyder, A. Z., Schlaggar, B. L., & Petersen, S. E. (2012). Spurious but systematic correlations in functional connectivity MRI networks arise from subject motion. *NeuroImage*, *59*(3), 2142–2154. https://doi.org/10.1016/j.neuroimage.2011.10.018

Power, J. D., Mitra, A., Laumann, T. O., Snyder, A. Z., Schlaggar, B. L., & Petersen, S. E. (2014). Methods to detect, characterize, and remove motion artifact in resting state fMRI.

Neuroimage, *84*, 320–341.

Power, J. D., Plitt, M., Laumann, T. O., & Martin, A. (2017). Sources and implications of whole-brain fMRI signals in humans. *Neuroimage*, *146*, 609–625.

Qiao, J., Li, X., Wang, Y., Wang, Y., Li, G., Lu, P., & Wang, S. (2022). The Infraslow Frequency Oscillatory Transcranial Direct Current Stimulation Over the Left Dorsolateral Prefrontal Cortex Enhances Sustained Attention. *Frontiers in Aging Neuroscience*, *14*, 879006. https://doi.org/10.3389/fnagi.2022.879006

Raichle, M. E. (2006). The Brain's Dark Energy. *Science*, *314*(5803), 1249–1250. https://doi.org/10.1126/science.1134405

Rajah M., N., & D'Esposito, M. (2005). Region-specific changes in prefrontal function with age: A review of PET and fMRI studies on working and episodic memory. *Brain*, *128*(9), 1964–1983.

Rajimehr, R., Xu, H., Farahani, A., Kornblith, S., Duncan, J., & Desimone, R. (2022). Functional architecture of cerebral cortex during naturalistic movie-watching. *BioRxiv*, 2022.03. 14.483878. https://doi.org/10.1101/2022.03.14.483878

Raut, R. V., Mitra, A., Marek, S., Ortega, M., Snyder, A. Z., Tanenbaum, A., Laumann, T. O., Dosenbach, N. U., & Raichle, M. E. (2020). Organization of propagated intrinsic brain activity in individual humans. *Cerebral Cortex*, *30*(3), 1716–1734. https://doi.org/10.1093/cercor/bhz198

Raut, R. V., Snyder, A. Z., Mitra, A., Yellin, D., Fujii, N., Malach, R., & Raichle, M. E. (2021). Global waves synchronize the brain's functional systems with fluctuating arousal. *Science Advances*, *7*(30), eabf2709. https://doi.org/10.1126/sciadv.abf2709

Richman, J. S., & Moorman, J. R. (2000). Physiological time-series analysis using approximate entropy and sample entropy. *American Journal of Physiology-Heart and Circulatory Physiology*, *278*(6), H2039–H2049.

Rosenberg, M. D., Finn, E. S., Scheinost, D., Papademetris, X., Shen, X., Constable, R.

T., & Chun, M. M. (2016). A neuromarker of sustained attention from whole-brain functional connectivity. *Nature Neuroscience*, *19*(1), 165–171.

Rosenberg, M., Noonan, S., DeGutis, J., & Esterman, M. (2013). Sustaining visual attention in the face of distraction: A novel gradual-onset continuous performance task. *Attention, Perception, & Psychophysics*, *75*, 426–439.

Rosenblum, Y., Bovy, L., Weber, F. D., Steiger, A., Zeising, M., & Dresler, M. (2022). Increased Aperiodic Neural Activity During Sleep in Major Depressive Disorder. *Biological Psychiatry Global Open Science*, *3*(4), 1021–1029. https://doi.org/10.1016/j.bpsgos.2022.10.001

Ruskin, D. N., Bergstrom, D. A., Kaneoke, Y., Patel, B. N., Twery, M. J., & Walters, J. R. (1999). Multisecond Oscillations in Firing Rate in the Basal Ganglia: Robust Modulation by Dopamine Receptor Activation and Anesthesia. *Journal of Neurophysiology*, *81*(5), 2046–2055. https://doi.org/10.1152/jn.1999.81.5.2046

Sala-Llonch, R., BartrÃ©s-Faz, D., & JunquÃ©, C. (2015). Reorganization of brain networks in aging: A review of functional connectivity studies. *Frontiers in Psychology*, *6*. https://doi.org/10.3389/fpsyg.2015.00663

Salvador, R., Martinez, A., Pomarol-Clotet, E., Gomar, J., Vila, F., Sarro, S., Capdevila, A., & Bullmore, E. (2008). A simple view of the brain through a frequency-specific functional connectivity measure. *Neuroimage*, *39*(1), 279–289.

Samaha, J., & Postle, B. R. (2015). The Speed of Alpha-Band Oscillations Predicts the Temporal Resolution of Visual Perception. *Current Biology*, *25*(22), 2985–2990. https://doi.org/10.1016/j.cub.2015.10.007

Sasai, S., Homae, F., Watanabe, H., Sasaki, A. T., Tanabe, H. C., Sadato, N., & Taga, G. (2014). Frequency-specific network topologies in the resting human brain. *Frontiers in Human Neuroscience*, *8*. https://doi.org/10.3389/fnhum.2014.01022

Sasai, S., Koike, T., Sugawara, S. K., Hamano, Y. H., Sumiya, M., Okazaki, S., Takahashi, H. K., Taga, G., & Sadato, N. (2021). Frequency-specific task modulation of human

brain functional networks: A fast fMRI study. *Neuroimage*, *224*, 117375. https://doi.org/10.1016/j.neuroimage.2020.117375

Satterthwaite, T. D., Elliott, M. A., Gerraty, R. T., Ruparel, K., Loughead, J., Calkins, M. E., Eickhoff, S. B., Hakonarson, H., Gur, R. C., Gur, R. E., & Wolf, D. H. (2013). An improved framework for confound regression and filtering for control of motion artifact in the preprocessing of resting-state functional connectivity data. *Neuroimage*, *64*, 240–256. https://doi.org/10.1016/j.neuroimage.2012.08.052

Scalabrini, A., Ebisch, S. J., Huang, Z., Di Plinio, S., Perrucci, M. G., Romani, G. L., Mucci, C., & Northoff, G. (2019). Spontaneous brain activity predicts task-evoked activity during animate versus inanimate touch. *Cerebral Cortex*, *29*(11), 4628–4645.

Scalabrini, A., Vai, B., Poletti, S., Damiani, S., Mucci, C., Colombo, C., Zanardi, R., Benedetti, F., & Northoff, G. (2020). All roads lead to the default-mode network-global source of DMN abnormalities in major depressive disorder. *Neuropsychopharmacology*, *45*(12), 2058–2069. https://doi.org/10.1038/s41386-020-0785-x

Scheeringa, R., Fries, P., Petersson, K.-M., Oostenveld, R., Grothe, I., Norris, D. G., Hagoort, P., & Bastiaansen, M. C. M. (2011). Neuronal Dynamics Underlying High- and Low-Frequency EEG Oscillations Contribute Independently to the Human BOLD Signal. *Neuron*, *69*(3), 572–583. https://doi.org/10.1016/j.neuron.2010.11.044

Scheinost, D., Tokoglu, F., Shen, X., Finn, E. S., Noble, S., Papademetris, X., & Constable, R. T. (2016). Fluctuations in global brain activity are associated with changes in whole-brain connectivity of functional networks. *IEEE Transactions on Biomedical Engineering*, *63*(12), 2540–2549. https://doi.org/10.1109/TBME.2016.2600248

Schölvinck, M. L., Maier, A., Frank, Q. Y., Duyn, J. H., & Leopold, D. A. (2010). Neural basis of global resting-state fMRI activity. *Proceedings of the National Academy of Sciences of the United States of America*, *107*(22), 10238–10243.

Schrantee, A., Lucassen, P. J., Booij, J., & Reneman, L. (2018). Serotonin transporter occupancy by the SSRI citalopram predicts default-mode network connectivity. *European*

Neuropsychopharmacology, *28*(10), 1173–1179. https://doi.org/10.1016/j.euroneuro.2018.07.099

Schreiber, T., & Schmitz, A. (2000). Surrogate time series. *Physica D: Nonlinear Phenomena*, *142*(3–4), 346–382. https://doi.org/10.1016/S0167-2789(00)00043-9

Schwalm, M., Schmid, F., Wachsmuth, L., Backhaus, H., Kronfeld, A., Aedo Jury, F., Prouvot, P.-H., Fois, C., Albers, F., Van Alst, T., Faber, C., & Stroh, A. (2017). Cortex-wide BOLD fMRI activity reflects locally-recorded slow oscillation-associated calcium waves. *eLife*, *6*, e27602. https://doi.org/10.7554/eLife.27602

Shannon, C. E. (1948). A mathematical theory of communication. *The Bell System Technical Journal*, *27*(3), 379–423.

Shine, J. M., Bissett, P. G., Bell, P. T., Koyejo, O., Balsters, J. H., Gorgolewski, K. J., Moodie, C. A., & Poldrack, R. A. (2016). The Dynamics of Functional Brain Networks: Integrated Network States during Cognitive Task Performance. *Neuron*, *92*(2), 544–554. https://doi.org/10.1016/j.neuron.2016.09.018

Shmueli, K., Van Gelderen, P., De Zwart, J. A., Horovitz, S. G., Fukunaga, M., Jansma, J. M., & Duyn, J. H. (2007). Low-frequency fluctuations in the cardiac rate as a source of variance in the resting-state fMRI BOLD signal. *NeuroImage*, *38*(2), 306–320. https://doi.org/10.1016/j.neuroimage.2007.07.037

Shrout, P. E., & Bolger, N. (2002). Mediation in experimental and nonexperimental studies: New procedures and recommendations. *Psychological Methods*, *7*(4), 422.

Siegel, M., Donner, T. H., & Engel, A. K. (2012). Spectral fingerprints of large-scale neuronal interactions. *Nature Reviews Neuroscience*, *13*(2), 121–134. https://doi.org/10.1038/nrn3137

Smith, D., Wolff, A., Wolman, A., Ignaszewski, J., & Northoff, G. (2022). Temporal continuity of self: Long autocorrelation windows mediate self-specificity. *NeuroImage*, *257*, 119305. https://doi.org/10.1016/j.neuroimage.2022.119305

Sokunbi, M. O., Fung, W., Sawlani, V., Choppin, S., Linden, D. E. J., & Thome, J. (2013). Resting state fMRI entropy probes complexity of brain activity in adults with ADHD. *Psychiatry Research: Neuroimaging*, *214*(3), 341–348. https://doi.org/10.1016/j.pscychresns.2013.10.001

Spoa, M., Monti, S., Bjekić, J., Guerra, A., Fiorenzato, E., Cauzzo, S., Bertoldo, A., & Antonini, A. (2025). Resting-state EEG changes associated with cognitive decline in Parkinson's disease: A systematic review. *Journal of Neural Transmission*. https://doi.org/10.1007/s00702-025-03065-0

Stark, E. A., Cabral, J., Riem, M. M., Van IJzendoorn, M. H., Stein, A., & Kringelbach, M. L. (2020). The power of smiling: The adult brain networks underlying learned infant emotionality. *Cerebral Cortex*, *30*(4), 2019–2029. https://doi.org/10.1093/cercor/bhz219

Stein, R. B., Gossen, E. R., & Jones, K. E. (2005). Neuronal variability: Noise or part of the signal? *Nat Rev Neurosci*, *6*(5), 389–397. https://doi.org/10.1038/nrn1668

Steinberg, S. N., & King, T. Z. (2024). Within-Individual BOLD Signal Variability and its Implications for Task-Based Cognition: A Systematic Review. *Neuropsychology Review*, *34*(4), 1115–1164. https://doi.org/10.1007/s11065-023-09619-x

Takahashi, T., Yoshimura, Y., Hiraishi, H., Hasegawa, C., Munesue, T., Higashida, H., Minabe, Y., & Kikuchi, M. (2016). Enhanced brain signal variability in children with autism spectrum disorder during early childhood. *Human Brain Mapping*, *37*(3), 1038–1050.

Tanabe, S., Huang, Z., Zhang, J., Chen, Y., Fogel, S., Doyon, J., Wu, J., Xu, J., Zhang, J., Qin, P., Wu, X., Mao, Y., Mashour, G. A., Hudetz, A. G., & Northoff, G. (2020). Altered Global Brain Signal during Physiologic, Pharmacologic, and Pathologic States of Unconsciousness in Humans and Rats. *Anesthesiology*, *132*(6), 1392–1406. https://doi.org/10.1097/ALN.0000000000003197

Tarantini, S., Tran, C. H. T., Gordon, G. R., Ungvari, Z., & Csiszar, A. (2017). Impaired neurovascular coupling in aging and Alzheimer's disease: Contribution of astrocyte dysfunction and endothelial impairment to cognitive decline. *Experimental Gerontology*, *94*,

52–58.

Taylor, H. P., Huynh, K. M., Thung, K.-H., Lin, G., Lyu, W., Lin, W., Ahmad, S., & Yap, P.-T. (2026). Functional hierarchy of the human neocortex across the lifespan. *Nature*, *652*(8111), 955–964. https://doi.org/10.1038/s41586-026-10219-x

Teipel, S. J., Flatz, W. H., Heinsen, H., Bokde, A. L. W., Schoenberg, S. O., Stöckel, S., Dietrich, O., Reiser, M. F., Möller, H.-J., & Hampel, H. (2005). Measurement of basal forebrain atrophy in Alzheimer's disease using MRI. *Brain*, *128*(11), 2626–2644. https://doi.org/10.1093/brain/awh589

Thompson, W. H., & Fransson, P. (2015). The frequency dimension of fMRI dynamic connectivity: Network connectivity, functional hubs and integration in the resting brain. *Neuroimage*, *121*, 227–242.

Tian, L., Li, Q., Wang, C., & Yu, J. (2018). Changes in dynamic functional connections with aging. *NeuroImage*, *172*, 31–39. https://doi.org/10.1016/j.neuroimage.2018.01.040

Tomasi, D., & Volkow, N. D. (2012). Aging and functional brain networks. *Molecular Psychiatry*, *17*(5), 549–558.

Tong, C., Li, W., Zou, Y., Xia, Y., Pei, M., Zhang, K., Luo, Y., & Liang, Z. (2025). Norepinephrine-mediated arousal fluctuations drive inverted U-shaped functional connectivity dynamics. *Nature Communications*, *16*(1), 11318. https://doi.org/10.1038/s41467-025-66436-x

Tong, Y., & Frederick, B. D. (2010). Time lag dependent multimodal processing of concurrent fMRI and near-infrared spectroscopy (NIRS) data suggests a global circulatory origin for low-frequency oscillation signals in human brain. *Neuroimage*, *53*(2), 553–564. https://doi.org/10.1016/j.neuroimage.2010.06.049

Tong, Y., Hocke, L. M., & Frederick, B. B. (2019). Low Frequency Systemic Hemodynamic "Noise" in Resting State BOLD fMRI: Characteristics, Causes, Implications, Mitigation Strategies, and Applications. *Frontiers in Neuroscience*, *13*, 787. https://doi.org/10.3389/fnins.2019.00787

Tort, A. B., Komorowski, R., Eichenbaum, H., & Kopell, N. (2010). Measuring phase-amplitude coupling between neuronal oscillations of different frequencies. *Journal of Neurophysiology*, *104*(2), 1195–1210. https://doi.org/10.1152/jn.00106.2010

Tsvetanov, K. A., Henson, R. N. A., Jones, P. S., Mutsaerts, H., Fuhrmann, D., Tyler, L. K., Rowe, J. B., & Cam-CAN. (2020). The effects of age on resting-state BOLD signal variability is explained by cardiovascular and cerebrovascular factors. *Psychophysiology*. https://doi.org/ARTN%20e13714%2010.1111/psyp.13714

Turchi, J., Chang, C., Ye, F. Q., Russ, B. E., Yu, D. K., Cortes, C. R., Monosov, I. E., Duyn, J. H., & Leopold, D. A. (2018). The Basal Forebrain Regulates Global Resting-State fMRI Fluctuations. *Neuron*, *97*(4), 940-952.e4. https://doi.org/10.1016/j.neuron.2018.01.032

Turi, G. F., Teng, S., Chen, X., Lim, E. C., Dias, C., Hu, R., Wang, R., Zhen, F., & Peng, Y. (2025). *Serotonin modulates infraslow oscillation in the dentate gyrus during Non-REM sleep*. https://doi.org/10.7554/eLife.100196.3

Uddin, L. Q. (2017). Mixed Signals: On Separating Brain Signal from Noise. *Trends in Cognitive Sciences*, *21*(6), 405–406. https://doi.org/10.1016/j.tics.2017.04.002

Uddin, L. Q. (2020). Bring the Noise: Reconceptualizing Spontaneous Neural Activity. *Trends in Cognitive Sciences*, *24*(9), 734–746. https://doi.org/10.1016/j.tics.2020.06.003

Van Den Heuvel, M. P., & Hulshoff Pol, H. E. (2010). Exploring the brain network: A review on resting-state fMRI functional connectivity. *European Neuropsychopharmacology*, *20*(8), 519–534. https://doi.org/10.1016/j.euroneuro.2010.03.008

Van Essen, D. C., Smith, S. M., Barch, D. M., Behrens, T. E., Yacoub, E., Ugurbil, K., & W. U-Minn HCP Consortium. (2013). The WU-Minn Human Connectome Project: An overview. *Neuroimage*, *80*, 62–79. https://doi.org/10.1016/j.neuroimage.2013.05.041

Vij, S. G., Nomi, J. S., Dajani, D. R., & Uddin, L. Q. (2018). Evolution of spatial and temporal features of functional brain networks across the lifespan. *NeuroImage*, *173*, 498–508. https://doi.org/10.1016/j.neuroimage.2018.02.066

Von Stein, A., & Sarnthein, J. (2000). Different frequencies for different scales of cortical integration: From local gamma to long range alpha/theta synchronization. *International Journal of Psychophysiology*, *38*(3), 301–313. https://doi.org/10.1016/S0167-8760(00)00172-0

Vossel, S., Geng, J. J., & Fink, G. R. (2014). Dorsal and ventral attention systems: Distinct neural circuits but collaborative roles. *Neuroscientist*, *20*(2), 150–159. https://doi.org/10.1177/1073858413494269

Wager, T. D., Davidson, M. L., Hughes, B. L., Lindquist, M. A., & Ochsner, K. N. (2008). Prefrontal-subcortical pathways mediating successful emotion regulation. *Neuron*, *59*(6), 1037–1050.

Wainio-Theberge, S., Wolff, A., Gomez-Pilar, J., Zhang, J., & Northoff, G. (2022). Variability and task-responsiveness of electrophysiological dynamics: Scale-free stability and oscillatory flexibility. *Neuroimage*, *256*, 119245.

Walters, J. R., Hu, D., Itoga, C. A., Parr-Brownlie, L. C., & Bergstrom, D. A. (2007). Phase relationships support a role for coordinated activity in the indirect pathway in organizing slow oscillations in basal ganglia output after loss of dopamine. *Neuroscience*, *144*(2), 762–776. https://doi.org/10.1016/j.neuroscience.2006.10.006

Wang, X., Liao, W., Han, S., Li, J., Zhang, Y., Zhao, J., & Chen, H. (2019). Altered dynamic global signal topography in antipsychotic-naive adolescents with early-onset schizophrenia. *Schizophrenia Research*, *208*, 308–316. https://doi.org/10.1016/j.schres.2019.01.035

Wang, Y., Ao, Y., Yang, Q., Liu, Y., Ouyang, Y., Jing, X., Pang, Y., Cui, Q., & Chen, H. (2020). Spatial variability of low frequency brain signal differentiates brain states. *PLOS ONE*, *15*(11), e0242330. https://doi.org/10.1371/journal.pone.0242330

Wang, Y., Chen, W., Ye, L., Biswal, B. B., Yang, X., Zou, Q., Yang, P., Yang, Q., Wang, X., Cui, Q., Duan, X., Liao, W., & Chen, H. (2018). Multiscale energy reallocation during low-frequency steady-state brain response. *Human Brain Mapping*, *39*(5), 2121–2132.

https://doi.org/10.1002/hbm.23992

Wang, Y., Huang, X., Yang, X., Yang, Q., Wang, X., Northoff, G., Pang, Y., Wang, C., Cui, Q., & Chen, H. (2019). Low Frequency Phase-locking of Brain Signals Contribute to Efficient Face Recognition. *Neuroscience*, *422*, 172–183. https://doi.org/10.1016/j.neuroscience.2019.10.024

Wang, Y., Wang, X., Ye, L., Yang, Q., Cui, Q., He, Z., Li, L., Yang, X., Zou, Q., Yang, P., Liu, D., & Chen, H. (2019). Spatial complexity of brain signal is altered in patients with generalized anxiety disorder. *Journal of Affective Disorders*, *246*, 387–393. https://doi.org/10.1016/j.jad.2018.12.107

Wang, Y., Yang, C., Li, G., Ao, Y., Jiang, M., Cui, Q., Pang, Y., & Jing, X. (2023). Frequency-dependent effective connections between local signals and the global brain signal during resting-state. *Cognitive Neurodynamics*, *17*(2), 555–560. https://doi.org/10.1007/s11571-022-09831-0

Wang, Y., Zou, Q., Ao, Y., Liu, Y., Ouyang, Y., Wang, X., Biswal, B., Cui, Q., & Chen, H. (2020). Frequency-dependent circuits anchored in the dorsal and ventral left anterior insula. *Scientific Reports*, *10*(1), 16394. https://doi.org/10.1038/s41598-020-73192-z

Wang, Y.-F., Dai, G.-S., Liu, F., Long, Z.-L., Yan, J. H., & Chen, H.-F. (2015). Steady-state BOLD Response to Higher-order Cognition Modulates Low-Frequency Neural Oscillations. *Journal of Cognitive Neuroscience*, *27*(12), 2406–2415. https://doi.org/10.1162/jocn_a_00864

Wang, Y.-F., Liu, F., Long, Z.-L., Duan, X.-J., Cui, Q., Yan, J. H., & Chen, H.-F. (2014). Steady-State BOLD Response Modulates Low Frequency Neural Oscillations. *Scientific Reports*, *4*(1), 7376. https://doi.org/10.1038/srep07376

Wang, Y.-F., Long, Z., Cui, Q., Liu, F., Jing, X.-J., Chen, H., Guo, X.-N., Yan, J. H., & Chen, H.-F. (2016). Low frequency steady-state brain responses modulate large scale functional networks in a frequency-specific means: lfSSBRs Modulate Brain Networks. *Human Brain Mapping*, *37*(1), 381–394. https://doi.org/10.1002/hbm.23037

Waschke, L., Kloosterman, N. A., Obleser, J., & Garrett, D. D. (2021). Behavior needs neural variability. *Neuron*, *109*(5), 751–766. https://doi.org/10.1016/j.neuron.2021.01.023

Watrous, A. J., Tandon, N., Conner, C. R., Pieters, T., & Ekstrom, A. D. (2013). Frequency-specific network connectivity increases underlie accurate spatiotemporal memory retrieval. *Nature Neuroscience*, *16*(3), 349–356.

Watson, B. O. (2018). Cognitive and Physiologic Impacts of the Infraslow Oscillation. *Frontiers in Systems Neuroscience*, *12*, 44. https://doi.org/10.3389/fnsys.2018.00044

Wei, D., Zhuang, K., Ai, L., Chen, Q., Yang, W., Liu, W., Wang, K., Sun, J., & Qiu, J. (2018). Structural and functional brain scans from the cross-sectional Southwest University adult lifespan dataset. *Scientific Data*, *5*(1), 180134. https://doi.org/10.1038/sdata.2018.134

Werner, G., & Mountcastle, V. B. (1963). The variability of central neural activity in a sensory system, and its implications for the central reflection of sensory events. *Journal of Neurophysiology*, *26*(6), 958–977. https://doi.org/10.1152/jn.1963.26.6.958

West, K. L., Zuppichini, M. D., Turner, M. P., Sivakolundu, D. K., Zhao, Y., Abdelkarim, D., Spence, J. S., & Rypma, B. (2019). BOLD hemodynamic response function changes significantly with healthy aging. *Neuroimage*, *188*, 198–207.

Wilckens, K. A., Ferrarelli, F., Walker, M. P., & Buysse, D. J. (2018). Slow-Wave Activity Enhancement to Improve Cognition. *Trends in Neurosciences*, *41*(7), 470–482. https://doi.org/10.1016/j.tins.2018.03.003

Wingfield, A., & Grossman, M. (2006). Language and the Aging Brain: Patterns of Neural Compensation Revealed by Functional Brain Imaging. *Journal of Neurophysiology*, *96*(6), 2830–2839. https://doi.org/10.1152/jn.00628.2006

Wolff, A., Berberian, N., Golesorkhi, M., Gomez-Pilar, J., Zilio, F., & Northoff, G. (2022). Intrinsic neural timescales: Temporal integration and segregation. *Trends in Cognitive Sciences*, *26*(2), 159–173. https://doi.org/10.1016/j.tics.2021.11.007

Wolff, A., Di Giovanni, D. A., Gomez-Pilar, J., Nakao, T., Huang, Z., Longtin, A., &

Northoff, G. (2019). The temporal signature of self: Temporal measures of resting-state EEG predict self-consciousness. *Hum Brain Mapp*, *40*(3), 789–803. https://doi.org/10.1002/hbm.24412

Wolman, A., Çatal, Y., Klar, P., Steffener, J., & Northoff, G. (2024). Repertoire of timescales in uni – and transmodal regions mediate working memory capacity. *NeuroImage*, *291*, 120602. https://doi.org/10.1016/j.neuroimage.2024.120602

Wolman, A., Çatal, Y., Wolff, A., Wainio-Theberge, S., Scalabrini, A., Ahmadi, A. E., & Northoff, G. (2023). Intrinsic neural timescales mediate the cognitive bias of self – temporal integration as key mechanism. *NeuroImage*, *268*, 119896. https://doi.org/10.1016/j.neuroimage.2023.119896

Wolman, A., Lechner, S., Angeletti, L. L., Goheen, J., & Northoff, G. (2024). From the brain's encoding of input dynamics to its behavior: Neural dynamics shape bias in decision making. *Communications Biology*, *7*(1), 1538.

Wolters, A. F., Van De Weijer, S. C. F., Leentjens, A. F. G., Duits, A. A., Jacobs, H. I. L., & Kuijf, M. L. (2019). Resting-state fMRI in Parkinson's disease patients with cognitive impairment: A meta-analysis. *Parkinsonism & Related Disorders*, *62*, 16–27. https://doi.org/10.1016/j.parkreldis.2018.12.016

Wong, C. W., DeYoung, P. N., & Liu, T. T. (2016). Differences in the resting-state fMRI global signal amplitude between the eyes open and eyes closed states are related to changes in EEG vigilance. *Neuroimage*, *124*(Pt A), 24–31. https://doi.org/10.1016/j.neuroimage.2015.08.053

Wong, C. W., Olafsson, V., Tal, O., & Liu, T. T. (2013). The amplitude of the resting-state fMRI global signal is related to EEG vigilance measures. *NeuroImage*, *83*, 983–990. https://doi.org/10.1016/j.neuroimage.2013.07.057

Woods, S. J., Silcox, J. W., & Payne, B. R. (2024). Evaluating Aperiodic and Periodic Neural Activity as Markers of Listening Effort in Speech Perception. *Auditory Perception & Cognition*, *7*(3), 203–218. https://doi.org/10.1080/25742442.2024.2395217

Wright, P. W., Brier, L. M., Bauer, A. Q., Baxter, G. A., Kraft, A. W., Reisman, M. D., Bice, A. R., Snyder, A. Z., Lee, J. M., & Culver, J. P. (2017). Functional connectivity structure of cortical calcium dynamics in anesthetized and awake mice. *PLoS One*, *12*(10), e0185759. https://doi.org/10.1371/journal.pone.0185759

Wu, C. W., Gu, H., Lu, H., Stein, E. A., Chen, J.-H., & Yang, Y. (2008). Frequency specificity of functional connectivity in brain networks. *Neuroimage*, *42*(3), 1047–1055. https://doi.org/10.1016/j.neuroimage.2008.05.035

Wu, G., Liao, W., Stramaglia, S., Ding, J., Chen, H., & Marinazzo, D. (2013). A blind deconvolution approach to recover effective connectivity brain networks from resting state fMRI data. *Medical Image Analysis*, *17*(3), 365–374.

Wu, G. R., Colenbier, N., Van Den Bossche, S., Clauw, K., Johri, A., Tandon, M., & Marinazzo, D. (2021). rsHRF: A toolbox for resting-state HRF estimation and deconvolution. *Neuroimage*, *244*, 118591. https://doi.org/10.1016/j.neuroimage.2021.118591

Wutz, A., Melcher, D., & Samaha, J. (2018). Frequency modulation of neural oscillations according to visual task demands. *Proceedings of the National Academy of Sciences*, *115*(6), 1346–1351. https://doi.org/10.1073/pnas.1713318115

Xia, Y., Chen, Q., Shi, L., Li, M., Gong, W., Chen, H., & Qiu, J. (2019). Tracking the dynamic functional connectivity structure of the human brain across the adult lifespan. *Human Brain Mapping*, *40*(3), 717–728. https://doi.org/10.1002/hbm.24385

Xiang, L., Harel, A., Todorova, R., Gao, H., Sara, S. J., & Wiener, S. I. (2023). Locus coeruleus noradrenergic neurons phase-lock to prefrontal and hippocampal infra-slow rhythms that synchronize to behavioral events. *Frontiers in Cellular Neuroscience*, *17*, 1131151. https://doi.org/10.3389/fncel.2023.1131151

Xie, L., Wang, X., Lin, X., Wen, J., Ma, T., Leong, A. T. L., & Wu, E. X. (2025). Brain-wide resting-state fMRI network dynamics elicited by activation of single thalamic input. *Nature Communications*, *16*(1), 11247. https://doi.org/10.1038/s41467-025-66104-0

Xie, W., Peng, C. K., Shen, J., Lin, C. P., Tsai, S. J., Wang, S., Chu, Q., & Yang, A. C.

(2020). Age-related changes in the association of resting-state fMRI signal variability and global functional connectivity in non-demented healthy people. *Psychiatry Res*, *291*, 113257. https://doi.org/10.1016/j.psychres.2020.113257

Xie, Y. C., Chan, A. W., McGirr, A., Xue, S. C., Xiao, D. S., Zeng, H. K., & Murphy, T. H. (2016). Resolution of High-Frequency Mesoscale Intracortical Maps Using the Genetically Encoded Glutamate Sensor iGluSnFR. *Journal of Neuroscience*, *36*(4), 1261–1272. https://doi.org/10.1523/Jneurosci.2744-15.2016

Yan, C. G., Wang, X. D., Zuo, X. N., & Zang, Y. F. (2016). DPABI: Data Processing & Analysis for (Resting-State) Brain Imaging. *Neuroinformatics*, *14*(3), 339–351. https://doi.org/10.1007/s12021-016-9299-4

Yang, A. C., Huang, C. C., Yeh, H. L., Liu, M. E., Hong, C. J., Tu, P. C., Chen, J. F., Huang, N. E., Peng, C. K., & Lin, C. P. (2013). Complexity of spontaneous BOLD activity in default mode network is correlated with cognitive function in normal male elderly: A multiscale entropy analysis. *Neurobiology of Aging*, *34*(2), 428–438.

Yang, C., Xiao, K., Ao, Y., Cui, Q., Jing, X., & Wang, Y. (2023). The thalamus is the causal hub of intervention in patients with major depressive disorder: Evidence from the Granger causality analysis. *NeuroImage: Clinical*, *37*, 103295. https://doi.org/10.1016/j.nicl.2022.103295

Yang, G. J., Murray, J. D., Glasser, M., Pearlson, G. D., Krystal, J. H., Schleifer, C., Repovs, G., & Anticevic, A. (2016). Altered Global Signal Topography in Schizophrenia. *Cerebral Cortex*, cercor;bhw297v1. https://doi.org/10.1093/cercor/bhw297

Yang, H., Zhang, J., & Cheng, J. (2021). Effects of donepezil on the amplitude of low-frequency fluctuations in the brain of patients with Alzheimer's disease: Evidence from resting-state functional magnetic resonance imaging. *NeuroReport*, *32*(11), 907–912. https://doi.org/10.1097/WNR.0000000000001659

Yang, L., Yan, Y., Wang, Y., Hu, X., Lu, J., Chan, P., Yan, T., & Han, Y. (2018). Gradual Disturbances of the Amplitude of Low-Frequency Fluctuations (ALFF) and Fractional ALFF

in Alzheimer Spectrum. *Frontiers in Neuroscience*, *12*. https://doi.org/10.3389/fnins.2018.00975

Yellin, D., Berkovich-Ohana, A., & Malach, R. (2015). Coupling between pupil fluctuations and resting-state fMRI uncovers a slow build-up of antagonistic responses in the human cortex. *NeuroImage*, *106*, 414–427. https://doi.org/10.1016/j.neuroimage.2014.11.034

Yeshurun, Y., Nguyen, M., & Hasson, U. (2021). The default mode network: Where the idiosyncratic self meets the shared social world. *Nat Rev Neurosci*, *22*(3), 181–192. https://doi.org/10.1038/s41583-020-00420-w

Yu, H., Liu, X., Zheng, C., Wang, Z., Wang, M., Zhang, C., Hao, Q., Liu, R., & Wang, Y. (2025). Frequency-specific modulations for subcomponents of executive functions in the infra-slow frequency range—A combined O-tDCS and fNIRS study. *International Journal of Clinical and Health Psychology*, *25*(2), 100575.

Zalesky, A., Fornito, A., Cocchi, L., Gollo, L. L., & Breakspear, M. (2014). Time-resolved resting-state brain networks. *Proceedings of the National Academy of Sciences*, *111*(28), 10341–10346. https://doi.org/10.1073/pnas.1400181111

Zeng, L.-L., Wang, D., Fox, M. D., Sabuncu, M., Hu, D., Ge, M., Buckner, R. L., & Liu, H. (2014). Neurobiological basis of head motion in brain imaging. *Proceedings of the National Academy of Sciences*, *111*(16), 6058–6062. https://doi.org/10.1073/pnas.1317424111

Zhang, C., Wang, Y., Jing, X., & Yan, J. H. (2023). Brain mechanisms of mental processing: From evoked and spontaneous brain activities to enactive brain activity. *Psychoradiology*, *3*, kkad010. https://doi.org/10.1093/psyrad/kkad010

Zhang, H., Yang, S. Y., Qiao, Y., Ge, Q., Tang, Y. Y., Northoff, G., & Zang, Y. F. (2022). Default mode network mediates low-frequency fluctuations in brain activity and behavior during sustained attention. *Human Brain Mapping*, *43*(18), 5478–5489. https://doi.org/10.1002/hbm.26024

Zhang, H., Zhang, L., & Zang, Y. (2015). Fluctuation amplitude and local synchronization of brain activity in the ultra-low frequency band: An fMRI investigation of

continuous feedback of finger force. *Brain Research*, *1629*, 104–112.

Zhang, J., Huang, Z., Tumati, S., & Northoff, G. (2020). Rest-task modulation of fMRI-derived global signal topography is mediated by transient coactivation patterns. *PLOS Biology*, *18*(7), e3000733. https://doi.org/10.1371/journal.pbio.3000733

Zilio, F., Gomez-Pilar, J., Cao, S., Zhang, J., Zang, D., Qi, Z., Tan, J., Hiromi, T., Wu, X., & Fogel, S. (2021). Are intrinsic neural timescales related to sensory processing? Evidence from abnormal behavioral states. *Neuroimage*, *226*, 117579. https://doi.org/10.1016/j.neuroimage.2020.117579

Zuo, X. N., Biswal, B. B., & Poldrack, R. A. (2019). Reliability and reproducibility in functional connectomics. *Frontiers in Neuroscience*, *13*, 117.

Zuo, X.-N., Di Martino, A., Kelly, C., Shehzad, Z. E., Gee, D. G., Klein, D. F., Castellanos, F. X., Biswal, B. B., & Milham, M. P. (2010). The oscillating brain: Complex and reliable. *NeuroImage*, *49*(2), 1432–1445. https://doi.org/10.1016/j.neuroimage.2009.09.037